UNIVERSITÀ DEGLI STUDI DI PADOVA

UNIVERSITÀ DEGLI STUDI DI PADOVA

Dipartimento di ingegneria industriale DII

Corso di laurea magistrale in Ingegneria dei Materiali

FATIGUE BEHAVIOUR OF COMPOSITES

Relatore: Prof. Massimo Guglielmi

Correlatore: Prof. Alojz Ivankovic

Laureanda: MARTA ARTUSO

ANNO ACCADEMICO 2017/2018

Abstract

This work is the product of almost six months spent at University College Dublin. It consists on fatigue tests done in CFRPs with and without steel fibres inside. The idea of insert a different fibre material layer inside CFRPs is proposed to improve fracture toughness and especially delamination behaviour that is one of the mechanism that brings to failure.
These material samples were tested statically in a previous research project and the team at UCD was interested in testing them also under fatigue solicitation to compare results and behaviours. CFRP is studied because can be applied in aerospace and automotive field so there is a lot of interest in discovering how it behaves in particular under a cyclic force. After a first fatigue test, samples were tested again in fatigue to see how they replied to a second cyclic load. Repeating fatigue tests is a study of big interest nowadays because it can bring to a better material's characterisation and it can simulate a real phenomenon which happens during material's life. In order to do experiments, standards and rules are necessary to regulate procedures and obtain proper results. From data analysis it is possible to see that, as happened in static tests, fibres improve material's behaviour and increase fracture toughness. As future work, it is suggested to continue the investigation of fatigue in these materials, especially to work on repeating fatigue tests because it is necessary to find new standards in order to better describe and understand how samples react to solicitation.

To my family,

Contents

Introduction

1.1 Background

Due to the impressive strength to weight properties of composite materials, and the easy manufacturing, such materials have been favoured as an alternative to metals in a wide range of industries. The properties of composite structures can be changed in modifying the fibres, their orientations, amount and matrix formulations to fulfill design requirements. It is possible to get components of complex geometries with lighter designs than the metal ones, Figure 1.1, and with excellent surface finish and corrosion resistance.
The manufacture of Fibre Reinforced Polymers (FRPs) for structural application gained traction in the 1940's, where new moulding methods found application in the motor and marine industries. During the 1960's the marine industry was the largest consumer of fibre reinforced composite materials, and in subsequent years composites have become preferred materials in many aspects of aircraft and spacecraft construction.

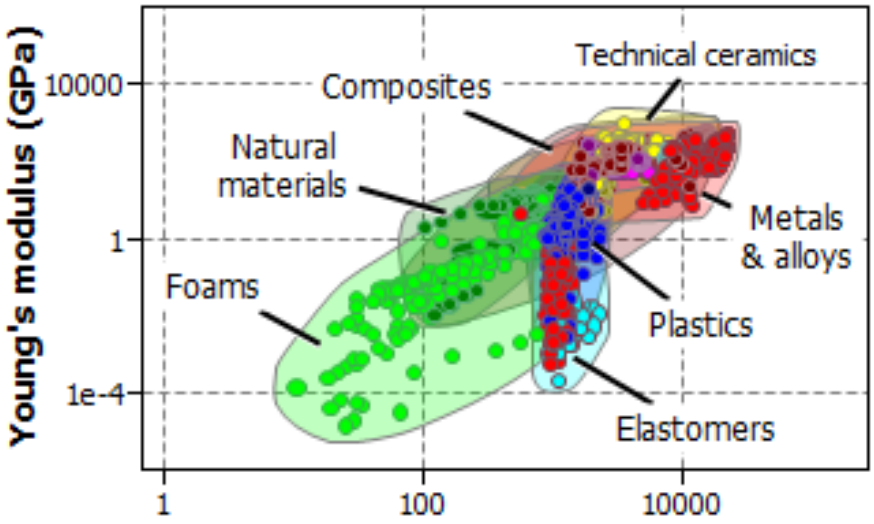

Figure 1.1 High specific strength of CFRP compared to metals. Data obtained from the CES materials database

The use of composite materials as a replacement for traditional steel and thermoplastic materials has brought with it a number of challenges. The use of different fibre orientations and matrix formulations bring to different mechanical properties under a variety of modes of loading.

It is important to characterise composites' behaviour in all forms of stress, in particular under fatigue loading. Ideally loads occur in the same plane as the fibres, however the major weakness in the layered structure of composite laminates is a load in the plane perpendicular to the fibres. Under fatigue loading conditions, delamination can initiate and grow to a critical length, significantly

reducing the structural integrity of the material, leading to failure. A standardised test method exists for the composite material's mode I fracture toughness under quasi-static loading conditions [1][2], however some such standards exist for experimental determination of its behaviour under fatigue loading conditions (ESIS-TC4-Protocol), which is the most common cause of failure in the material. The thesis aim is to study fatigue behaviour of composite materials during fatigue stress. In particular the work is based on a comparison between a carbon fibre composite and the same material with a layer of steel fibres inside indeed the materials tested in this job are CFRP and CFRP with steel fibres put in different positions (longitudinally and transversally) and in a different amount. The purpose is to discover if also during fatigue tests the material with fibres has a higher toughness so it is more resistant to crack propagation as resulted in previous static tests.

1.2 Motivation

Fatigue delamination of composite materials is a subject that has received much research attention in recent years. The European Structural Integrity Society Technical Committee have conducted several round robin tests with the aim of establishing a standardised test procedure. The choice of specimen geometry is the double cantilever beam, which is also employed in quasi-static testing. The major interest has been placed on establishing a procedure of relatively short test duration (7 hours) to describe the behavior of the material, however it would be also necessary to characterise the threshold value of the material – its behaviour at short crack growth rates, but this requires longer test durations under displacement control, so it is not studied in this thesis. The main law, used to characterise and compare samples is Paris relationship which represents the crack growth in composites as a function of the strain energy release rate. The work presented in this thesis has been carried out at University College Dublin School of Mechanical and Materials Engineering for a period of almost six months. It is the continuation of previous static tests done on the same samples and it will be part of a future paper. The aim of this study is to find a solution to increase the weak points of composites: delamination and low fracture toughness. The idea is to use steel fibres inside the a CFRP material to get an improvement. Two fatigue tests are done on the material to study the phenomenon in the virgin material and in a sample with a crack damage created during the first test.

1.3 Project Scope & Objectives

The main purpose would be to show an increase of the energy necessary to the crack growth and how it changes using different quantity and disposition of steel fibres inside the CFRP. This project is limited to the observation of mode I (opening) fatigue delamination and fatigue properties of carbon fibre reinforced polymer. The objectives of the project are as follows:

- To manufacture and prepare double cantilever beam specimens for delamination fatigue analysis

- To create satisfactory conditions for the employment of a draft test procedure prepared by ESIS TC4

- To conduct fatigue tests and repeat them on the specimens using Instron 250kN machine

- To analyse the data from the test and get a final conclusion

1.4 Thesis structure

This thesis consists of nine chapters. The second chapter provides an overview on composite materials and their applications. The third chapter focuses on CFRPs, their composition, properties and applications. Fourth chapter is about fracture mechanics to describe delamination growth in composites, and presents up-to-date developments in experimental standardisation and crack growth representation, while fifth is on material's manufacturing and specimens' preparation. Chapters six and seven talk about testing procedure and samples' preparation for the test. Chapter eight resumes previous quasi-static tests done on the same material in order to compare static and fatigue behaviour and the final chapter show data analysis and results obtained from tests. Then project conclusions are presented.

Chapter 2

A composite can be defined as a combination of two materials, usually a fibre and a matrix or resin, with the purpose of getting the beneficial properties of both materials. Fibre Reinforced Polymers (FRP) are materials made by two or more constituent materials (where one of them is in form of fibre) with significantly different physical or chemical properties that, when combined, produce a material with characteristics different from the individual components. The individual components remain separate and distinct within the finished structure (Figure 2.1).

The many component materials and different processes that can be used make composites extremely versatile and efficient. They typically result in lighter, stronger, more durable solutions compared to traditional materials. In many cases, the fibre reinforcement attributes to high strength and stiffness with low density. The matrix allows for flexibility, possessing good shear properties and also low density. Carbon fibre reinforced polymers (CFRP), with carbon fibre inside the matrix, are characterised by a high strength-to-weight ratio and rigidity. They are mostly used in aerospace, automotive, civil engineering, sports goods and an increasing number of other consumer and technical applications.

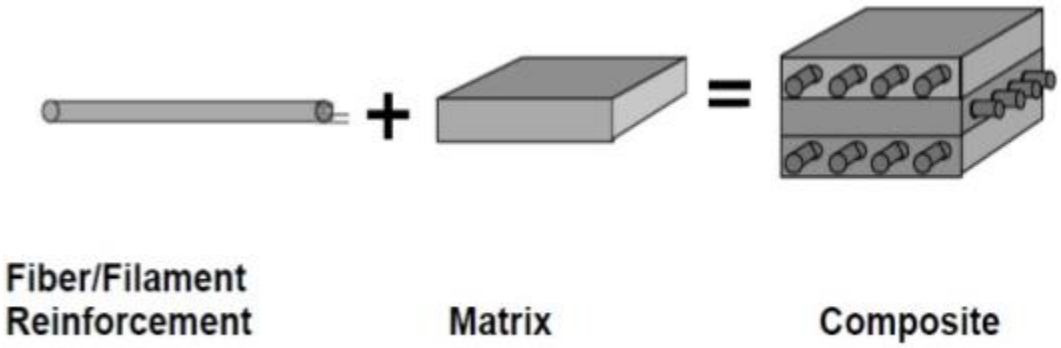

Figure 2.1 Scheme of a composite material

CFRPs have been replacing traditional materials, such as steel and aluminium, in critical load bearing applications in a wide range of industries including aerospace, automotive and renewable energy generation. These composite materials are selected and used for their low weight, high strength, corrosion resistance and high stiffness. However, their critical points are poor out-of plane impact resistance, low fracture toughness, poor delamination resistance and high cost.
The wider introduction of these composite materials into industries has been a slow process. It was difficult to replace metals with CFRP, however, by replacing a metal part with a composite equivalent, the weight and the cost could be reduced, while mechanical properties can increase.

2.1 Composite Materials

Composite materials are made from two or more distinct constituent materials. These constituent materials are categorised as either a matrix phase or a reinforcement phase. The matrix and reinforcement phases act together to produce a material with properties substantially different to those of either of the constituent materials. These input materials remain distinct and do not merge or dissolve in the final composite material [3]. Actually, the binding polymer (matrix) is often a thermoset resin such as epoxy, but other thermoset or thermoplastic polymers can be introduced. The composite may contain aramid (e.g. Kevlar, Twaron), carbon fibers, aluminium, ultra-high-molecular-weight polyethylene (UHMWPE) or glass fibers. The properties of the final CFRP product can also be affected by the type of additives introduced to the binding matrix. The many component materials and different processes that can be used make composites extremely versatile and efficient. They typically result in lighter, stronger, more durable solutions compared to traditional materials [4].

2.1.1 Natural and traditional composite materials

Natural composites exist in both animals and plants. Wood is a composite indeed it is made from long cellulose fibres (a polymer) held together by a much weaker substance called lignin. The two substances – lignin and cellulose – together form a much stronger one. The bone in body is also a composite. It is made from a hard but brittle material called hydroxyapatite (which is mainly calcium phosphate) and a soft and flexible material called collagen (which is a protein). Collagen combines with hydroxyapatite to give bone the properties that are needed to support the body.

Man-made composites are not a recent development. Wattle and daub has been used as a construction material for at least 6,000 years. It consists of a matrix of wet soil, clay, sand, animal dung and straw (daub), with small wooden strips (wattle) as the reinforcement phase (Figure 2.2a). Similarly, concrete, is also classified as a composite. It is manufactured by combining Portland Cement, aggregates, sand and water. Here the cement acts as the matrix material, while the aggregates and sand represent the reinforcement phase (Figure 2.2b).

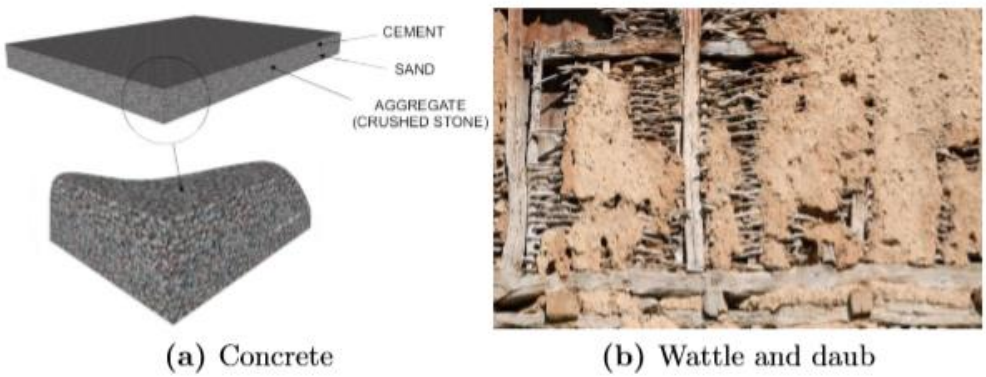

Figure 2.2 Examples of first composite: (a) concrete, (b) wattle and daub

2.1.2 Modern Composite Materials

In more recent times, high-performance materials have been developed by using fibres to reinforce polymers. Fibre Reinforced Polymers (FRP) often consist of carbon or glass fibres in either an epoxy, vinyl ester or polyester matrix. There are different types of fibres [3] [5]:

- **Glass fibres**: the first modern composite material was fiberglass and although many forms of fiber are used as reinforcement in composite laminates, glass fibers account for more than 90 percent of the fibers used in reinforced plastics because they are cheaper and have relatively good strength-to weight characteristics. They are widely used today for boat hulls, sports equipment, building panels and many car bodies. The matrix is a plastic and the reinforcement is glass that has been made into fine threads and often woven into a sort of cloth. The plastic matrix holds the glass fibres together and also protects them from damage by sharing out the forces acting on them. Glass is generally a good impact resistant fiber but weighs more than carbon or aramid. Glass fibers have excellent mechanical characteristics, stronger than steel in certain forms. The lower modulus requires special design treatment where stiffness is critical. Glass fibers are transparent to radio frequency radiation and are used in radar antenna applications.
- **Carbon fibres**: some advanced composites are now made using carbon fibres instead of glass. These materials are lighter and stronger than fibreglass but more expensive to produce. They are used in aircraft structures and expensive sports equipment such as golf clubs. Carbon nanotubes have also been used successfully to make new composites. These are even lighter and stronger than composites made with ordinary carbon fibres but they are still extremely expensive.
- **Aramid fibers**: it is an aromatic polyimide that is a man-made organic fiber for composite reinforcement. Aramid fibers offer good mechanical properties at a low density with the added advantage of toughness or damage/impact resistance. They are characterized as having reasonably high tensile strength, a medium modulus, and a very low density as compared to glass and carbon. Aramid fibers are insulators of both electricity and heat and increase the impact resistance of composites. They are resistant to organic solvents, fuels and lubricants. Aramid composites are not as good in compressive strength as glass or carbon composites. Aramid is the predominant organic reinforcing fiber replacement for steel belting in tires.
- **New fibres**: polyester and nylon thermoplastic fibers have recently been introduced both as primary reinforcements and in a hybrid arrangement with fiberglass. Attractive features include low density, reasonable cost, and good impact and fatigue resistance. Although polyester fibers have fairly high strengths, their stiffness is considerably below that of glass. More specialized reinforcements for high strength and high temperature use include metals and metal oxides such as those used in aircraft or aerospace applications.

Other composites have particles, nanotubes or other shape materials as reinforce. Properties change with the disposition of these elements inside the matrix.

2.2 Advantages and applications

It is important to understand why industries are using FRP in increasing quantities. Composite materials have a number of advantages over their metallic counterparts. For example:

• Composites can have higher strength and bigger specific modulus of other common engineering materials. This helps to reduce weight and increase fuel efficiency in the aerospace and automotive industries.

• The mechanical properties of composite parts can also be tailored for specific applications by controlling the orientation of the fibre reinforcement or type of fibre used.

• Composite materials can be moulded to virtually any shape. This allows components to be manufactured as a single piece, thereby often reducing the need for additional expensive machining or finishing operations. This also helps to greatly reduce the number of individual components needed in the assembly of larger structures, thus reducing manufacturing time as well as labour costs.

2.2.1 Aerospace

The civil aerospace industry has been the key market for composites over the last number of decades. Rising fuel costs, environmental regulations and an increase in airline traffic have helped drive the increasing use of composite materials in the aerospace industry. Composites are used in military, business and commercial aircraft of all sizes, including spacecraft. They are used in particular on aircrafts: the reduction in weight resulting from the use of composite materials, coupled with the development of more fuel efficient engines, has made these new aircraft designs considerably more economical to operate than previous models. The Boeing 787 Dreamliner was the first major commercial plane to have a composite fuselage and composite wings (Figure 2.3a). It famously achieved 50% composite materials by weight, resulting in 20% weight saving compared to a more conventional aluminium design. The reduced fatigue and corrosion risks result in 35% lower maintenance hour requirements versus the smaller 767 aircraft.
Another major new application of composites is in the construction of unmanned aerial vehicles (UAV). UAV's are well known for their use in the military as drones (Figure 2.3b) or unmanned combat aerial vehicles (UCAV) (Figure 2.3c). However, UAV's are also used in commercial applications such as crop spraying and in situations in which it would be too dangerous to employ a manned aerial vehicle.

Figure 2.3 On the left (a) Boeing 737, in the middle (b) UAV drone, on the right (c) UCAV

2.2.2 Automotive

The main advantages composites offer the automotive applications are in cost reduction, weight reduction and recyclability. Composites offer many structural and weight advantages over traditional steel and injection moulded automotive parts.
The use of composite in automotive industry is an help also in reducing carbon emissions. Central to this plan is the development of electric cars. Composite materials are set to play a central role in these developments. Composite materials are now being considered as alternatives to steel and aluminium in the construction of regular cars because they would be 30% lighter than aluminium and 50% lighter than steel. A total reduction in weight of around 10% can be achieved with the use of composites without compromising performance or handling and with the benefit of increased fuel efficiency and lower carbon emissions.

The 1981 McLaren MP4/1 was the first F1 car to be built with a carbon fibre monocoque. Composite improved rigidity and weight without reducing its safety.[6]

BMW is the major company investing on these new materials. They have opened and expanded a $300 million hydro-powered carbon fibre manufacturing plant in Washington. The plant will produce 9,000 tonnes of the material a year. This will reduce the cost of the material, while increasing the reliability of their supply chain. An example of application of these fibres is into the BMW ”i” line of cars. The BMW i3 was the first mass production car to have most of its internal structure made from carbon fibre. This weight shedding helps offset the heavy lithium-ion batteries, therefore increasing range and energy consumption.

Figure 2.4 BMW i3

Moreover, thermoplastic composites offer excellent crash performance compared with traditional steels. While steel typically absorbs only 35J/kg of energy, thermoset composites can absorb about twice this, and thermoplastics can absorb 7-8 times the energy of steel.

Hans-Juergen Karkosch, Conti Tech Vibration and Control, and Holger Klink, BASF, introduced heavy duty lightweight composite engine mounts and cross members. Most engine mounts are made of aluminium. They are replacing the engine mounts with a lighter weight material: 50% glass fibre and rubber modified polyamide (PA). The engine mounts weigh less, reduce front axle load, reduce plant complexity, and lower noise.

The Italian company Fiat introduced on the market Abarth 124 GT with carbon composite roof, which Fiat claims is the only one on the market made entirely from CFRP. The new material allows a weight reduction and a bigger compactness. [7]

Also the use of natural fibres in composite materials is increasing, especially in automotive field, due to the idea of reuse and recycle materials, which is leading to an increase in the bio-based material content in automotive applications. Natural fibres are eco-friendly, lightweight, strong and low cost, so they have already started to replace glass and mineral fillers in numerous engineering applications in automobiles, furniture, packaging and construction. The automobile industry has discovered the advantages to be gained from natural fibres and the Natural-Fibre Composites (NFC) made through the combination of natural fibres with different polymers such as: Polypropylene (PP) (Figure 2.5), Polyethylene (PE), and Polyvinylchloride (PVC). Their main properties are high mechanical resistance and dimensional stability added to a low weight. However, the use of natural fibres also has some limitations. They are moisture sensitive and their bonding with polymer matrices is weak. [8]

Figure 2.5 Application of natural fibres in a car

2.2.3 Renewable Energy Generation

The Electricity Supply Board (ESB), an Irish energy company, has recently announced an investment program in renewable energy generation. The program will invest in energy generation from wind, air and biomass. The turbine blades are manufactured from composites to help reduce weight and also improve corrosion and fatigue resistance. First they were made by glass fibres composites then new technologies moved to carbon fiber to obtain bigger and lighter blades to increase the collection of energy. Composites are also being used in the generation of renewable energy from wave and ocean sources. The turbine blades and casing are manufactured from composite materials (Figure 2.6) [9].

Figure 2.6 Composites wind turbine blades

Chapter 3

This chapter describes different methods to obtain carbon fibres used in CFRP, moreover it focuses on the material's applications indeed in the last years CFRPs have become very popular and they are more and more used in aerospace, automotive and in sport applications.

3.1 Carbon Fiber Reinforced Plastic

Carbon fibres were first manufactured in the second half of the 19th century by Joseph Swan and Thomas Edison as a cheaper alternative filament material to platinum for incandescent lightbulbs. These filaments were produced by carbonising plant threads. Otherwise, these fibres did not have the desirable high tensile strength that would make them suitable for structural use. The next development was achieved in 1958 by Roger Bacon who produced carbon fibres by carbonising strands of an artificial cellulose based material called rayon. These fibres began to show some potential as a structural material and in order to reach a high strength it was necessary the carbon rings to be orientated and crystalised along fibre axis. So when the hot-stretching process was developed for rayon it was possible to produce fibres with a Young modulus of 170 GPa. Simultaneously, a Japanese researcher Dr. Akio Shindo produced carbon fibres, with a Young Modulus of 142 GPa, from the oil derivative polyacrylonitrile (PAN) but as Britain was the first to put them in commerce it took the lead in production. PAN became, and still is, the most popular base material for manufacturing high quality carbon fibres for CFRPs. PAN's fibres are fused and stretched to align chains on CH_2 then to get graphite fibre it is necessary to stabilise and oxidise them in an inert atmosphere to let O_2 create links among chains. To get higher properties, fibres are maintained in tension and after these processes there is the carbonisation phase using temperature of 400/450°C to obtain a completely carbon fibres. At this point, fibres are made by amorphous carbon crystals, so a process of crystallization is used to increase the mechanical properties. This last step is done in an inert atmosphere and increasing temperature until 2000°C. Higher temperature brings to higher properties. Carbon fibres obtained from PAN have a non-circular section with holes and pores. Analysing the structure, it alternates pores, amorphous and crystalised zones. The last are orientated casually and fibres have a medium diameter of 10 micron.

Japan developed another technology starting from pitch, a residue of oil, cheaper than PAN. To get a carbon fiber, pitch is treated in an inert atmosphere at 200/300°C to obtain a 'mesophasic' pitch. Then a thermal treatment and spinning are used to obtain fibres maintaining the material in tension; after oxidation and carbonisation are done to obtain higher properties. These fibres have a high Young Modulus but lower mechanical resistance than carbon fibres obtained from PAN. They have a circular section and the graphite's planes are arranged radially (Figure 3.2) [10].

PAN fibres have high toughness with E=200-300 MPa and σ=7000 MPa, while pitch fibres have higher Young Modulus but lower toughness with E=900 MPa and σ=3400 MPa.

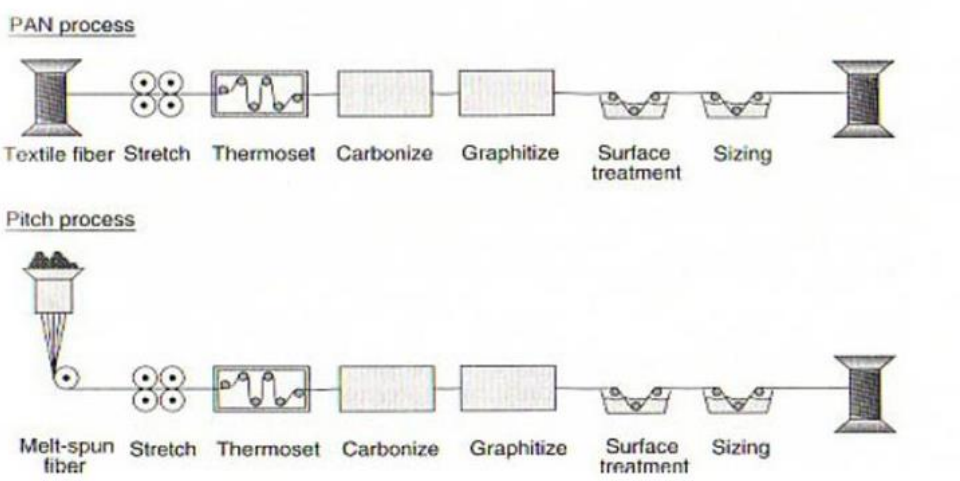

Figure 3.1. Carbon fibres process starting from PAN and pitch

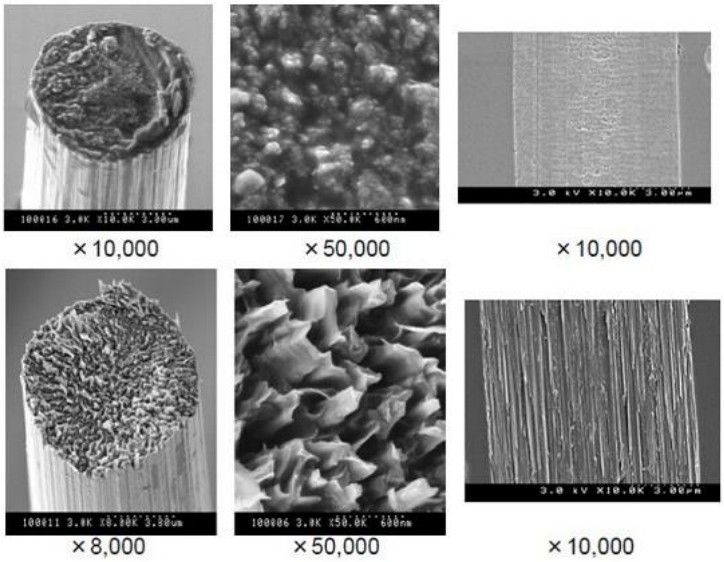

Figure 3.2 Comparison between PAN and pitch fibres

3.2 Applications of Carbon Composites Materials

When CFRPs were initially proposed, as a high-performance structural material, its anisotropic properties caused hesitation and skepticism. However, new technologies, falling costs and improved understandings of carbon composite behaviours brought to its proliferation. Although CFRPs have a remarkably high stiffness and strength to weight ratio, the high price is still a problem. Thus, its use only becomes justified in applications that require high stiffness and/or are very weight sensitive. Some of its most well noted applications are in the aerospace, automotive and sport equipment industries.

3.2.1 Aerospace

Composite materials are particularly attractive to aviation and aerospace applications because of their exceptional strength and stiffness-to-density ratios and superior physical properties. In aerospace field it is required light-weight, high reliability, aerodynamic performance, fatigue and corrosion resistance. Further, the structure has to meet the requirements of fuel sealing and provide access for easy maintenance of equipment respecting safety standards.
Rolls-Royce was the first to implement CFRPs in the aerospace industry. They used this material to manufacture engine compressor blades, significantly reducing the weight of heavy engines. The use of CFRP for a wide range of critical and non-critical components has become common place. The Boeing 787 Dreamliner (Figure 3.3) was the first major commercial plane to have a composite fuselage and composite wings. The use of composite materials brought to 20% weight saving compared to a more conventional aluminium design, it increased fatigue resistance and reduced corrosion risks. This allowed a 35% lower maintenance hour requirements and so the reduced amount of fuel used and the decrement of maintenance costs helped to offset the greater upfront cost [11].

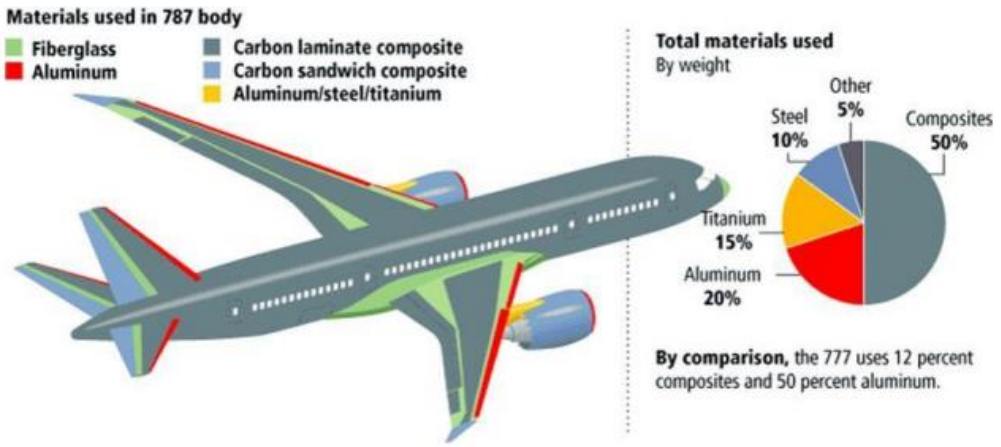

Figure 3.3 Boeing 787 composition

An Italian start-up company manufactured the world's first single-engine, light-sport aircraft composed almost entirely of carbon fiber reinforced polymer (CFRP). NASHERO, based in San Giovanni in Croce, Italy, says composites offer several advantages over the aluminum alloys typically used in small aircraft construction. They are lower in weight and resist better to corrosion, but at the same time have excellent fatigue strength and stiffness. Because manufacturers can mold them into sculpted shapes, composites also offer greater design flexibility and have the potential for better surfaces. With its lighter, stronger overall structure, the CFRP aircraft is able to accommodate a lighter engine and a larger payload and CFRP show excellent crash absorption properties. NASHERO selected a range of CFRP materials for the aircraft and developed an innovative vacuum infusion process to produce aircraft parts with the lowest possible void content in the structure [5].

Other examples of CFRPs in space application include: fairings, manipulator arms, antennae reflectors, solar array panels and optical platforms and benches. They have also recently been used

for primary structure applications. They combine stiffness and strength, they have an excellent thermal stability and they are very important for weight reduction.

3.2.2 Sports Equipment

The high-strength, high modulus (stiffness) and light-weight properties of carbon fiber have taken sporting goods to the next level of performance. Golf shafts, racquets, skis, snowboards, hockey sticks, fishing rods, bats, and bicycles have all been advanced through carbon fiber reinforcements and the opportunities to further improve sporting good applications are boundless. The reason for using carbon fiber for sporting good applications is not only its light-weight and durable properties, but also the freedom it provides when designing highly-specific applications. The precise feeling and shape of a piece of equipment, which is critical to its performance, are easily achieved when working with carbon fiber materials.
One of fields of application of CFPRs is cycling. The monocoque fibreglass by Bowden Spacelander is regarded as the first all composite mass production bike frame. Producing carbon fibre bike frames there is a drastic reduction in weights, when compared to aluminium alternatives. Carbon fibre is selected as it is light weight, corrosion resistant and strong. Additionally its anisotropic properties mean that it can be made stiffer in some directions to withstand peddling stresses, while simultaneously being more compliant in others for comfort. This is not achievable with traditional isotropic metallic components.
A graphite golf club shaft was invented by Frank Thomasin 1969. The lighter and more compliant composite shafts facilitated higher speed and torques, resulting in longer range shots. As a consequence of the larger torques, composite shafts have a tendency to have reduced accuracy, Figure 3.4.

Figure 3.4 CFPRs golf shafts

The deepest penetration of carbon fiber in the sports equipment can been seen also in tennis rackets. Players can hit faster ball with the lighter racket and control the ball better with larger area of the racket. The high, middle-grade tennis rackets in the world today are mostly made of carbon fiber composite materials. The carbon fiber used in tennis racket were introduced by United States Chemold in 1974. Carbon fiber composite materials have a good shock absorption performance and let a free design. Carbon fiber used in modern tennis racket compared with wood (Figure 3.5), used in the past, considering the same weight, can have a can's increased about 115 times and also the

tension of cable is increased by 20% ~ 45%. Vibration damping performance is outstanding and design has high degrees of freedom.

Figure 3.5 Comparison between wood (top) and CFRP (bottom) racket

CFPRs are also used in skiing and snowboarding. General skis have wood, metal and fiber composites (general glass fiber). Wood skis are light and cheap, but easily affected by damps. Aluminum alloy metal skis have higher price and lower adaptability to the snow. Fiber composites in skis is suitable for any types of snow and easy in maintenance. Skis are typically on the market performance of sandwich composite materials. The skis core material is made from wood or PU, PVC, etc, to allow elasticity; carbon fiber is located in the upper core layer, to strengthen the skis flexion degree while glass fiber is in between the core layer and carbon fibre plane as connection between the carbon panel and the core layer and increase the toughness.

3.2.3 Automotive

Carbon fiber has emerged as one of the promising options as automakers work hard to reduce vehicle weight to meet US corporate average fuel economy (CAFE) and European Union (EU) carbon dioxide (CO_2) gas emission requirements. As more carbon composites are used for automotive applications, the future of the composites industry looks bright [4].

In 2015, worldwide demand for carbon composite products in the automotive industry — roof panels, body frame, closure panels and more — reached a value of US$2.4 billion. The market is expected to grow to US$6.3 billion in 2021. This growth in global carbon composites will be due largely to strong demand for carbon fiber-reinforced plastics (CFRP) in luxury cars, race cars and other high-performance cars. To decrease CO_2 emissions, automotive brands are trying to make their vehicles lighter without compromising occupant safety. Due to this, they are looking into lightweight materials, such as advanced high-strength steel (AHSS, steel with tensile strength that exceeds 780 MPa), aluminum, magnesium and CFRP for their product design. Of all the material options, only CFRP offers the potential for weight savings greater than 50%. For that reason, this advanced material is receiving great attention. Currently, most major automakers, such as BMW,

Mercedes, Ford and GM, are focusing on incorporating CFRP in mass-volume cars as a means to meet the stringent government guidelines.

The 1981 McLaren MP4/1 was the first F1 car to be built with a carbon fibre monocoque. It improved not only rigidity and weight, but also its safety [4]. In 1988 Ferrari F40 (Figure 3.6) was the first car with a significant number of carbon fibre components. For example, passenger compartment was encased in carbon fibre panels which reduced its kerb weight significantly, while simultaneously increasing stiffness.

Figure 3.6 Ferrari F40

The ultra-expensive McLaren F1, introduced in 1992, became the first road car to have its monocoque built entirely from carbon fibre. The BMW i3 (Figure 2.4) was the first mass production car to have most of its internal structure made from carbon fibre. This weight shedding helps offset the heavy lithium-ion batteries, therefore increasing range and energy consumption [12].

Chapter 4

This chapter presents strong and weak points of CFRP composite, focusing in particular on delamination which is the phenomenon linked to fatigue. It describes steps that bring to material's damage and methods to increase the fracture toughness focusing on the addiction of steel fibres. Last paragraphs explain modes and types of fracture, analysing steps that bring to material's damage and failure.

4.1 CFRP properties and disadvantages

The implementation of Carbon Fibre Reinforced Plastics (CFRPs) has become commonplace in many high-end structural applications. These composite materials are selected and used for their properties like low weight, high strength, corrosion resistance and high stiffness. However, they have also some weak points such as: poor out-of-plane impact resistance, low fracture toughness and poor delamination resistance. They are susceptible in particular to impact damage from out of plane impacts which generate delamination.

Considering that composite laminates, they consist of layers of fibre reinforcement bonded by a thermoset polymer matrix, such as epoxy resin. The propagation of delamination is confined to the matrix material bonding them, following the path of least resistance. Indeed matrices are susceptible to delamination (or interlaminar fracture) because of their highly cross-linked structure that causes an inherently low fracture toughness and hence poor resistance to fracture because of the separation of plies. Delamination is perhaps the most common cause of failure in composite structures and the separation of the resin-rich interface between the layers of fibre reinforcement results in a significant decrease in stiffness and strength that contribute to the structural integrity of the material [13], and can ultimately result in structural collapse via fibre breakage or buckling. In comparison with other engineering materials, composites exhibit a very high strength to weight ratio, or specific strength, however in spite of the materials high effective elastic modulus in the fibre direction, its transverse shear modulus is significantly lower. Delamination of the material is caused mostly by transverse shear stresses, which are parabolic in magnitude through the thickness of a beam[14]. High interlaminar stresses are naturally likely to occur at sections in the structural design that require discontinuity of the composite material, such as cut-outs, holes, joints and ply-drops. The differences in Young's Moduli of the fibre and matrix is the cause for the high local stresses present at the interface of the two [15].

4.2 Increasing of fracture toughness

Many of the mechanical properties come from highly cross-linked nature of thermoset epoxy resins. The epoxy resins have good temperature resistance and low creep properties, but they are brittle, so it often causes the crack initiation and propagation in the resin-rich interlaminar region, producing a

component with low fracture toughness. To enhance fracture toughness, several techniques have been researched and developed.
Some solutions to this problem have been proposed, in particular working on the structure of the matrix to decrease the brittleness using rubber or thermoplastic particle inside epoxies, also the addiction of nanoparticles helps to increase the ductility of the matrix[16,17]. Extensive research has been performed on the epoxy toughening by adding different types of nanoparticles, such as silica particles [18,19], rubber particles [20,21], carbon nanotubes [22–24] graphene [25,26] and nano-clays[27–30], with great success achieved. However, the addition of nano-additives will considerably increase the viscosity of epoxy matrices and hence cause manufacturing difficulties and product defects of the FRPs.
Significant increases in delamination resistance and impact damage tolerance have been achieved by common through-thickness reinforcement techniques such as: 3D weaving, stitching and braiding [31] [32]. These techniques, studied by Dexter and Funk [33] are only suitable for dry fibre preforms and they can come at a high cost premium when compared to uni-directional laminates.
The use of Z-pins is another option. Z-pinning is a technique to insert reinforcing fibres along the Z-direction of continuous fibre-reinforced plastics (Figure 4.1). Z-pins act as fine nails that provide support in the direction normal to the plies through a combination of adhesion and friction, and is employed in some composite aircraft structures. The pins are usually constructed of titanium, steel or fibrous composite. Z-pinning has shown to largely improve composites interlaminar properties, showing increases in through thickness modulus as a large scale bridging zone is created. They typically have diameters in the range of 0.2-1.0 mm and only make up around 1 % vol of the composite. However, Z-pins can be responsible for some reductions in in-plane mechanical properties [34] [35].

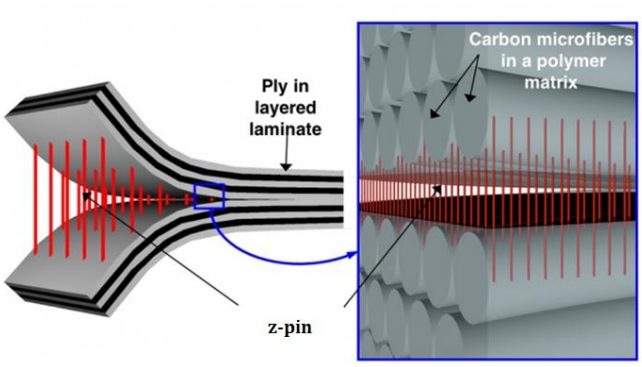

Figure 4.1 Z-pin structure

Another option to increase fracture resistance is surface treatments. Studies of the effects of surface treatment with Ar^+ irradiation and the more environmentally friendly oxygen plasma have observed an increase in interlaminar fracture toughness of a carbon/epoxy prepreg by 24% and 20% respectively [15]. Another solution is to pay attention on the design, Kim [36] suggested that the reinforcement of free edges is an effective way to prevent and/or delay initiation of delamination. His study has indicated that the reinforcement of edges of various delamination prone laminates by fiber glass cloth significantly delays or prevents the initiation of edge delamination.
Otherwise, the primary mechanism for the enhancement of interlaminar fracture toughness (ILFT)

is through the bridging of crack/micro-cracks. The compatibility of the interlayer with the matrix material has been shown to be particularly important. This may be assessed for any interlayer/matrix pairing by a combination of wettability, solubility and peel testing. For a given areal density, smaller diameter fibres have been shown to provide a greater increase in mode I ILFT. This has been attributed to the increased coverage that they provide [37] [38] [39]. Smaller diameter fibres have also been observed to support a more stable crack propagation [40].

Introducing interlayer materials at the mid-plane of FRPs is another route to achieve FRP enhancement. The interlayer is usually applied in one of three forms: particle, film or polymer nano-fibre. The compatibility of the interlayer with the matrix material has been shown to be particularly important. The addition of a ductile thermoplastic material to the inter-laminar region can significantly enhance the fracture toughness of the composite. Materials with high tensile strengths and large percentage-elongation-to-break values tend to work well as interlayers, provided they are suitably inserted to be effective at absorbing energy during fracture. [37] [39] [41]
Recently the blending of a small quantity (0.5 wt%) of multi-walled carbon nanotubes (MWCNTs) into the CFRP laminate has been shown to deliver a substantial increase in toughness. Samples were tested in mode I (DCB test) and an addiction of 0.5% of carbon nanotubes increased the energy for the crack propagation of 25%. [42]

Based on the literature review, it is generally accepted that fibre bridging is one of the main toughening mechanisms for fibre interleaved FRPs. Previous work, as explained in chapter 8, exploits outstanding advantage of stainless steel fibres for introducing significant fibre bridging in the fracture process of CFRPs. It has been demonstrated that the addition of stainless steel fibre could significantly enhance G_{IC}. This is the reason why in this thesis it is investigated how to increase the material's fracture toughness and increase the energy necessary to let the crack grow in the material adding steel fibers in CFRPs. Next paragraph resumes previous studies done using steel fibers in a composite.

4.2.1 Fibrous metallic interlayers: stainless steel filaments

Few works have yet been carried out to investigate the efficacy of fibrous metallic interlayer at enhancing CFRPs. Thin metallic fibres show potential as they possess high ductility and high stiffness. However, the weight additions of only a thin layer of metallic fibres can significantly impact the light-weight attribute of the composite.
During last years a big interest has been developed on how stainless steel fibres can reinforce polymer composites and this steel filaments have a high stiffness of 193 GPa and a high strain-to-fail of approximately 20%. Heat treatment also allows to maintain the ductility of the fibres without altering the stiffness. One of the work done in this subject was by Callens et al., their research compared the increasing of resistance with steel fibers in a brittle and ductile matrix. The diameters of the steel filaments they used in the CFRPs, were 30 microns or less. The strain-to-failure (STF) of a composite made from these fibres was 3-4 times that of a CFRP material. However, it was noted that even a ductile matrix material was not sufficient on its own to fully facilitate the 20% STF of the stainless steel fibres.. The mechanism of failure is proposed was first a debonding

between fibre and matrix, strain magnification and then necking at local weak point (Figure 4.2) [43][44][45].

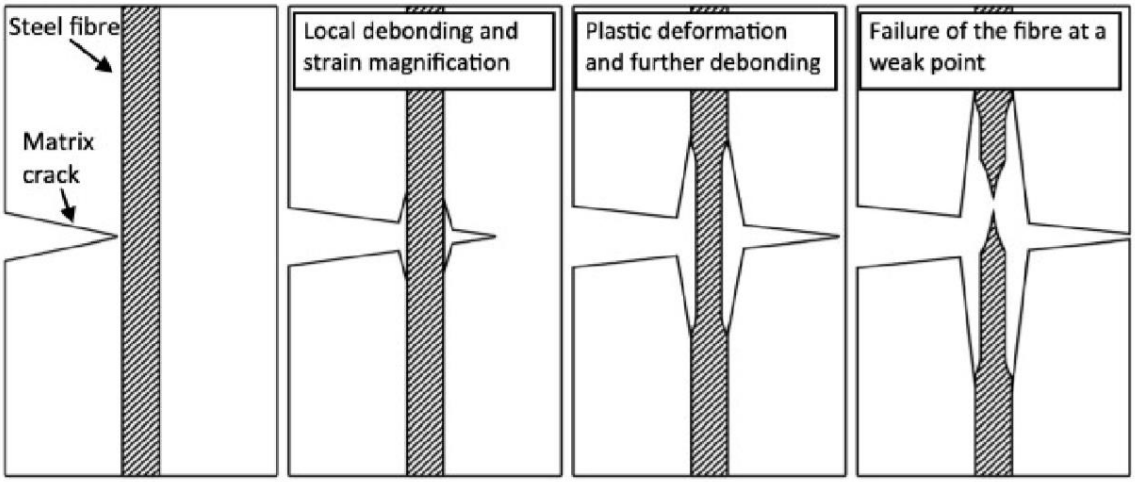

Figure 4.2 Proposed failure mechanism of ductile steel fibres in a brittle matrix

Subsequent work looked at addressing this issue by enhancing the adhesion at the fibre-resin interface. By hindering the development of micro-cracks, enhanced adhesion has resulted in a higher strength composite with a higher strain-to-failure. However, an optimal level of adhesion must be found as excessive levels can result in the localisation and magnification of strain, causing premature failure of the fibres.

Another work was done by Swolf et al. They proposed the hybridization of self-reinforced polypropylene (SRPP) with steel fibres producing a hybrid composite with two ductile materials. They observed that thank to steel filaments stiffness and strength increased by a factor of 5 and 3 respectively and also the impact resistance increased without altering the specific modulus of the material. [46]

Callens, Verpoest et al. studied how the distribution of steel fibres in the epoxy resin could influence the behaviour of the material. They proposed a higher amount of fibres concentration (Q-UD) and a more homogeneous distribution (P-UD). They concluded that in both cases fibres enhanced stiffness and strain-to-failure but the presence of tightly packed bundles (Q-UD) increase the failure strain because it delays the necking that is the cause of failure. [45] The mechanism of fracture for (Q-UD) and a (P-UD) is shown in Figure 4.3. High fibre packing in bundles (Q-UD) increases the strength of 0° layers. By causing the crack to initially grow in the resin rich region around the bundles, fibre debonding and necking is postponed. Additionally, for closely bundled fibres, once necking begins, the stressfield experienced by the neighbouring fibres is positively affected, increasing the measured strength of the overall composite.

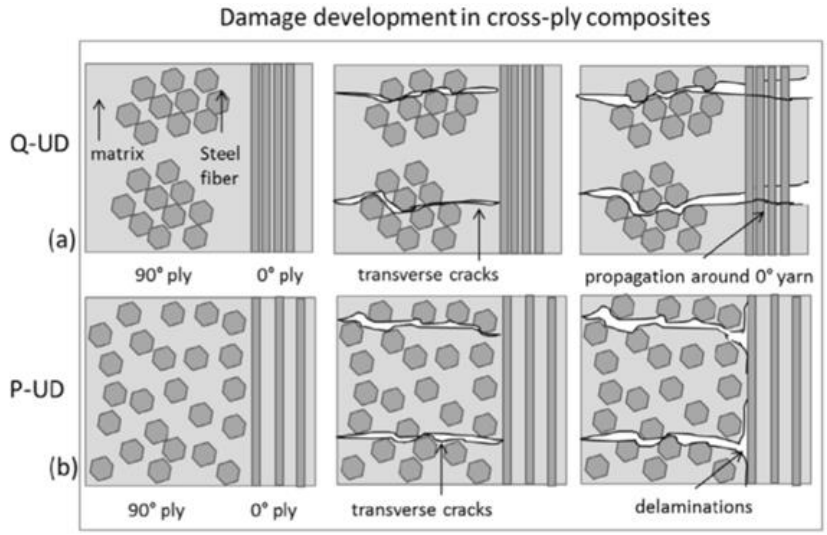

Figure 4.3 Q-UD and P-UD mechanism of fracture

Published work was also carried out by Callens who looked at the effect of fibre architecture on the tensile and impact behaviour of stainless steel fibre reinforced polypropylene composites. The 3 architectures that were investigated were (Figure 4.4): a quasi-unidirectional weave, a basket weave and a satin weave. The STF was shown to be independent of the crimp. However, the high-crimp basket weave expectedly had the lowest stiffness and yield stress. This arrangement had significant out-of-plane deformation during tensile loading; this was facilitated by the polypropylene matrix's low stiffness and yield stress. Impact testing produced positive results when compared to other composites. After accounting for density, the specific absorbed energy of the stainless steel reinforced polymer was equal to that of glass fibre reinforced polymers (GFRPs) and greater that than of CFRP [47].

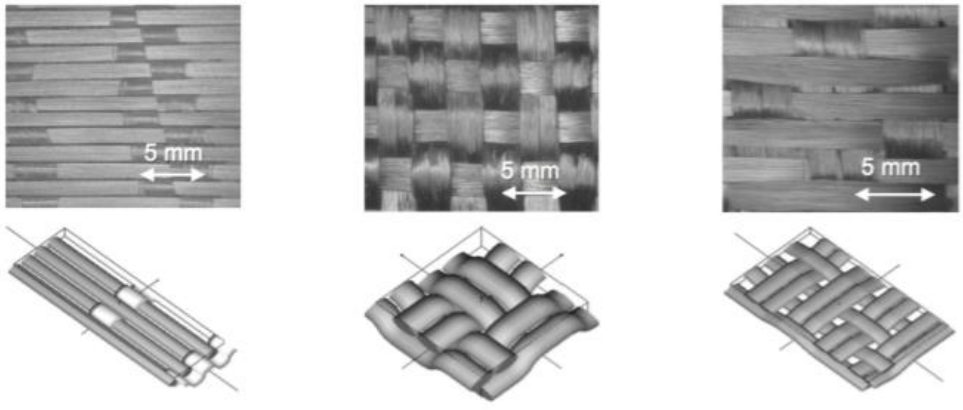

Figure 4.4 Different disposition of steel fibre inside the matrix: quasi unidirectional weave, basket weave and satin weave

4.3 Modes of Fracture

There are three pure modes of loading, which are as follows (Figure 4.5):

- Mode I - Opening

- Mode II - In-Plane Shear

- Mode III - Out-of-Plane Shear

Testing is usually carried out solely in one of the three pure modes of loading, however, in practice fracture usually takes place in a combination of these loading modes. This thesis carries out testing in mode-I.

The three main types of fracture are ductile fracture, brittle fracture and stick-slip fracture. They are best characterised by load-displacement curves.
Ductile fracture is represented on the load-displacement curve by a large increase in displacement with a small drop off in load, represented by figure 4.6a. This corresponds to a ductile material undergoing large amounts of strain and plastic deformation as the crack propagates. Whereas, brittle fracture is represented on the load-displacement curve by a small amount of displacement relative to a large sudden drop off in load, represented by figure 4.6b. Corresponding to a brittle material which undergoes little strain and plastic deformation as the crack propagates. Stable crack growth occurs for both ductile and brittle fracture types. Meaning that the crack grows continuously as the displacement is increased.

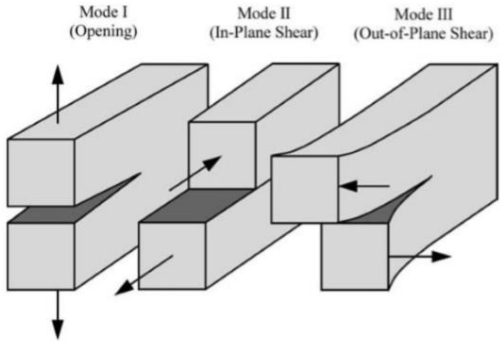

Figure 4.5 Three pure modes of loading

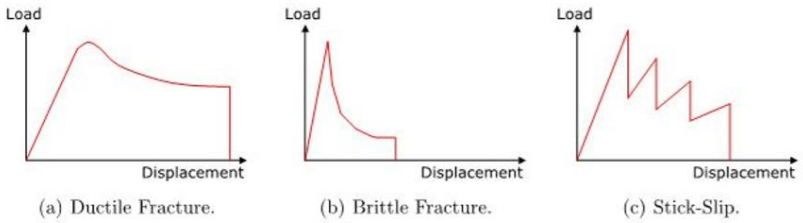

(a) Ductile Fracture. (b) Brittle Fracture. (c) Stick-Slip.

Figure 4.6 Examples of load-displacement curves for different fracture types

Stick-slip fracture is represented on the load-displacement curve by a saw tooth appearance, represented by figure 4.6c. This fracture type has an unstable crack propagation and is not ideal to carrying out quasi-static testing on due to the dynamic nature of the sudden ”slip” or crack propagation. The only fracture toughness information that can be gathered from a stick-slip fracture is the initiation and arrest values of each saw tooth [48].

4.4 Damage of composite material

Composites have high mechanical performances and good fatigue durability so they offer definite advantages compared to more traditional materials. However, mechanisms involved when they are tested are complex and the variability of the mechanical properties due to anisotropy, heterogeneity and defects (due to materials but also processing technologies) have to be considered. [49] The inhomogeneity of the microstructure provides numerous paths in which loads can be redistributed around the damage region. Thus the ability to predict the strength of high performance composite materials under complex loading conditions is required for design with such materials. Because composite materials are frequently used in structures subjected to dynamic loads it is also important to fully understand their response to cyclic loads.
Due to the inhomogeneity of the microstructure of composites, the integrity and response of the composite are affected more by the effective accumulated sub-critical damage than by any single damage event. For laminated composites this subcritical damage takes the form of matrix cracks: delamination, debonding, and fiber fractures. [17]

In recent years many researchers tried to the investigate the damage in composite material but they have not reach a conclusion because they could not understand the individual details that combine to form the damage state which controls the fracture of composites.
In 1987 Allen and Harris studied the evolution of matrix cracking in cross-ply laminates subjected to fatigue loading condition. They found that the stress distribution behaviour is dependent on the load amplitude. They also reported the existence of other types of damage such as delamination that alter the redistribution of stress along the plies [50]. Adams et al. studied damage in reinforced plastics and reported that damage in specimens fabricated from reinforced plastics could be detected by a reduction in stiffness and an increase in damping [51]. Manivasagam et al. studied the characterisation of damage progression in composites using the fundamental frequency degradation of layered composite materials with damage progression [52].

In service, failure of parts results from a combination of concomitant factors which degrades the local characteristics of the material and fatigue can be one of these factors. Carbon composite materials are known to have excellent mechanical performances under cyclic loading but under certain loading conditions, fatigue can occur and leads to the catastrophic in-service failure of structures. The main factors that could cause fatigue fractures of composite part or structure are numerous:

- Environment: temperature, contact with chemicals, humidity (influence on mechanical properties mainly at low number of cycles)

- Inadequate or faulty design: over-estimation of the strength of the material, underestimation of actual stress,

- Type of stress: especially compression and shear,

- Presence of manufacturing defects.

To understand the cause of failure, it is essential to identify and quantify all of these influential factors and assess their interactions.
The damage in composite materials is linked to a large number of microscopic events that will develop very gradually over a large volume of the material. This is due to the heterogeneity of the material on a microscopic scale, as the matrix and reinforcement have different mechanical behaviors. In composites, in term of damage, the damage appears not only on the surface but also in the bulk material and so its type depends on the anisotropy of the material and not only on the loading. Also viscosity and ductility of matrix may be influent parameters in fatigue and other parameters such as the fibre nature, their length, size and the type of draping may also play an important role in the anisotropy of the material and may confer to the material different properties. Comparing composite with metals, it has been seen that the notch effect is less sensible for composite than for metallic materials. In compression, cyclic loadings generate important damage with a decrease of 30% in fatigue strength for composite in comparison with metal. In the composite, more than 50% of damage occurs in the first 20% of life which means that a structure or a component can live in its environment with the presence of cracks. In metal, crack initiation (damage) occurs generally after more than 75% of fatigue life. [49] (Figure 4.7)

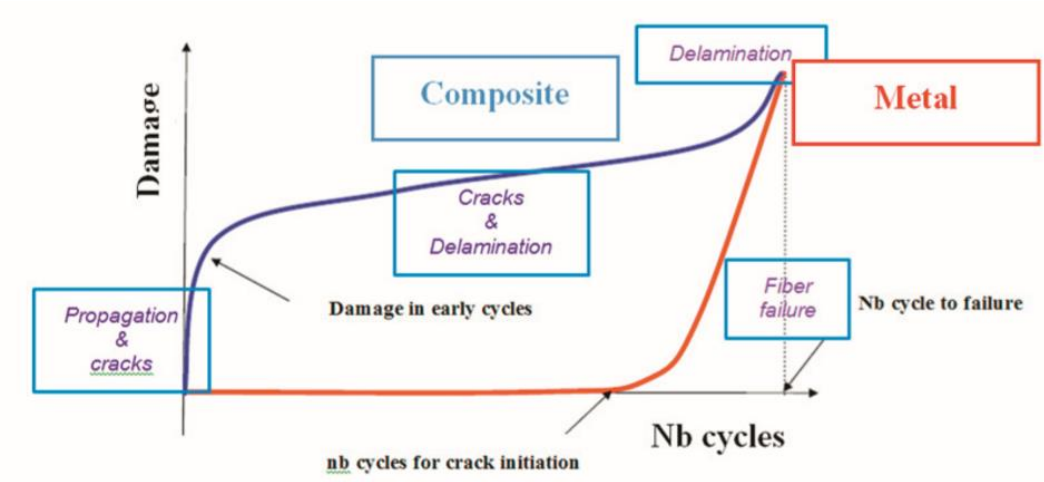

Figure 4.7 Comparison between composites and metals fatigue behaviour

4.5 Steps of damaging

The damage process described below depends on the type and direction of the reinforcement and the mechanical stresses applied. However, the damage process happens in two stages: the first damage occurring requires low energy consumption (interface or matrix failure), while the second stage (fiber breakage) require more significant energy level.

The first step of damage begins in zones of lower strength such as the matrix fibre interfaces and the matrix itself, with failure over small distances. The first one are called interlaminar cracks (see Figure 4.8a), while the second are called intralaminar cracks. Intralaminar damages mainly appear in the areas where fibres are not oriented in the axis of the load, so the strain in the matrix reaches its breaking strain. In general intralaminar cracks are parallel and regularly spaced. In the case of a laminated composite, in addition to the intralaminar damage, there is also another damage called delamination (see Figure 4.8b). When cracks develop in a ply, the propagation is stopped by the adjacent plies. At the intralaminar crack tip, the singularities of stress make the cracks propagate at the interface between two adjacent plies layers. In the case of a laminated composite with different directions plies, delamination can also initiate because of differences of stiffness of the different plies forming the laminate or it may develop during manufacture due to incomplete curing or may result from the interlminar stresses created by impact. Delamination may grow under cyclic loading and this growth redistributes the stresses in the plies of the laminate, and may influence residual stiffness, strength and fatigue life.

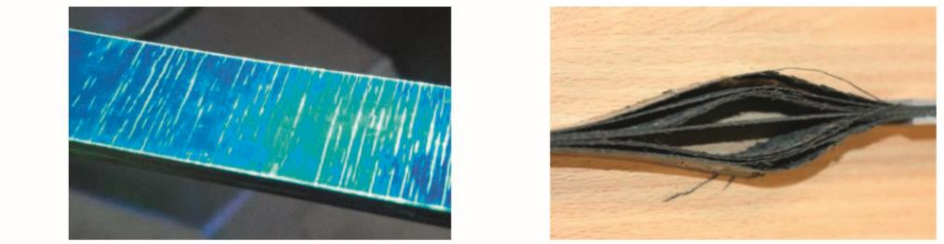

Figure 4.8. (**a)** (left) Penetrant inspection showing a large density of interlaminar cracks; (**b)** (right) delamination during tensile test due to the differences of stiffness

Analysing the causes of delamination it is possible to see that it may result from interlaminar stresses created by impact, eccentricities in structural load paths or from discontinuities in the structure. Besides mechanical loads, also moisture and temperature may cause interlaminar stresses in a laminate. The phenomenon occurs in particular near free edges were stress is intensified or it can be caused by an impact. The hit generates highly localised deformation gradients which cause large transverse shear and normal stresses that can cause the damage to propagate and eventually failure of the laminate. This amount and type of damage in the laminate depends upon the size, type and geometry of the laminate, impact energy and the loading at the time of impact. Another cause of delamination development in a laminate is the matrix cracking in off-axis plies. These interlaminar stresses frequently cause local delamination which grow along ply interface near matrix cracks. [17]

Finally, when the volume ratio of the matrix damage reaches a certain level, the final stage of damage corresponds to the failure of the fibres, called translaminar failure. This type of damage is mainly involved in the final stages of ruin in areas where fiber orientation more or less coincides with the axis of stress. This is usually the case in the high stress-applying region of the parts. The SEM observations in Figure 4.9 sum up the 3 main failure modes: (a) interlaminar failure; (b) intralaminar failure;(c) translaminar failure.

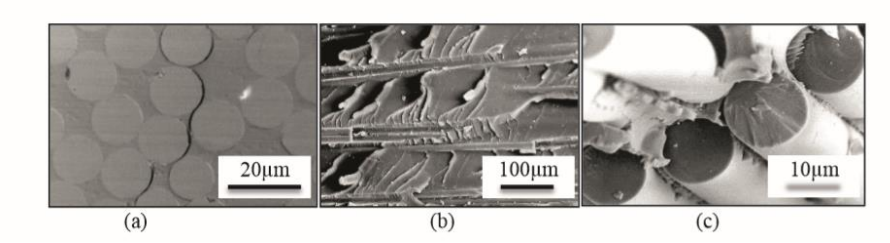

Figure 4.9 Modes of failure

The matrix damage (intra and interlaminar failures) in mode I (opening mode) grows by forming characteristic events like rivers or other events (see Figure 4.10).

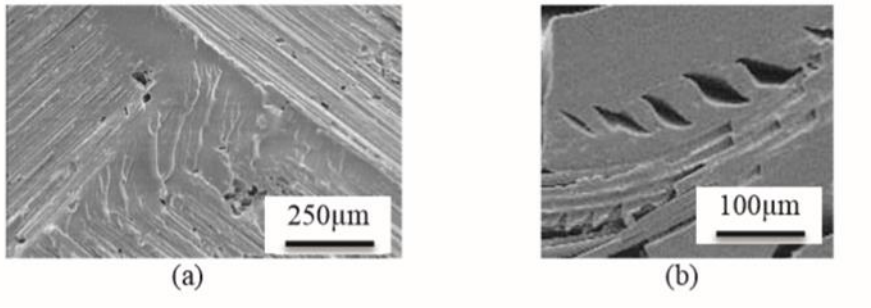

Figure 4.10 (**a)** Rivers; (**b)** Formation of cups

At macroscopic scale, the type and the order of occurrence of the mechanisms of damage resulting from monotonic or fatigue loadings are fairly similar. The greater damage differences are observable at microscopic level (striations, rollers, etc.). Most of the time, in service, fatigue failure shows unusually large and smooth translaminar failures (in comparison with static failure). As mentioned previously, the two first steps of damage are fracture of fibre/matrix interfaces and then fracture inside the matrix. These two types of fracture can present fatigue striations that are often much localized and can be difficult to find. Under cyclic tensile stress, fibers in particular with different orientations sometimes break in a single plan and show smooth and flat individual facture. This feature is never observed in case of static loading. Figure 4.11 shows the process of fatigue fibers breakage.

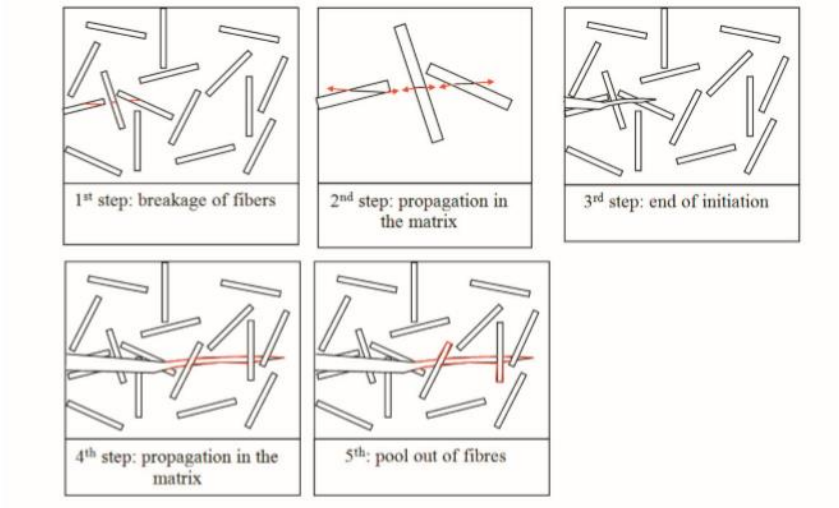

Figure 4.11 Steps of fatigue initiation

Resuming, the damage development is always driven by the same process: the first damage occurring requires low energy consumption (rupture interface or matrix), while the last stages (fibre breakage) requires more energy to appear. The greater damage differences are observable only at microscopic level and most of the time, in service, fatigue failure shows unusually large and smooth translaminar failures (in comparison with static failure) [49].

Chapter 5

This chapter argues the manufacturing of the material used during the experiments. It will be described which type of resin and fibres are used and all the steps necessary to get the final composite material. The samples were manufactured at UCD and, after obtaining a sheet of composite, the samples were cut with proper dimensions in order to follow fatigue test standards.

5.1 Materials

5.1.1 Carbon Fibres

Dry carbon fibres (Figure 5.1) used as the reinforcement phase in the composite were biaxial non-crimp fabric (Toray T700Sc 50C) in a 0/90° or +45/-45° form provided by Saertex GmbH, (Germany). Both ±45◦ and 0/90◦ non-crimp sheets of carbon fibre were used to reduce the anisotropy of the specimens.

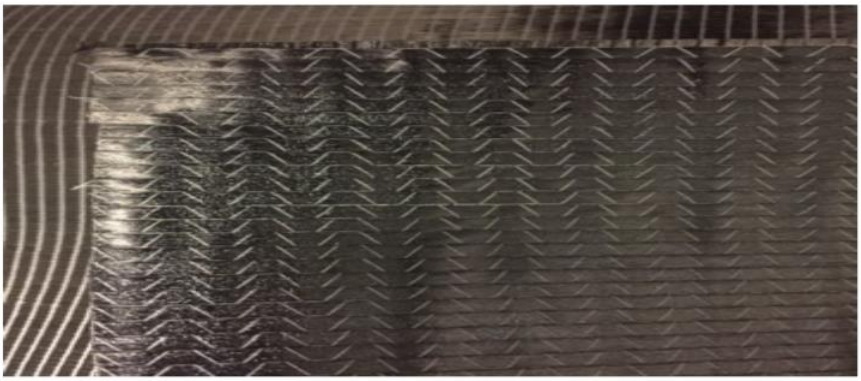

Figure 5.1 Dry carbon fibres 0/90°

5.1.2 Resin

Aerospace grade epoxy resin was used as the matrix phase of the composite. The Cytec Cycom 890 one part liquid resin was supplied by Bombarider Aerospace. Its commercial name is CYCOM 890 RTMs and its viscosity is low enough at 80°C (250 cps) to allow injection without excessive heating of either the resin or the transfer pipework. When the resin is heated to cure temperature its viscosity is further reduced, helping to ensure full wet-out of the reinforcing fibres. The resin is fully cured after two hours at 180°C. It is compatible with the range of reinforcing fibres used in manufacturing composite components, i.e., carbon, glass, aramid, etc.

5.2 Interlayers

5.2.1 Interlayer Type One: Thin Carbon Fibre Veil

The thin non-woven carbon fibre veil was supplied by Fibre Glast Developments Corporation. It has the form of a thin ply of continuous strand fibres that are looped randomly throughout the material and it is similar to that of tissue paper. A light polyester binder is used to hold the veil together. The veil has a low areal density of 6.8g/m^2, with an average thickness of 0.053 mm. The veil was carefully manufactured to ensure that the tensile strength was equal in both the longitudinal direction also called machine direction (MD) and cross direction (CD), with a value of 5.17- 36.19 kPa. The elongation to failure in both the MD and CD ranges from 0.2-1.8%. It is compatible with all common resin types: Vinyl Ester, Polyester and Epoxy. One interlayer placed between the central two plies increases the overall weight of the specimens by approximately 0.1%. Therefore placing a veil in every interlaminar region in the component would result in a 0.7% increase in mass.

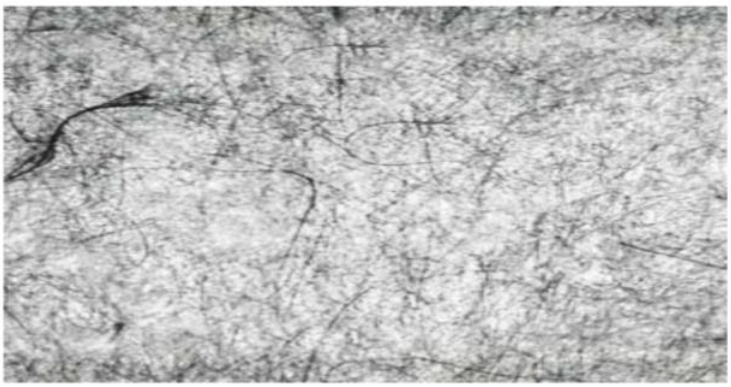

Figure 5.2 Thin carbon fibre interlayer veil

5.2.2 Interlayer Type Two: Stainless Steel Filaments

The 22 micron diameter stainless steel filaments, used in the composite, were supplied by Bekaert (Belgium). Stainless steel has a percentage-elongation-to-break of over 50%, a stiffness of 193GPa and a strain to failure of 20% and this makes it a promising interlayer material. The material was provided in bundles of 4000 filaments which were spread out by hand to deliver the required areal densities (Figure 5.3). The addition of steel fibres increase the weight, for example one interleaved region, comprising of 4,000 such filaments every 25 mm, would increase the mass of a specimen by approximately 7.5%. Therefore if an interlayer was to be inserted into each of the 7 interlaminar regions in a component, a substantial 52% weight increase would be incurred.

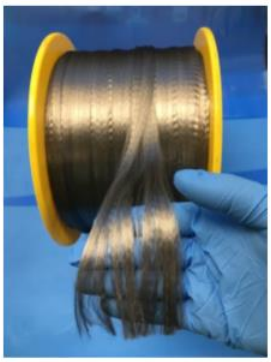

Figure 5.3 Stainless steel bundle

5.3 Manufacturing

5.3.1 Pre-Curing Steps

The number of required test specimens from each given manufactured panel dictates its size. Allowances of 20 mm along each edge of the panel and several millimeters for each cut were also factored in. Once the required size was determined the carbon fibre and additional materials required for the process were cut. Four sheets each of both the ±45◦ and 0/90◦ non-crimp carbon fibre were required for each panel. The epoxy resin required was weighed out to be one-half of the mass of the dry fibres. As the holes in the aluminum base and the copper tubing connecting the inner vacuum area to the pump become clogged with cured resin, they must be respectively re-drilled and replaced after each use.

5.3.1.1 Laying-up of the control panel

An important phase of the pre-curing step is the laying-up of the control panel. The lay-up procedure for the control panel consists of:

- Cleaning the aluminium base plate and then applying a layer of agent.
- Application of a protective PTFE film on the plate, as seen in Figure 5.4. PTFE is impregnable to the epoxy resin, therefore prevents the curing on the base plate so it is possible to easily remove it. The film had the same area as the carbon fibre fabrics.

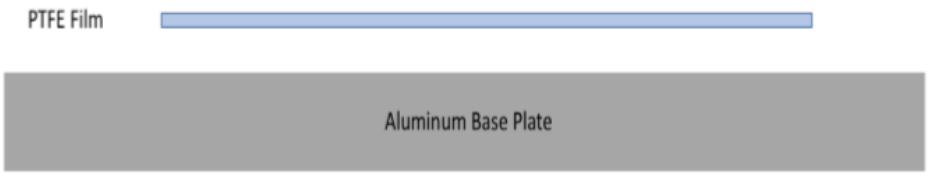

Figure 5.4 Laying down PTFE film on aluminum base plate.

- After, as in Figure 5.5, a sheet of 234HP Release Ease was then placed on top of the PTFE film. This layer was partially permeated by the resin, resulting in a more visually pleasing and dimensionally accurate surface upon removal post-curing.

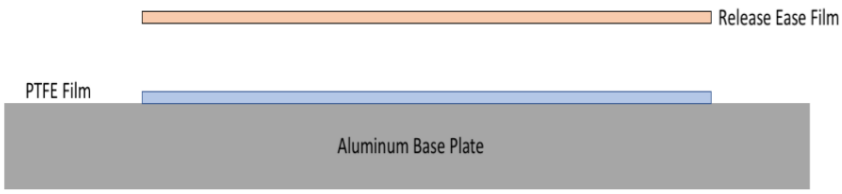

Figure 5.5 Semi-permeable release-ease film was added.

- Then layers of carbon fibre were added as illustrated in Figure 5.6. The orientation of the carbon fibre fabric sheets was determined by the requirement that the fibres at the centre of the specimens are aligned with the direction of the crack growth. Additionally, the fabric has one glossy side and one matt side and they must be layered glossy-to-matt.

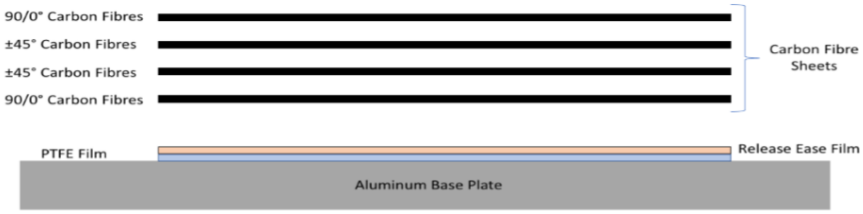

Figure 5.6 The first half of the carbon fibre sheets were added.

- The thin PTFE crack-starter films were added next, as shown in Figure 5.7. PTFE, as explained before, is impregnable to the resin so the laminates in each side of the crack-starter will not cure with fibres sheets. The presence of the film ensured that the crack would start in the central inter-laminar zone. These films also determined the precise location of the origin of the crack. The film was positioned so that it covered the first 57.5 mm of each sample as in Figure 5.8. A clean cut on the leading edge of the film is important and it had to be insured that this edge is precisely transverse across the sample. The accuracy of the positioning of the crack-starter can be aided by sticking it in place with small drops of the resin.

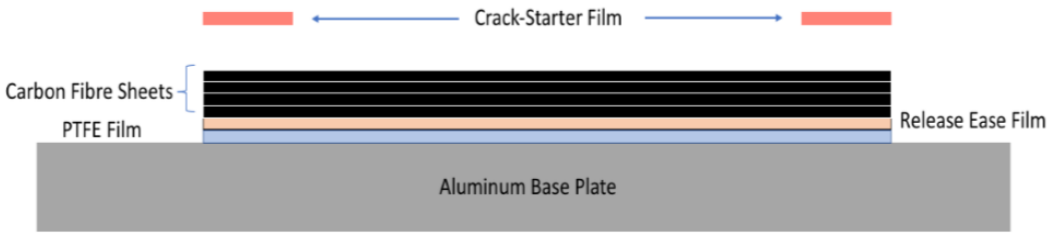

Figure 5.7 The crack-starter film placed on carbon fibres sheets

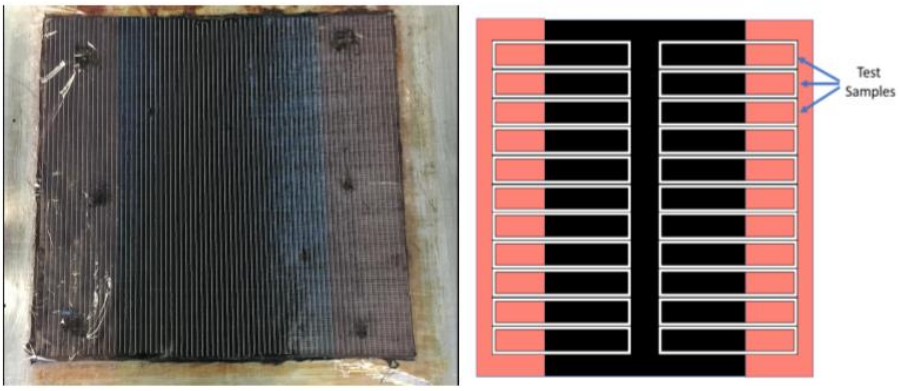

Figure 5.8 Positioning of the crack-starter. On the left, PTFE crack-starter film is held in place by drops of resin. On the right, illustrative explanation of the layout of samples within a panel where the pink section is the PTFE layer.

- The remaining carbon fibre fabric sheets were added on the top. These were ordered using the same principles as the bottom carbon fibre sheets, resulting in a layup that is symmetrical about the centre plane as shown in Figure 5.9.

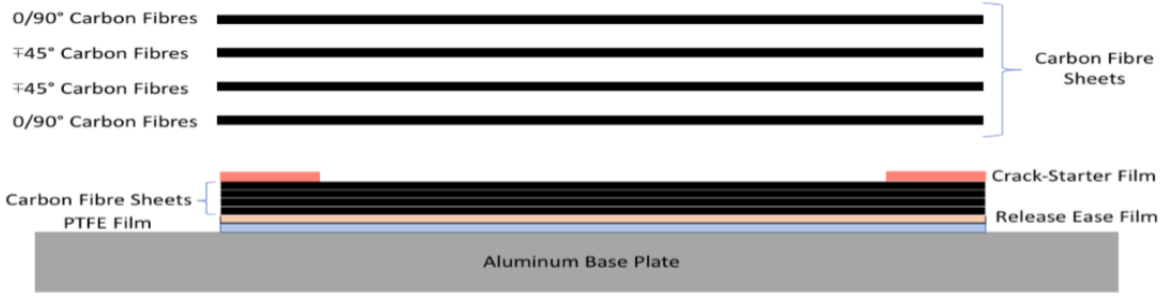

Figure 5.9 Second half of the carbon fibre sheets insertion

- Then, another layer of release-ease was applied. This served the same purpose as the bottom release-ease layer. A layer of distribution mesh was placed immediately on top of the release ease, as shown in Figure 5.10. The purpose of this layer was to ensure that the surrounding bagging film could not be sucked flat on to the layup beneath. Consequently the resin was better able to travel along the top of the layup and therefore more thoroughly and homogeneously wet all of the fibres. Small cuttings of mesh were also placed over the vacuum holes, ensuring that the bag was not sucked down, blocking them entirely.

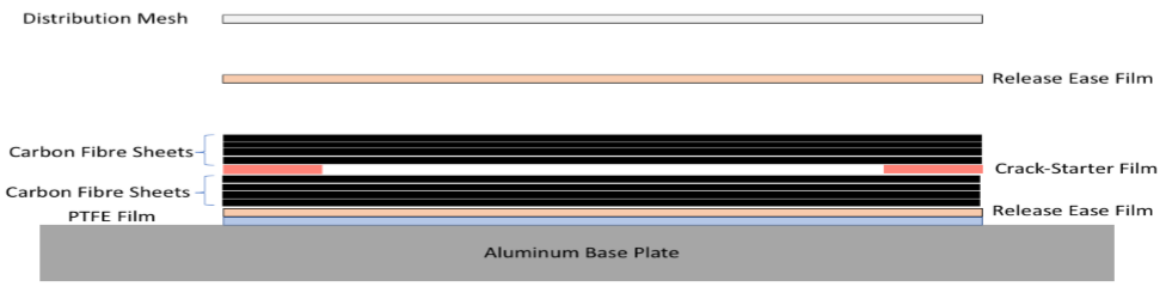

Figure 5.10 Insertion of the second release ease film was placed down and distribution mesh

- After the second release ease film, resin and top PTFE film were added as in Figure 5.11. The resin at room temperature was weighed out to be half the weight of the dry fibres. At 20°C, the curing takes 10 days, and any degradation in the resin due to partial curing can be detrimental to the final composite. Additionally, it was necessary to minimize the contact that the resin had with the air as air bubbles containing steam are to be avoided in the resin.
  The resin was placed on the top PTFE film so that when the film was put in place the resin would be off centre and to the opposite side of the vacuum holes (Figure 5.12). This ensured a better wetting of the fibres.

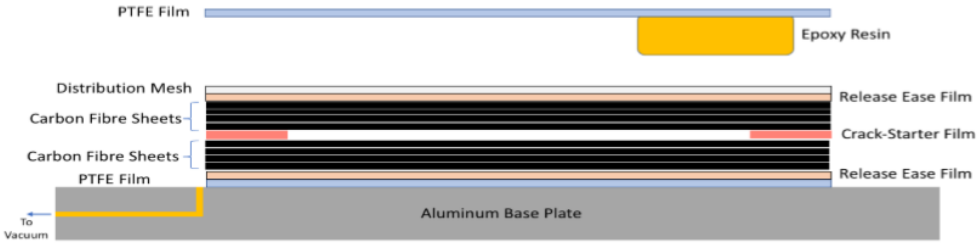

Figure 5.11 Addiction of the epoxy resin and upper sheet of PTFE film.

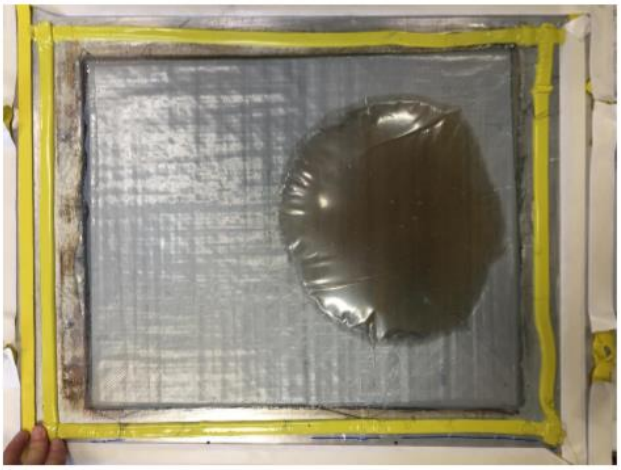

Figure 5.12 Positioning of the epoxy resin on the opposite side of the layup

- The inner vacuum bagging film was added next, as in Figure 5.13. A layer of malleable tape was applied around the perimeter of the layup. The vacuum holes were included inside the tape. The bagging film was then placed down and secured on the tape. It facilitated the vacuum diffusion and the spread of the resin through the fibres. The vacuum was temporary applied to check the eventually presence of air leaks which had to be resolved before any further layers addiction. In case of leaks the bagging film was pushed onto the tape and the corners were smoothed out where the tape overlapped.

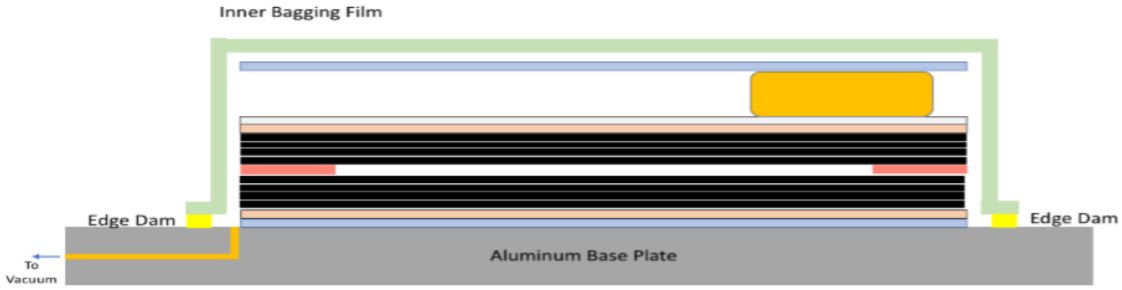

Figure 5.13 Inner bagging insertion

- A layer of breathing fabric was applied next, as shown in Figure 5.14. This layer ensured that the outer bagging film would not be sucked down onto the inner bagging film. The consequence of that would be a failure of the outer vacuum to be applied uniformly over the whole area of the layup, producing a panel with poor geometrical accuracy. Cuttings of the fabric were also placed over the hole connecting the outer vacuum pump, ensuring that the bag would not be sucked down and block the holes.

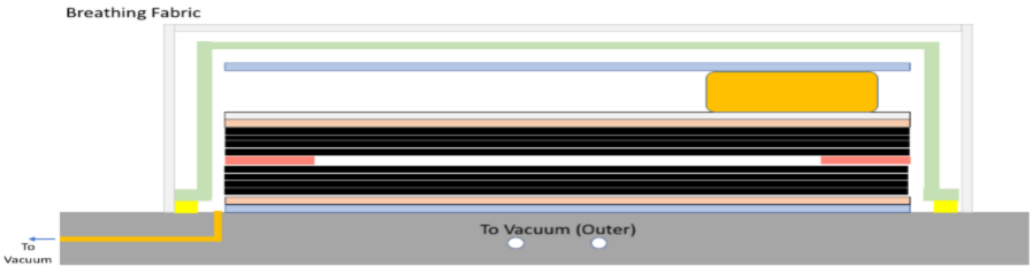

Figure 5.14 Application of the breathing fabric

- The outer vacuum bag was secured with sealant tape in the same way as the inner bagging film was with the edge dam. Similarly, the holes shown in Figure 5.15 must be connected to the outer vacuum pump and must be included in the bagged region. This vacuum bag was also checked for leaks.

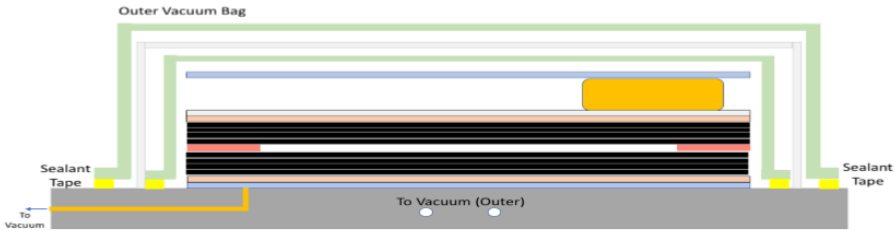

Figure 5.15 Outer vacuum bag positioning

- Sealant tape is then placed around the perimeter of the aluminium base. As seen in Figure 5.16, it was carefully ensured that the area around the pinholes would be properly sealed. An aluminium lid was then placed on top, and after the alignment of holes and pin, it was pressed down. A positive pressure of 5 bar was applied during the curing process through the aluminium lid in addition to the pressure applied by the two vacuum bags.

Figure 5.16 Sealant tape application

5.3.1.2 Interlayer Materials

We can find two interlayer materials in the composite:

- **Interlayer Material One: Carbon Fibre Veil.** The carbon fibre veil was added immediately after the crack-starter layer in the lay-up. This interlayer is in veil form so it didn't required a big preparation. The most important thing was to ensure that the veil was kept free of dampness, so it was necessary to handle it carefully to avoid damage.
- **Interlayer Material Two: Stainless Steel Filaments.** Four variants of this interlayer type were inserted among carbon fibres. Two sets of samples had the filaments laid out in the same direction as the crack would be propagating and they are called longitudinal samples (Figure 5.17a). The other two sets of samples had the fibres laid out with the filaments in the interlayer orientated perpendicularly to the direction in which the crack would grow. These samples are called the transverse samples (Figure 5.17b). Samples were produced for both of these orientations with two different areal concentrations of the fibres so their densities for

both types changed and the samples tested had respectively 4000 steel fibres every 12,5mm and 50mm.

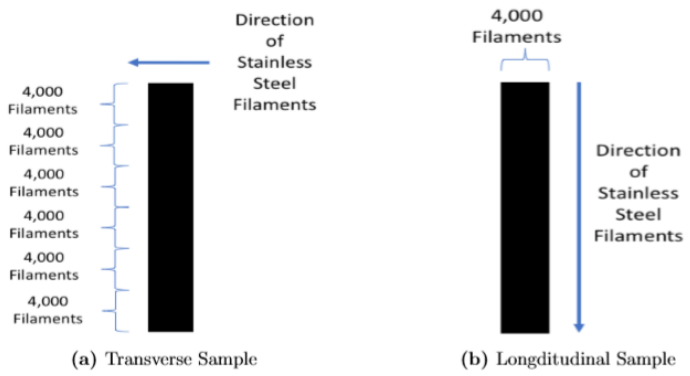

Figure 5.17 steel fibres disposition (a) transversal, (b) longitudinal

As this interlayer material came in the form of bundles of filaments, more work was required to ensure that they were evenly spread out over the area of the panel, and that they did not move as subsequent layers were put down. This was important to achieve a relatively consistent fibre density in the area closed to the propagation of crack tip. The fibres were heated in an oven to a low temperature in order to remove unwanted moisture.

5.3.2 Curing of the composite

The curing of the composite was done under considered conditions of pressure and temperature. The samples were manufactured in a bespoke press-clave. Hydraulic rams ensured that the lid remained firmly pressed down and the positive pressure was maintained inside. A system of 4 thermocouples maintained the selected temperature for all duration. The aluminium box was inserted into the press-clave and after the vacuum and positive pressure tubes were connected. The 4 thermocouples were then inserted into the back of the aluminium box and correct program was input. The process consisted on 2 hours of heating up to 180°C and then maintaining that temperature for an additional 2 hours.
The press was then closed and set to apply 500 kg to the aluminium box which contained the layup. The inner vacuum was then turned on and the temperature cycle was started. After approximately 40 minutes the temperature was risen to 80°C and the resin could be seen to flow out. As soon as the resin was seen to emerge, the line was clamped and the inner pump was turned off. The outer vacuum pump was immediately turned on and the positive pressure was set to 2.5 bar.
This resulted in some additional resin being pushed out to the tubing. Once the resin had stopped flowing the pressure was increased to 5 bar. It was important to clamp the tubing in the same location for each panel as this dictated the amount of resin extruded and therefore had an effect on the panel thickness.

The curing process only required occasional checks over the next few hours. After approximately 7 hours the temperature of the system had dropped below 100°C and the system press, pumps and pressure reservoir could be shut-off or disconnected.

Figure 5.18 Resin extrusion in the vacuum tube

5.3.3 Post curing step

The following morning, the composite was removed from the press-clave, having been left to cool overnight. The aluminium lid was then removed to reveal the cured composite (Figure 5.19).

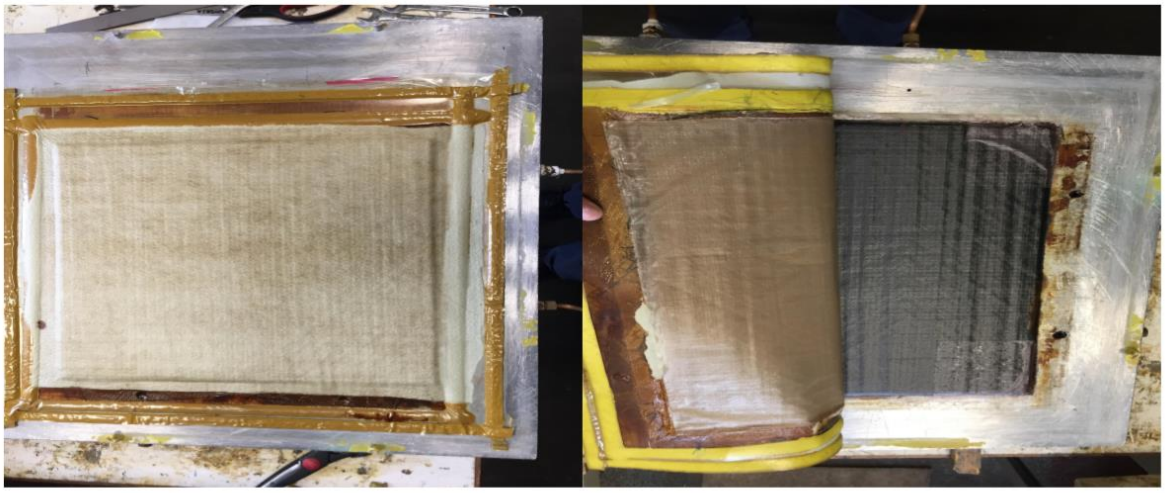

(a) Compsite after lid removed. (b) Peeling away additional layers.

Figure 5.19 Composite material removal after press-clave

The composite panel was then marked up in order to be cut into standard specimens. The folded over PTFE was used to determine the beginning of the crack-starter and the other measurements were based on this. The standard size for DCB tests is 150 mm X 20 mm, with crack-starter in the first 57.5 mm of the sample.
Once the panel was marked up it was cut into samples using an enclosed circular saw. Carbon fibre composite is a very brittle material and has a tendency to create a substantial quantity of very fine dust particles when cut.

Chapter 6

This chapter describes the way of testing samples and mode I fatigue delamination propagation in reinforced materials. Composite materials often fail by delamination and this behaviour needs to be fully characterized. It can be used a test method to characterise the delamination growth under mode I fatigue loads and it is useful to do a short test whose duration is below 24 hours to allow its application in an industrial environment. Thus this test method allows to get results within reasonable time (test duration of almost 7h per specimen). In this chapter, test methods and standard procedures for DCB fatigue testing are outlined referring to the International Standards Organisation (ISO) and the International Association for Testing Materials (ASTM) [1, 53]. It is also reported the European Structural Integrity Society (ESIS) protocols developed for mode-I DCB fatigue testing.

6.1 Test specimen rules

In Double Cantilever Beam (DCB) specimens according to ISO 15024, load blocks on the edges must be used as shown in Figure 6.1. Following Brunner and Stelzer suggestions it is better to maintain the precrack length under 30mm from the load line, however a crack too close to the load line increases the stiffening effect on the beam arms. Thus, the load blocks were placed so that the load line was 15mm from the tip of the insert so the distance of the initial delamination after precracking from the load line is 25mm. The choice of this short distance (a_0=25mm) by ESIS is also due limited displacement capabilities of the machine. Moreover, a shorter value of a_0 allows for lower crosshead displacement, therefore higher test frequency, but a longer value of a_0 is also beneficial, as it decreases the stiffening effect inherent with the use of load blocks; so the positioning of blocks takes into account both phenomenon. These requirements guarantee that the load line displacement values do not become too high and the test system is able to follow the displacement signals at higher test frequencies. As CFRP composite is relatively flexible there was a relatively large amplitude so a frequency of over 2 Hz was the higher possible during tests in order to reach the necessary displacement. Indeed it is necessary to find a compromise between precrack lengths from the load line and test frequency - a shorter precrack allows for a faster test as it enables a higher frequency to be used, however it also increases the stiffening effect due to the load blocks.

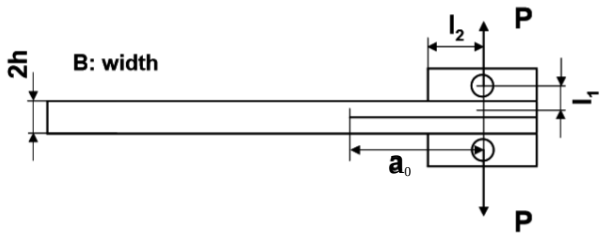

Figure 6.1 DCB specimen with load blocks

Table 6.1 shows values used in this work referring to the previous figure.

Table 6.1 DCB specimen dimensions

	Length (mm)
a_0 (precrack)	25
l_1	14,5
l_2	12,5
2h	4
B	20

6.2 Data recording and Documentation

The test is carried out in two stages; testing from the insert and testing from the precrack. In this paragraph rules used into two stages of DCB test are described. First stage is a quasi-static test used to create a precrack in the sample to allow the creation of a natural sharp crack tip instead of using as crack tip the one created artificially using the teflon film during manufacturing. In this stage the programme used is Bluehill and the sample is submitted to a tensile test. Once the wanted crack length has been reached, the test is stopped and the specimen is immediately unloaded. Data from the tensile test are used for the second part, in particular the maximum tensile strain is used for the calculation of the maximum and minimum displacement, the end point for the fatigue test and the amplitude. Second test stage is a fatigue test where crack is allowed to propagate to characterise the material's behaviour under a cyclic load. Two stages are better explained in the following sections.

6.2.1 Quasi-Static Mode I Pre-cracking

In this phase a machine with a load cell is used and according to EN ISO 75001 the load range should be in between 0-500 N but preferably in the load range of 0-200 N. This step is carried out on the Instron machine using its own software "Bluehill". The test uses fixed-grip conditions, this means that the test is controlled with respect to the linear displacement of the machine. This stage is done to make a natural precrack in the specimen under displacement control and it is necessary to record precracking data, according to ISO 15024, with a fixed crosshead speed of 1 mm/min. In the first set of tests, with virgin samples, precracking is stopped when a delamination length increment of 10 mm is reached; while in the second set of test, using samples already tested under fatigue, the quasi-static test was stopped when the load-displacement curve showed a drop in order to let the crack propagation during the second stage (Figure 6.2). It is important to not remove the specimen after unloading from the precrack.

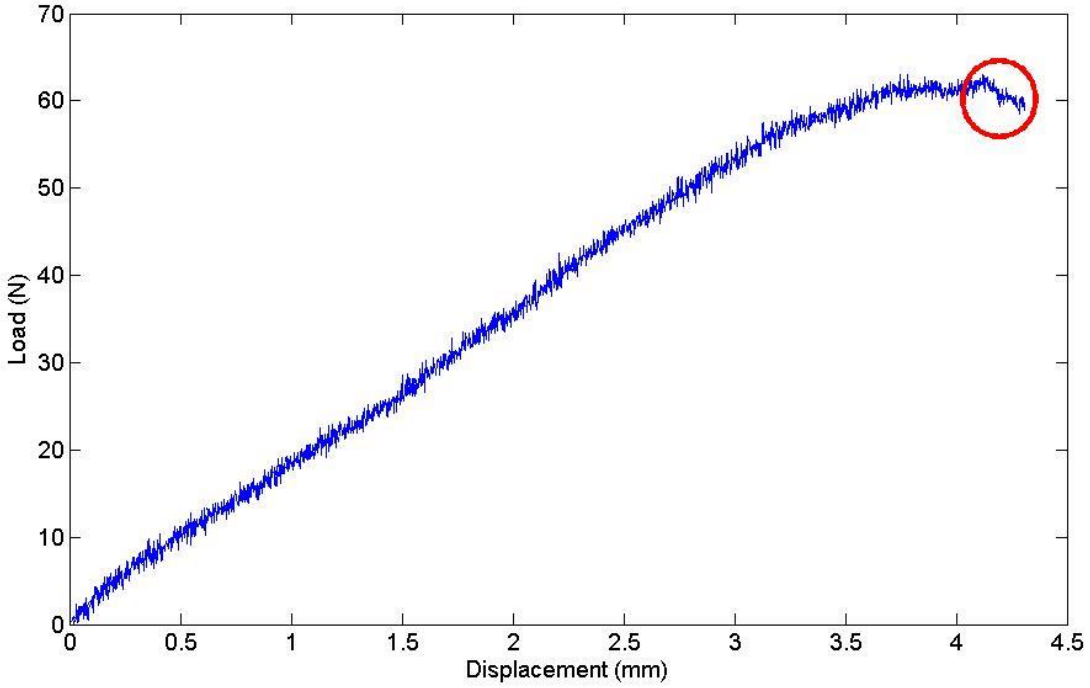

Figure 6.2 Example of load-displacement curve under quasi-static test during the second set of testing

6.2.2 Fatigue Testing

It is performed a mode I cyclic fatigue test from the quasi-static precrack, under displacement control, using the last displacement value from the quasi-static test before unloading as δ_{max} (maximum displacement in the fatigue test) as shown in figure 6.4. The minimum displacement δ_{min} is estimated using a R-ratio of 0.1 so $\delta_{min}/\delta_{max} = 0.1$ and it is suggested in ESIS protocol to avoid heat generation in the sample. Following standards, test frequencies should be set to either 10, 5, 3 Hz or less depending on the required displacement. The test under mode I loading should be performed at an as high as possible frequency, but to reach the maximum displacement and dodge the heating, it is necessary to calibrate it. In this work, a 2Hz frequency is used during the first set of tests, while in the second set of fatigue sometimes lower frequencies are required. The test goes on until a number of 50000 cycles is reached, when it is possible. The cyclic loading shall start from the mean displacement calculated from the tensile quasi-static test with:

$$\delta_{mean} = \frac{\delta_{max}+\delta_{min}}{2} \tag{6.1}$$

The amplitude of the oscillation is:

$$Amp = \frac{\delta_{max}-\delta_{min}}{2} \tag{6.2}$$

As mentioned above, the Instron testing machine has its own suite of softwares and the one used for fatigue testing is the Instron-Wavematrix. Before beginning each test, the amplitude, the starting displacement and the frequency of the test are input. WaveMatrix is a flexible material testing software system that allows both static ramps and cyclic waveforms to be generated. It displays the stages of each test in a graphical form. A program was written for use in this fatigue test that

consists of 2 static ramping stages proceeded by a number of cyclic load stages that depends on the number of intended pauses in the test. During the static ramp the sample was open to δ_{mean} then the fatigue test started applying the proper amplitude. In table 6.2 it is summarised how the program works.

Table 6.2 Summary of Wavematrix program

Stage name	Action	Data recorded	How often data is saved
Static Ramp to δmin.	Displacement checked on console	N/A	N/A
Static Ramp to δmean	Displacement checked on console. Crack length visually measured for N = 0 cycles	A	N/A
N = 1 – 100	Cyclic loading at 2 Hz or less	Pmax, Pmin, δmax, δmin, N, a	Every 10 cycles
N = 100-1000	“	“	Every 100 cycles
N = 1000-10000	“	“	Every 1000 cycles
N = 10000-30000	“	“	Every 2000 cycles
N = 30000-50000	“	“	Every 5000 cycles

During the fatigue test it is recorded the values of P_{max}, P_{min} (maximum and minimum load, respectively), δ_{max}, δ_{min} (maximum and minimum displacement). The crack length detection shall be performed directly from the operator or with the use of a camera. In these tests it is used a digital microscope camera.

During the running of the test, the sine wave indicating the measured displacement was visible, and a displacement-number of cycles curve was displayed. The displacement sine wave was checked to be sure that the correct amplitude was consistently being applied during the test.
The software is used for recording a number of parameters from the test. The parameters that are needed to determine the fatigue crack growth rate and the fracture toughness of the specimen are the maximum values of both the load and displacement at each corresponding cycle recorded. The crack length is monitored manually with a digital optical microscope as done in the first part of the test. The crack length is measured in relation to the number of cycles complete. Using this method, it is possible to relate the crack length to a corresponding load for a specific cycle and in doing so, the IFT for that specific cycle can be computed.
The crack growth rate (da/dN) was computed using the crack length recorded at specified cycles. More detail is given on this in the fatigue calculation section of data analysis §6.3. Moreover, by

plotting the energy for the crack propagation G_I against the crack growth rate it is possible to obtain Paris plot. [48]

6.3 Data Acquisition and Analysis

The computer records a set of data during the test (load, displacement, cycle counter). From them it is possible to calculate the delamination growth rate and the energy release rate.

6.3.1 Delamination growth rate, da/dN

There are two possible ways to determine delamination growth rates da/dN:

1) Method A: da/dN can be computed by calculating the slope of the straight line connecting two adjacent points on the delamination length, a, versus cycle number, N, curve (eq. 6.3). This approximation is reasonable if the delamination length increments are small. This method is called 'Secant method'.

$$\frac{da}{dN} = \frac{a_{i+1} - a_i}{N_{i+1} - N_i} \tag{6.3}$$

   For the determination of the cyclic strain energy release rate the average delamination length, ā, is normally used with:

$$\bar{a} = \frac{1}{2}(a_{i+1} - a_i) \tag{6.4}$$

2) Method B: da/dN can be calculated according to a standardised method described in ASTM E647 – 00.
   This incremental polynomial method for computing da/dN involves fitting a second order polynomial (parabola) to sets of (2m+1) successive data points, where m is usually 1, 2, 3 or 4. The regression parameters are determined by the least squares method, that is minimisation of the square of deviations between observed and fitted values of delamination length. Since this method is not able to describe the delamination rates between the first and the last pair of data points, these have to be evaluated using the secant or point-to-point technique which simply involves calculating the slope of the straight line connecting two adjacent data points on the a vs. N curve as described above (method A). For the second and the second to last set of data points the 3-point-method is used (m=1), that is, the regression polynomial is applied to the first and last three data points and evaluated for the medium point (i. e., the second or second to last). Analogous, for the third and third to last data point m=2 (5-point-method) and for all further data m=3 (7-point-method). The first and last data points are evaluated using a secant technique that involves calculating the slope of the straight line connecting two consecutive values of a. A schematic illustration of this incremental polynomial method is depicted in Figure 6.3 [54]. In Paris plot it is used the 7 point method on y axis.

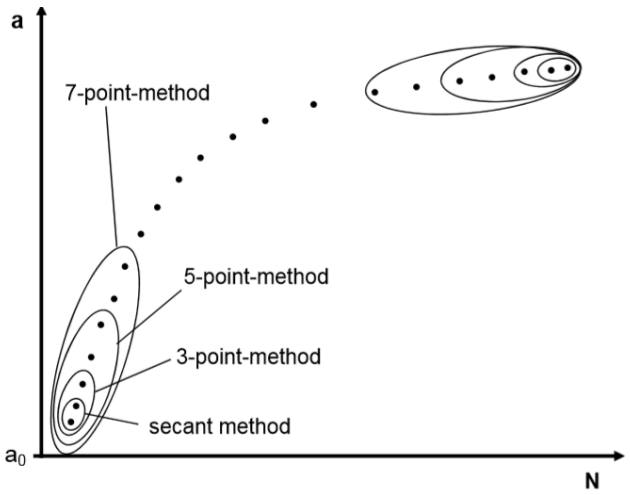

Figure 6.3 Schematic illustration of a typical a vs N graph (displacement control) for the determination of the cyclic interlaminar crack growth rate, da/dN

6.3.2 G_I calculation with beam theory (BT)

The double cantilever beam (DCB) test is used to determine the pure mode I fracture toughness of composites or adhesive joint systems. Figure 6.4 shows a simple illustration of the DCB test and loading conditions. The DCB specimen is centrally cracked (i.e. $h_1 = h_2 = h$). The loading is symmetrical such that the momentum applied is M = Pa.

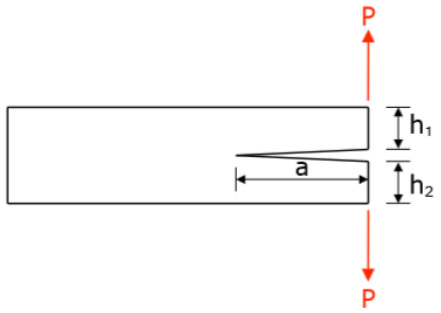

Figure 6.4 Illustration of a DCB test

The equation used to calculate the mode I fracture toughness, G_I (J/m^2) is:

$$G_I = \frac{P^2}{2B}\frac{dC}{da} \tag{6.5}$$

Where P is the load (N) and B the width (m). DCB test is commonly adopted in literature and is internationally standardised for composite because samples are easy to manufacture and test, and results analysis is simple. For displacement control conditions (method used in this thesis), first it is necessary to define the compliance C starting from the displacement δ (m), measured from the crack axis:

$$\delta = \frac{2Pa^3}{3EI} \tag{6.6}$$

Where a is the crack length (m), E the flexural modulus measured with a three point bending test (Pa) and considering the moment of inertia, $I = \frac{Bh^3}{12}$, due to the rectangular section of one arm of the crack and h is the half thickness (m), then the elastic compliance in a DCB geometry is defined as

$$C = \frac{\delta}{P} = \frac{2a^3}{3EI} \tag{6.7}$$

Thus

$$\frac{dC}{da} = \frac{2a^2}{EI} = \frac{24a^2}{EBh^3} \tag{6.8}$$

So it is possible to express the energy as:

$$G_I = \frac{P^2a^2}{IEB} = \frac{12P^2a^2}{B^2h^3E} = \frac{3P\delta}{2Ba} \tag{6.9}$$

Now, in order to express G in terms of δ and a, eq. 6.7 can be rearranged in:

$$P = \frac{3EI\delta}{2a^3} \tag{6.10}$$

And substituting eq. 6.10 into 6.9:

$$G_I = \frac{P^2a^2}{BEI} = \frac{9E^2I^2\delta^2}{4a^6}\frac{a^2}{BEI} = \frac{9\delta^2EI}{4Ba^4} \tag{6.11}$$

And under displacement control conditions:

$$\left(\frac{dG}{da}\right) = \frac{-9\delta^2EI}{Ba^5} = \frac{-4G}{a} \tag{6.12}$$

So under displacement control, as a increases the energy release rate G should decrease.

The equation 6.9 was used in C. Murphy thesis while he did fatigue tests at UCD and it is the one suggested from Stelzer and Bunner in 'Mode I delamination fatigue crack growth in unidirectional fiber reinforced composites: Results from ESIS TC4 round-robins'. It is the simplest equation to estimate energy but it is not so precise as it is explained in the next page [15] [54].

6.3.3 G_I calculation with correction factors (CBT)

The equations for the strain energy release rates previously outlined do not take into account various experimental effects that may influence the calculated values of G. These include large displacement and load block effects as well as root rotation or shearing of the substrate around the crack tip (see Figure 6.4). Williams derived corrections for each of these effects [55].

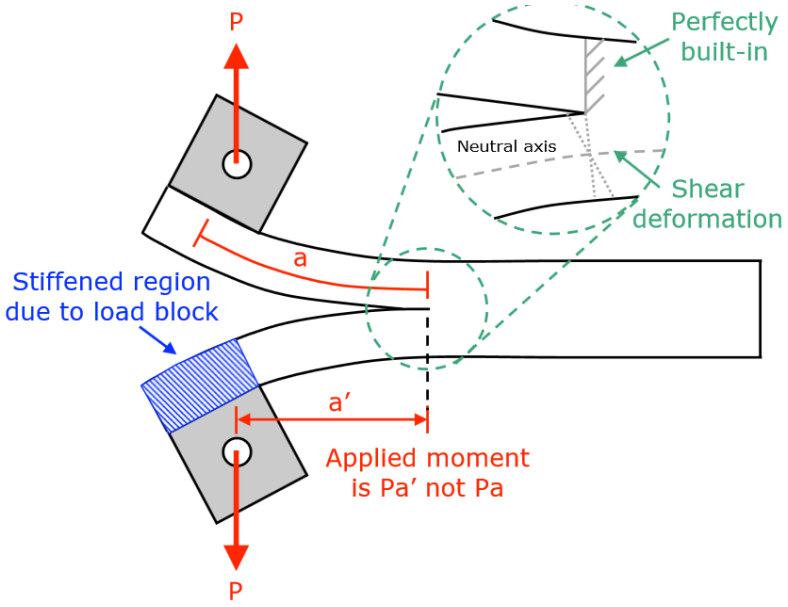

Figure 6.4 Real behavior of a specimen in DCB test

Figure 6.4 illustrates exaggerated deformation of the beam arms during a DCB test. The moment used in the calculation of G_I is Pa. However, it can be seen that the bending of the beams causes the moment arm to shorten. In general, the strain energy release rate for mode I, G_I, can be expressed according following equation obtained from linear elastic fracture mechanics (LEFM):

$$G_I = \frac{3 \cdot P \cdot \delta}{2 \cdot (a + |\Delta|)} \cdot \frac{F}{N} \tag{6.13}$$

where B is the specimen width (m), P the applied load (N), δ the displacement (m) and a the delamination length(m). By substituting P with the maximum load, the maximum strain energy release rates, G_{Imax} can be determined at every cycle.

F and N are the correction factors. The act of bonding a load block onto a DCB specimen that effectively stiffens the end of the moment arm is considered by dividing the displacement, δ, used in the calculation of G, by the load block correction factor, N. F is the displacement correction factor. F and N can be calculated with:

$$F = 1 - \frac{3}{10}\left(\frac{\delta}{a}\right)^2 - \frac{2}{3}\left(\frac{\delta l_1}{a^2}\right) \tag{6.14}$$

$$N = 1 - \left(\frac{l_2}{a}\right)^3 - \frac{9}{8}\left[1 - \left(\frac{l_2}{a}\right)^2\right]\frac{\delta l_1}{a^2} - \frac{9}{35}\left(\frac{\delta}{a}\right)^2 \tag{6.15}$$

Where l_1 and l_2 are the lengths in the figure 6.1. In addition, for both DCB geometry, the influence of beam root rotation on the compliance is taken into account, as well as the shearing of the substrate around the crack tip. This can be corrected for by incorporating an effective crack length that is greater than the corresponding physical crack length. In this approach, a constant, Δ, is added to each crack length measurement, a. The value of crack length correction factor Δ is determined experimentally. Δ is evaluated using the compliance of the test specimen at the visual initiation point and each propagation point when testing from the precrack. Plotting $(C/N)^{1/3}$ versus crack

length, a, it is possible to measure Δ from the x-axis intercept as shown in Figure 6.5, where C is the compliance and N the correction factor.

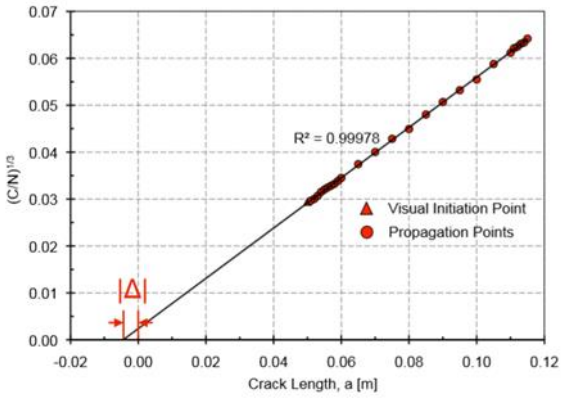

Figure 6.5 Determination of correction factor for root rotation of crack tip

6.3.4 Paris plot

A Paris plot is a log-log sigmoidal curve that describes three regions of fatigue crack growth. It reports the crack growth rate, da/dN, on y axis and the maximum level of energy for the propagation of the crack at a certain number of cycles, G_I, on x axis.

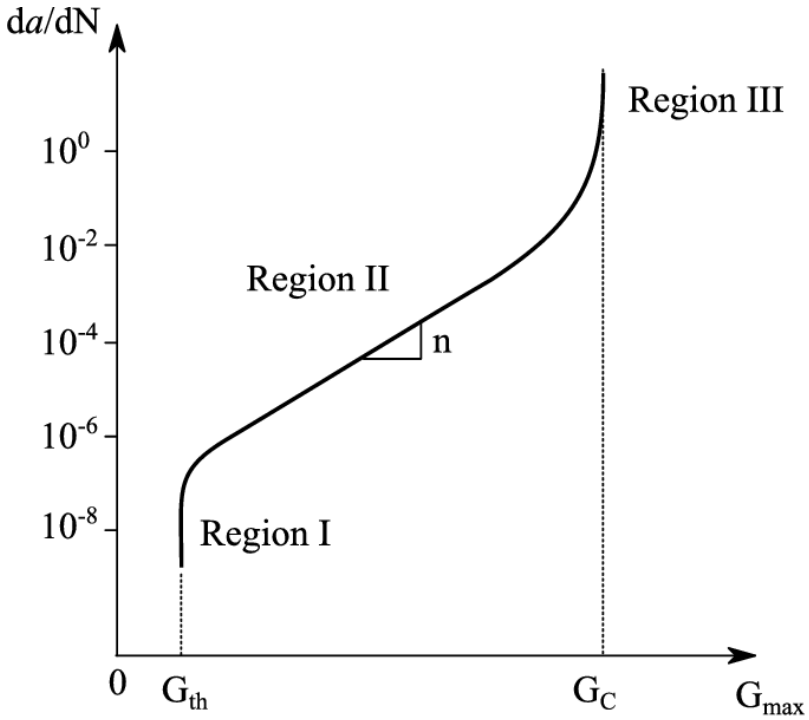

Figure 6.6 Example of Paris plot

In the fatigue crack propagation curve (Figure 6.6) it is possible to find 3 regions. Region I: region of crack arrest which is defined by the crack growth rate threshold (G_{th}) that happens at very low crack growth rates. Region II: linear growth in the logarithmic scale described by Paris law (slope n):

$$\frac{da}{dN} = C(\Delta G)^n \tag{6.16}$$

Region III: fast or unstable crack growth region defined by the fracture toughness (Gc). Cracks may nucleate quite early in the fatigue life of a material, however it is relatively more difficult at stress levels near the fatigue limit [56].

6.4 Machine set up for Mode I Fatigue Testing - (DCB)

Fatigue mode-I testing was carried out on the Instron-8502 250kN servo-hydraulic materials testing machine. Loading is applied by servo-hydraulic pumps that are capable of achieving relatively high frequencies which are needed to support fatigue testing. This system operates by attaching a load cell to the upper grip and keeping its position fixed, and the motion of the lower grip is controlled. It requires a flow of coolant supplied by a coolant tower through pump. This system uses approximately 50kW of power regardless of the test being conducted. The setup is illustrated in figure 6.7.

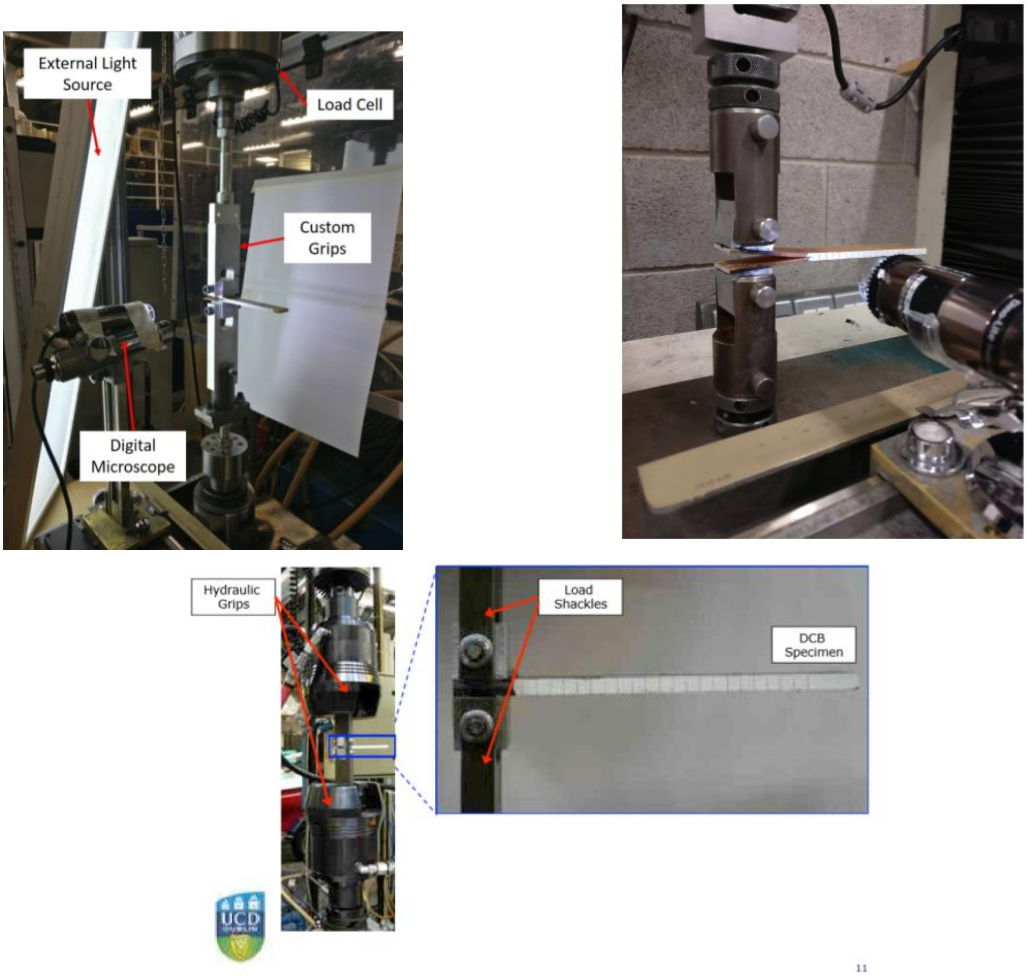

Figure 6.7: DCB Fatigue Setup on the Instron-8502 250kN Servo-Hydraulic Materials Testing Machine

A fatigue test constantly oscillates between a zero load and a tensile load. For this reason, it is important that there are no loose connecting parts. If this is not ensured, it can result in excessive noise in the system and so may cause false reading. To reduce the likelihood of this occurring, specifically machined pins and grips were designed, see figure 6.8. They were designed to create an interference fit between the pin and the load block but also maintain a sliding fit between the grips and the pins. This is done to ensure there is no frictional resistance but also maintain a tight fit. Steel grips contained a 6mm diameter hole, the same diameter as the load blocks. The load blocks were secured to the grips with a pin. The pin was sanded so that it allows rotation of the load block, but provides a tight enough fit to avoid any free movement of the load block. It was important to align as best as possible both grips and blocks in the sample to avoid torsion or compression being applied to the specimens due to asymmetrical load.

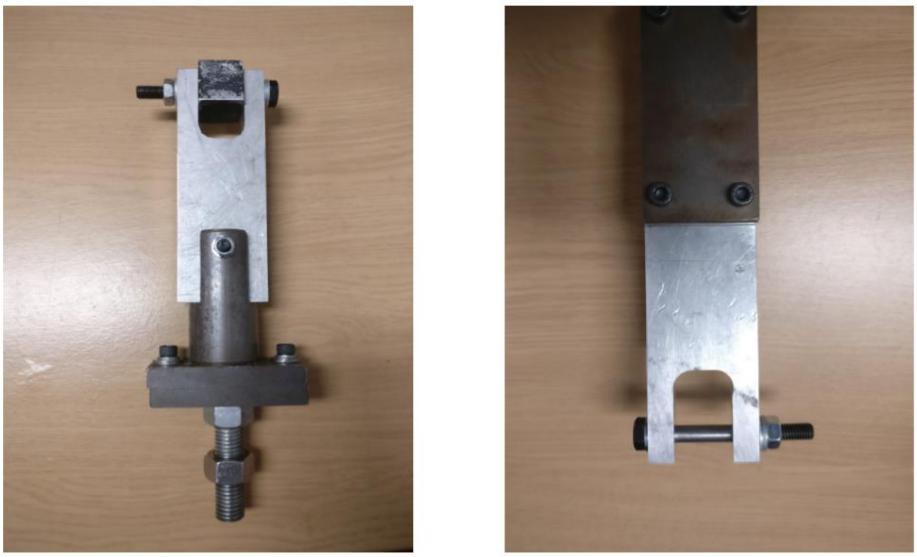

Figure 6.8. Custom built grips to improve stability

Chapter 7

This chapter is about the specimen preparation, the experimental setup, how to carry on the tests, samples' dimension and names. All these data are used in the next chapter for the analysis.

7.1 Material testing

A delamination fracture toughness test was carried out as per ISO 15024 or ISO 17212:2012 on 3 DCB specimens per each type of material. From the test it is possible to obtain the critical strain energy release rate $G_{I,}$ the crack growth rate da/dN and it lets the comparison between different samples. Attempts have been made in literature to normalise the bridging effect in fatigue testing using results from such quasi static tests but the correlation between it and fatigue is not already clear.

In total there were 15 samples and each of them was tested twice. Next table (Table 7.1) summarise the composites used in the test and their abbreviations.

Table 7.1 Material samples and abbreviations

Material	Abbreviation code
CFRP (control)	C1
	C2
	C3
CFRP + 4000 steel fibres in the longitudinal direction every 50 mm	50L1
	50L2
	50L3
CFRP + 4000 steel fibres in the transversal direction every 50 mm	50T1
	50T2
	50T3
CFRP + 4000 steel fibres in the longitudinal direction every 12,5 mm	125L1
	125L2
	125L3
CFRP + 4000 steel fibres in the transversal direction every 12,5 mm	125T1
	125T2
	125T3

Each fatigue test was repeated twice, the first on the virgin material and the second on the damaged increasing to see how it was the behaviour when a fatigue load was applied again in the same sample already damaged. This topic (repetition of fatigue tests) is of big interest in the last years and a lot of funds are destined to this research. Because of some problems with the machine the first set of test on the virgin material was repeated twice as the load at the initial displacement was far from zero.

7.2 Specimen preparation

The width of each specimen, B, was measured at three points (at the middle and at ~ 10mm from either end) using a ruler with a resolution of 0,5mm. The thickness of each specimen, h, was measured, at the same three points, using the same ruler. Also the length, L, was measured with the ruler. The average values of these measurements were used in the calculation of fracture energy, G_I.

During the preparation, one long edge of each sample was then machined smooth using a rotating polishing disc of P320 sandpaper. The samples were dried using paper towel and a hair-dryer to minimise any contamination from the water used in the process. Load blocks were attached to 30 mm from the beginning of each specimen, so the end of each block was 2,5mm far from where the crack initiator was located. The load blocks and each specimen were polished with sand paper and cleaned with an acetone solvent. Thus one surface was not perfectly flat, two epoxies were used. The load blocks were bonded with a room temperature curing epoxy black adhesive LOCTITE 480 on the flat side and with the two-component epoxy Loctite EA 3430 with a curing of 2 hours at 50°C in the oven on the rough side.

One side of each specimen was painted with a thin layer of water-based correction fluid (Tippex). Once the fluid had dried, vertical lines (or ticks) were drawn using a pen with a nib width of 0.1mm. The first tick was at the tip of the Teflon insert film. For the DCB specimen, ticks were drawn every 1mm for the first 15mm, then every 5mm for the next 50mm. The markers were repeated with a distance of 1mm for the second test from where the crack stopped at the end of the first test. The higher density of markings near the Teflon insert was required to capture in a more precise way the crack growth. Each line corresponds to a crack length at which data is recorded during the fracture test. An illustration of a fully prepared DCB specimen is shown in Figure 7.1 and a real sample is shown in Figure 7.2.

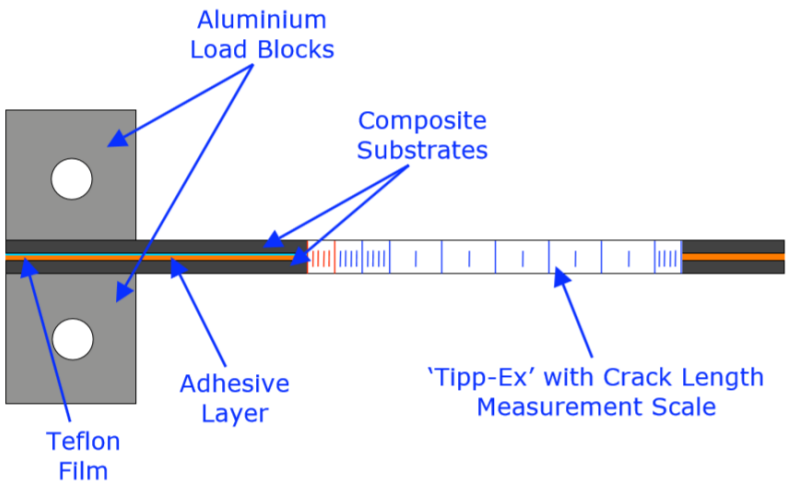

Figura 7.1 Example of DCB specimen component

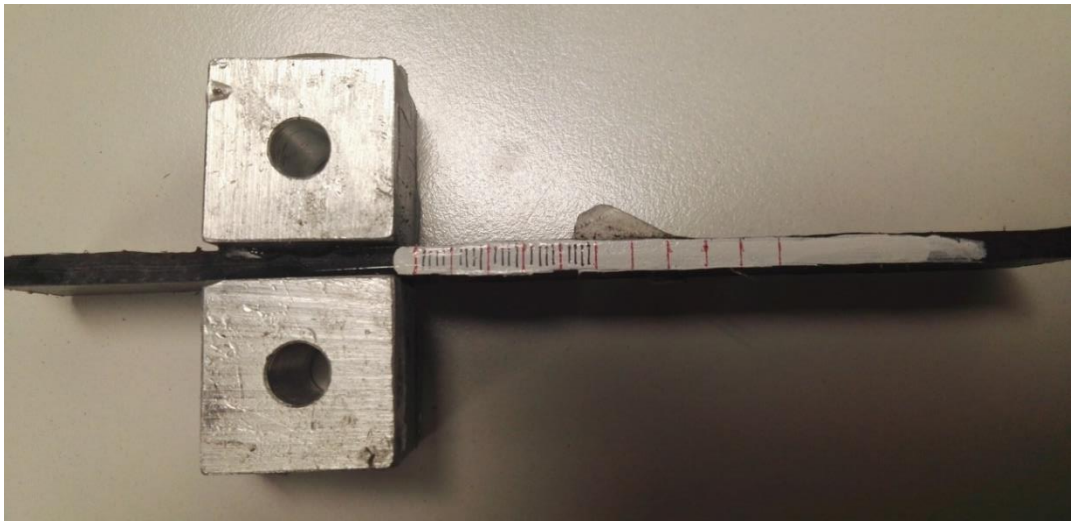

Figure 7.2 DCB real specimen

The specimens were cut to a nominal width of 20 mm. The DCB specimens were 150mm long with an initial crack starter length of 57,5mm, but the measured DCB specimen dimensions are shown in Table 7.2. DCB tests investigated only pure mode I.

Table 7.2 Samples dimensions

	B			**H**			**L**
Sample	**B1**	**B2**	**B3**	**h1**	**h2**	**h3**	
C1	2,05	2	2,05	4	4,2	4,2	15,11
C2	2,05	2,05	2	4	4,2	4	15
C3	1,95	2	2,05	4,5	4,3	4,2	15
12,5L1	1,95	1,95	2	5	4,5	5	14,93
12,5L2	1,95	1,95	1,9	5	4,5	4,9	14,9
12,5L3	2	1,95	2	4,7	5	5	14,9
12,5T1	2	1,95	2	4,5	5	5	15
12,5T2	1,95	1,95	1,95	5	4,5	4,5	14,9
12,5T3	1,96	2	2,05	4,8	5,1	5,1	15
50L1	1,95	2,03	2	4	4,2	4	14,9
50L2	1,95	1,9	2	4,4	4,5	4,2	15
50L3	1,95	1,95	1,95	4,4	4,2	4,4	14,9
50T1	2,05	2	1,95	4,5	4,5	4,3	14,9
50T2	1,95	1,95	2	4	4,5	4,5	14,9
50T3	2,05	2	2	4,5	4,4	4,5	14,9

7.3 Experimental Set-up

A 10kN load cell was used to record the applied load. The specimens were held in place using load shackles and loading pins as shown in Figure 7.3 and the dimensions used in the analysis are shown in Figure 7.4.

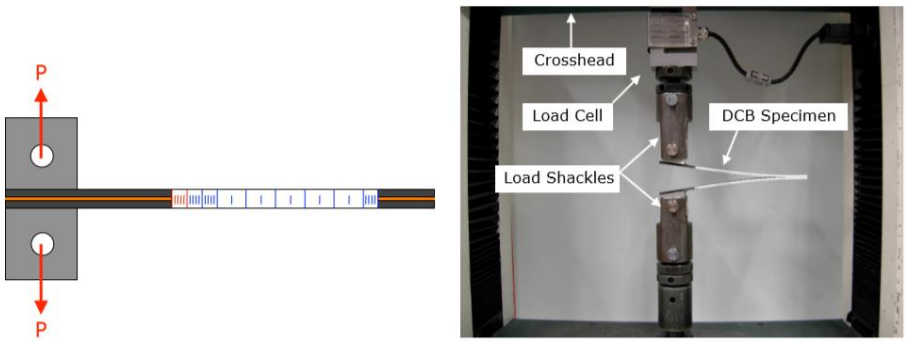

(a) DCB illustration. (b) DCB photo.

Figure 7.3 (a) DCB test, (b) DCB machine and clamps

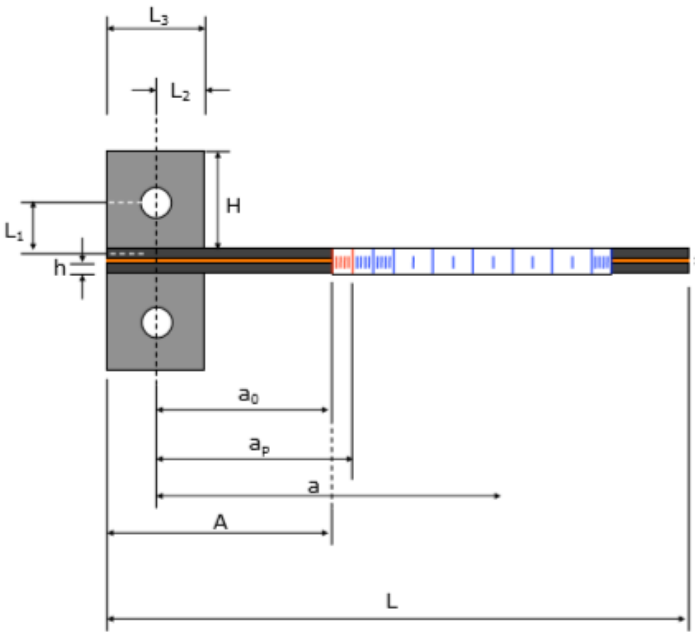

Figure 7.4 DCB specimen dimensions

In the next table (Table 7.3) are present the dimension mentioned in the previous figure for the first test done in the virgin samples. In table 7.4 are reported the values a_p for each samples as the static opening of the precrack was done until the load reached a drop so there is not a common length of

the precrack but sample dimensions are the same. For some samples data were lost due to problems with power supply in the laboratory.

Table 7.3 DCB specimen dimensions and values for the first fatigue test

Dimension	Length (mm)
H	25
H	2
L_1	12,5
L_2	12,5
L_3	25
L	150
a_o	15
a_p	25
A	17,5

Table 7.4 DCB specimen values for the second fatigue test

Sample	a_p
C1	34
C2	34
C3	35,5
50L1	45
50L2	40
50L3	38
50T1	43,5
50T2	-
50T3	35
12,5L1	43
12,5L2	-
12,5L3	40
12,5T1	39
12,5T2	43
12,5T3	42

An Excel spreadsheet was used to record crack length measurements during the test after a precise number of cycles. The crack growth was visually monitored using a travelling microscope. The crack length was observed at 10, 50, then every hundred until 1000, every thousand until 10000, every 2000 until 30000 and then every 5000 until 50000.

Chapter 8

In this chapter results from previous work are summarised. Quasi-static tests showed that the insertion of steel fibres increased the fracture toughness of the CFRP so samples were tested under a cyclic load to see if they show the same behaviour.

8.1 Quasi-static test procedure

Double cantilever beam (DCB) test was carried out to measure the mode-I fracture energy of CFRPs according to standard ISO:15024:2001. A schematic of the DCB test is shown in Figure 8.1. The specimens have a nominal width of 25 mm and length of 150 mm with an initial crack starter length of 45mm. The tests were conducted at room temperature with a constant displacement rate of 1mm/min. Four tests were repeated for each material.

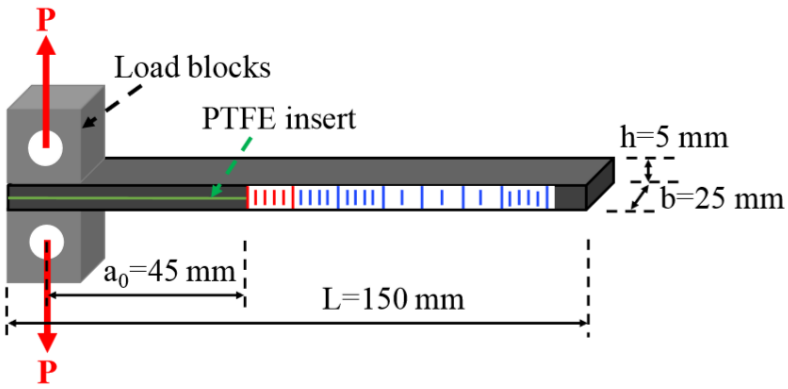

Figure 8.1 DCB quasi-static sample

Samples tested had different steel fibres orientations: longitudinal "L" and transversal "T". The number associated to L/T is the number of steel fibres that cover 1mm distance so L/T80 that means 80 fibres every mm correspond to 50L/T or rather 4000 filaments each 50mm and L/T320 correspond to 12,5L/T. Table 8.1 shows the correspondence between nomenclature used in quasi static and fatigue tests. Samples 160L/T were not tested in fatigue for reasons of time.

Table 8.1 Nomenclature

	Quasi static test	**Fatigue test**
Sample	Control	Control
	80L/T	50L/T
	160L/T	25L/T (not tested)
	320L/T	12,5L/T

During the test, load and displacement were measured from the machine while the crack propagation was detected by a camera.

8.2 Quasi-static test results

From quasi-static results, a Young's modulus of 46.8GPa, a tensile strength of 511MPa and a strain-to-failure of 1.17% were measured for the control (sample without steel fibres). Interlaying longitudinal steel fibres had negligible effects on the Young's modulus, tensile strength and strain-to-failure. However, negative effects on the mechanical properties were observed for adding steel fibres transversely to the loading direction, i.e. it decreased the Young's modulus, the tensile strength and the strain-to-failure. It was possible to see that the addition of steel fibres significantly decreased the size of the damage region. Moreover, no significant interlaminar delamination was observed for the samples containing steel fibres. This indicates a stronger interlaminar strength, which is further confirmed by the DCB test.

Example load versus displacement curves of DCB tests are shown in Figure 8.2. It is clear that interlaying steel fibres in CFRPs significantly and steadily increased the maximum load and also the maximum displacement increased. Moreover, the incorporation of steel fibres postponed the crack initiation as shown from the force drop that moved to the right in samples with steel fibres. Another obvious phenomenon is that, at the same steel fibre density, more pronounced improvement in maximum load is achieved for adding steel fibres transversely than longitudinally to the crack growth direction.

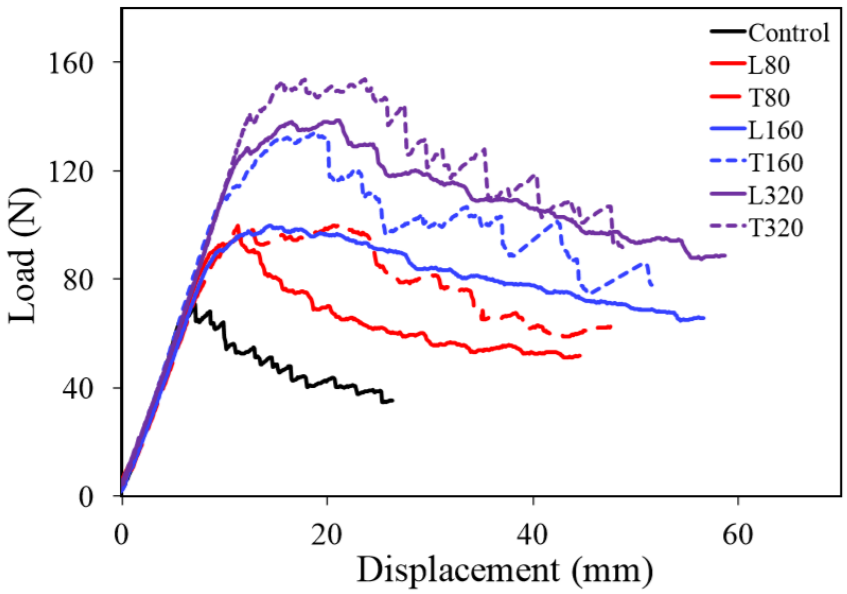

Figure 8.2 Load-displacement DCB test

R ('rising')-curve plot the fracture energy against the crack length and analysing Figure 8.3 it is observed an higher fracture energy immediately from the initial stage and this indicates an increasing damage zone ahead of the crack tip. Moreover the addition of steel fibre interlayers increased the crack resistance of CFRPs. For the same density of steel fibres, the improvement in G_{IC} was more pronounced when the steel fibres were placed transversely to the crack growth direction. Another significant advantage of using steel fibre as interlayers is that it can considerably reduce the crack growth speed.

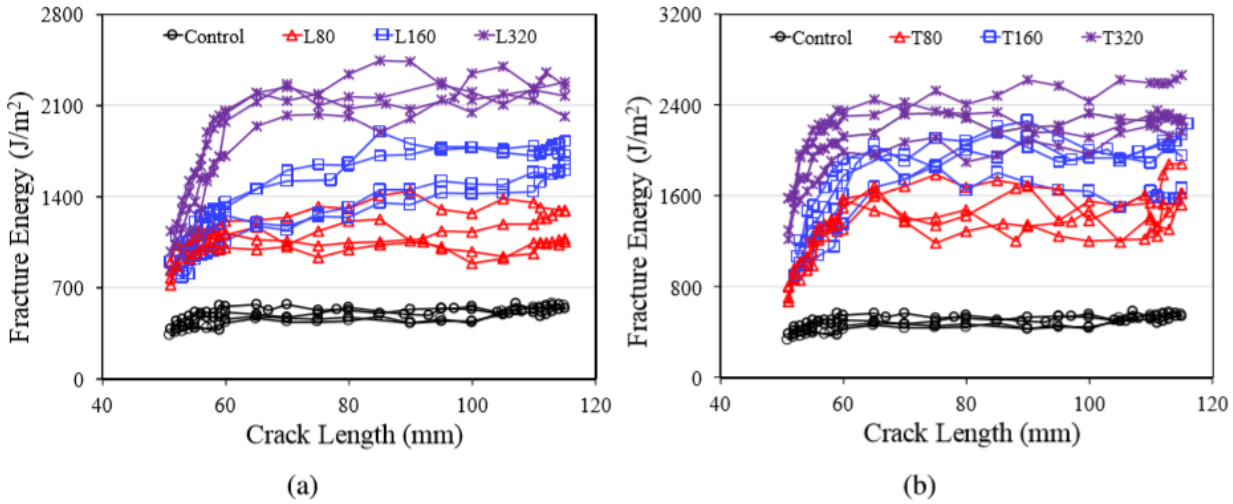

Figure 8.3 R curves comparing samples with longitudinal steel fibres (a) and transversal steel fibres (b)

Analyzing the fracture surface with a SEM it is confirmed the toughening mechanisms of steel fibre bridging and breakage. Moreover, the remained epoxy on the steel fibres indicates good adhesion between steel fibres and epoxy matrix (Figure 8.4)

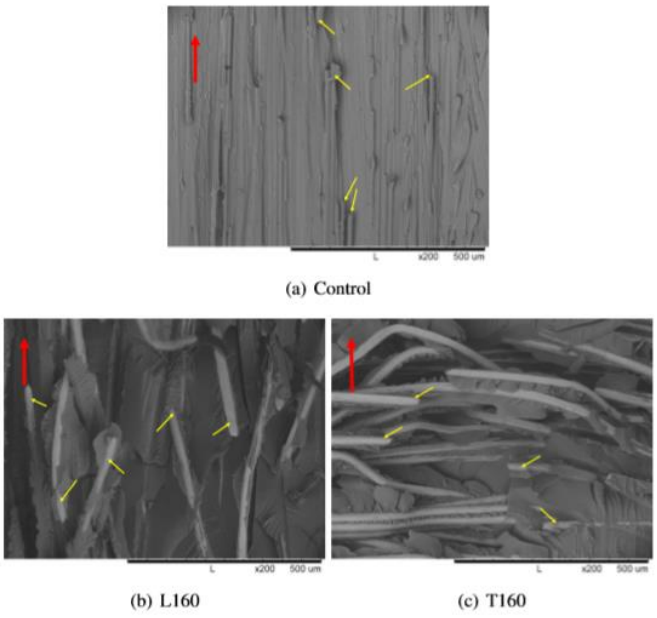

Figure 8.4 SEM images from quasi-static tests. The red arrow indicates the crack growth direction. The yellow arrow indicates damaged carbon fibre in (a) and damaged steel fibres in (b) and (c).

During fatigue tests, as it is possible to see in the next chapter, only control, 50L e 50T and 12,5L and 12,5T were tested because of time required to manage the tests. But this samples are enough to have a comparison with the quasi-static tests done before. Comparing quasi-static samples dimensions and that used during fatigue tests (see §6.1), it is possible to notice that in fatigue tests the thickness and the width of the samples are reduced and the reason of this choice is to shorten fatigue tests.

Chapter 9

This chapter focuses on data analysis obtained from fatigue tests in order to characterise the material's properties and compare the behaviours of the different CFRPs without steel fibres or with them in different amounts.
Main comparison is done using Paris plot for all samples but also other graphs are included to show the crack growth rate, fracture energy (calculated with BT and CBT §6.4.2; §6.4.3) and load-displacement curves.

9.1 First set of fatigue test analysis

9.1.1 Crack propagation rate

It is possible to describe crack propagation rate plotting crack length, measured using a microscope, against the number of cycles. As shown in the following figures, it is possible to see a higher growth speed in the first numbers of cycle; after the crack reaches a threshold so it is no more growing increasing the number of cycles. The following pictures show the crack growth during the fatigue test in controls considering all 3 samples (Figure 9.1) and in Figure 9.2 one sample per amount and disposition of steel fibres inside CFRPs material is plotted.

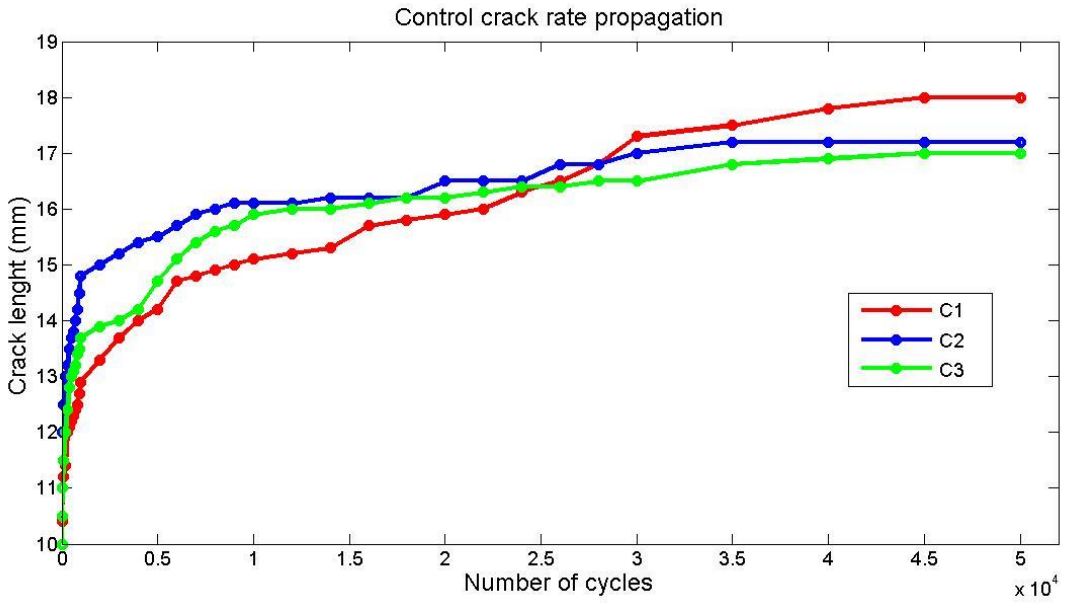

Figure 9.1 Control crack growth rate

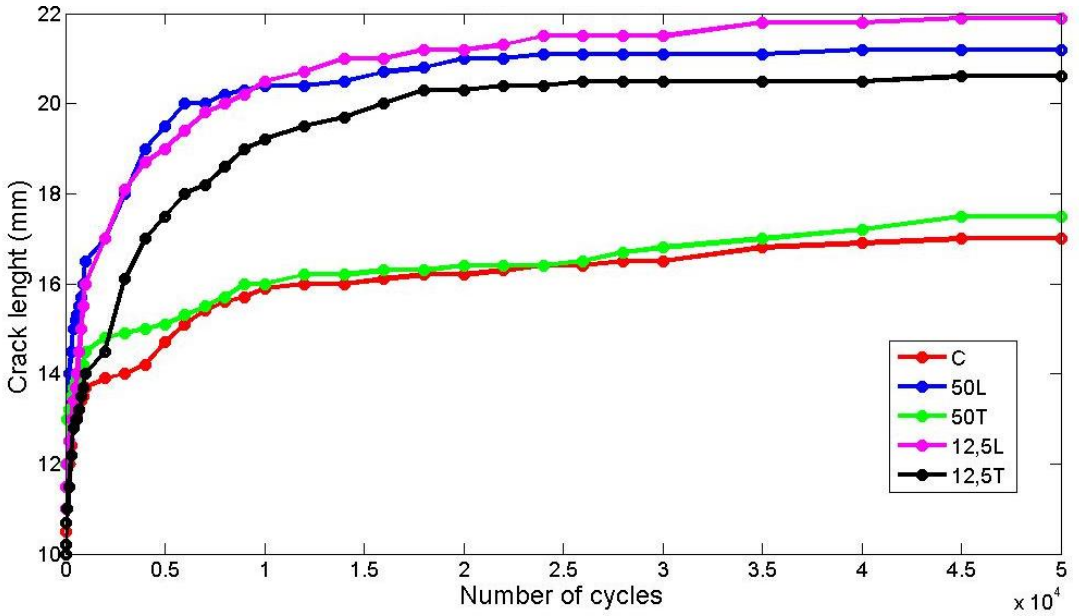

Figura 9.2 Crack rate propagation in different samples

In all curves it is possible to find 3 stages: the initiation of the crack where there is the fastest growth, then the second stage is the propagation where the crack growth rate decreases and the last stage is the crack growth stops because the load is too low to let the crack growing.

Comparing different specimens it is possible to see that in controls the crack length, with an average value of about 7mm, is generally lower than in the samples with steel fibres, where the mean measured crack goes from 10,5 to 14 mm, as shown in figure 9.3. This figure shows the average crack growth based on three samples for all types of specimens. Values in the graph are obtained subtracting from the final crack length measured the precrack.

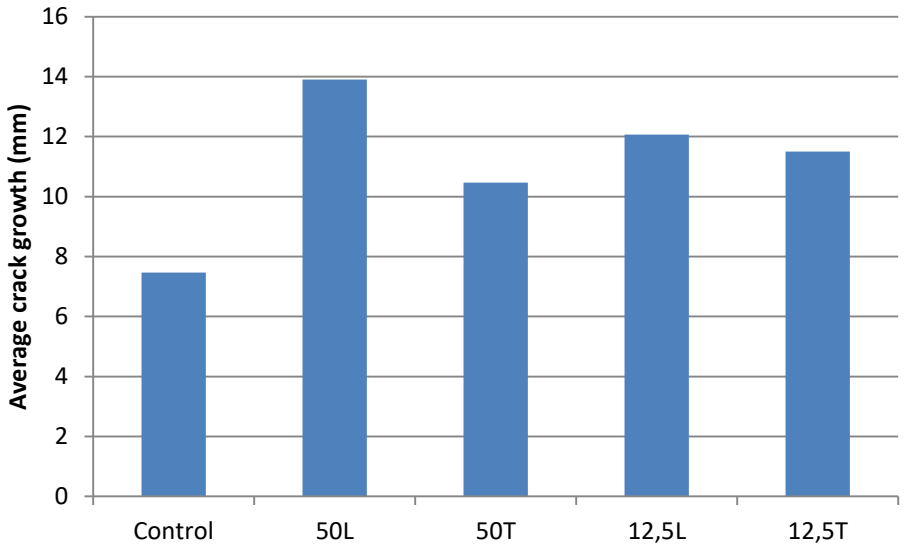

Figure 9.3 Crack growth during fatigue test

Moreover, comparing samples with longitudinal and transversal fibres it is possible to notice that the crack grows generally more when fibres are disposed longitudinally in CFRP.

9.1.2 Load analysis under fatigue test

Following ESIS protocols developed for mode-I DCB fatigue testing, the load during fatigue tests should decrease constantly with passage of time (i.e. number of cycles). But, as shown in Figure 9.4 below, the load has a decreasing trend only in controls while in other samples it is first decreasing and then it is increasing. This phenomenon could be associated to a mechanism of toughness of the material because it is mostly noticed in samples with steel fibres. It could also be associated to a bad sensitivity of the machine or to a bad alignment of grips during the set up of the machine.

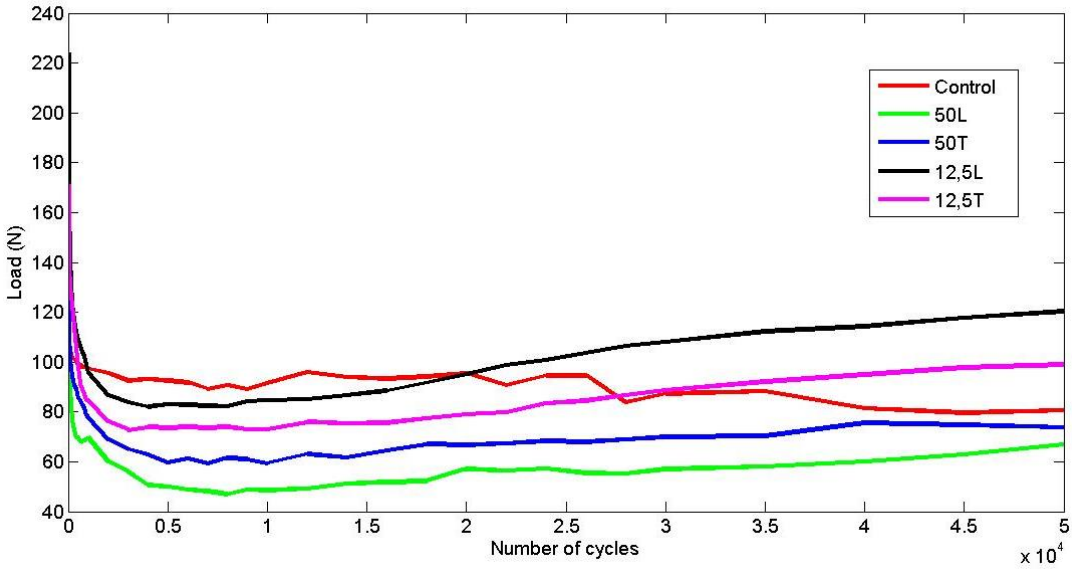

Figure 9.4 Load trend for some samples (sample number 2 for each type)

It is possible to notice that the control load trend is more in agreement with that in the standards because, ignoring some oscillations, the curve is generally decreasing. In samples with steel fibres it is possible to see a rise starting generally after 10000 cycles to the end of curves maybe associated to the bridging effect of the fibres inside the CFRP. This idea is also supported by some pictures taken during fatigue tests (Figure 9.5).

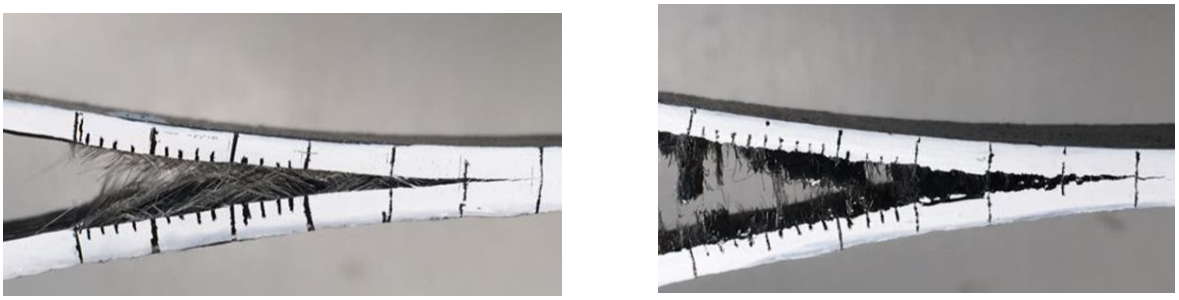

Figure 9.5 Fibres bridging on the longitudinal sample (left) and transversal sample (right)

9.1.3 Energy release rate G_I analysis

It is possible to compare different values of energy estimated using the BT method (see eq. 6.7) and CBT (eq. 6.11). A mean G_I and standard deviation was computed for each sample and from this an overall between-group mean and standard variation was computed. Table 9.1 gives the mean G_I values for each set of points along with its corresponding standard deviation. It is also calculated the coefficient of variation CoV to check reproducibility of values for each method.

Table 9.1 Mean energy values, standard deviation and CoV

	Control		**50L**		**50T**		**12,5L**		**12,5T**	
	BT	**CBT**	**BT**	**CBT**	**BT**	**CBT**	**BT**	**CBT**	**BT**	**CBT**
Mean G_I (J/m^2)	311,51	340,79	389,40	417,14	426,22	461,18	594,23	640,53	555,09	602,4
SD (+/-)	72,92	85,16	142,21	165,2	171,32	196,2	237,01	279,36	225,81	238,2
CoV	23,4	24,99	36,52	39,61	40,19	42,56	39,88	43,61	36,31	39,56

These calculations are also made in order to determine the G_I percentage difference between the control and the steel fibres reinforced specimens, as this is a simple and universal method that most journal articles use for comparison. Following picture shows the mean energy value for each type of sample (Figure 9.6). Energy plotted in this histogram (both BT and CBT) is the average value among every mean on the three samples for each type of specimen tested, as shown in table 9.2. A sample's energy rate G_I is the average energy calculated using energy values at each number of cycles where it was estimated.

Table 9.2 Samples energy and mean values

Sample	**Energy G_I (J/m^2) BT**	**Mean energy BT (J/m^2)**	**Energy G_I (J/m^2) CBT**	**Mean energy CBT (J/m^2)**
C1	387,80	311,51	426,39	340,80
C2	243,49		264,80	
C3	302,97		331,19	
50L1	328,07	389,40	349,17	417,14
50L2	469,76		503,22	
50L3	370,37		398,85	
50T1	560,68	426,22	606,61	461,18
50T2	352,58		377,89	
50T3	365,42		399,07	
12,5L1	626,71	594,23	671,08	640,53
12,5L2	1210,45		1351,20	
12,5L3	561,77		609,98	
12,5T1	600,66	555,09	646,57	602,37
12,5T2	556,43		604,08	
12,5T3	508,18		556,49	

In the calculation of mean energy of 12,5L it was not considered the sample 12,5L2 because its energy value was too high and different from other samples.

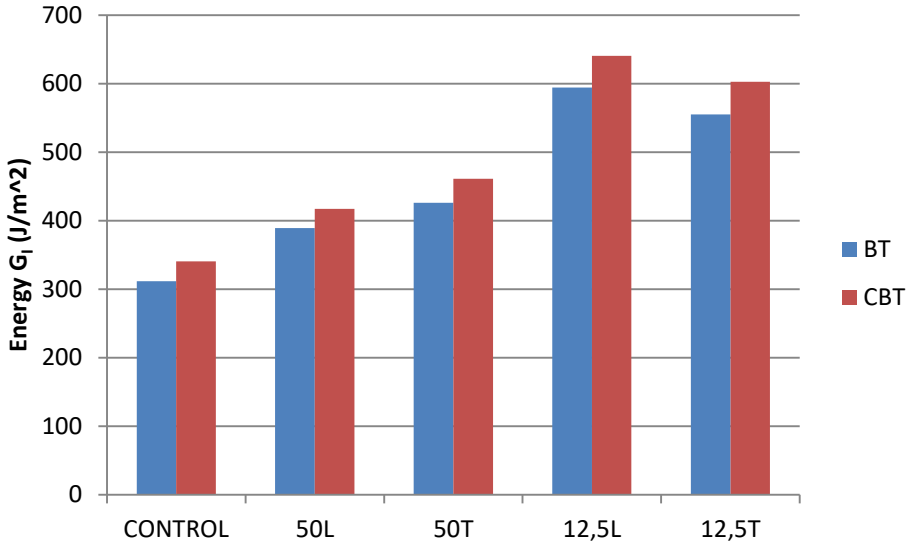

Figure 9.6 Energy mean values with different methods for each type of sample

From the graph it is possible see that energy values calculated with CBT are higher than that one calculated with BT due to the correction factors. Proportions are almost the same using two methods. Specimens with 4000 filaments every 12,5mm have highest energies with a mean value of BT energies of 594,23 and 555,09 J/m^2 respectively for longitudinal and transversal fibres and using CBT method, energies are 640,53 J/m^2 in samples with longitudinal fibres and 602,37 J/m^2 using transversal fibres. In general it is possible to say that the introduction of fibres increases the energy release so the fracture toughness of the material. Considering CBT calculation in samples 50L and 50T energy increased of 22,4% and 35,3% respectively compared to control, while for 12,5L and 12,5T of 87,9% and 76,8%. From literature it is also known that CBT is a more robust technique and is less sensitive to variations in the properties of the composite so values from this method will be used in following analysis. From table 9.1, observing CoV, it is possible to notice that controls show a bigger reproducibility so values of energy calculated are closer among samples than in samples with steel fibres.

Moreover, plotting energy G_I against the number of cycles where it was measured (Figure 9.7, 9.8), as happened for the load, it is evident that also energy is first decreasing and after some cycles increasing a bit due probably to the bridging effect. This behaviour is visible mostly in samples with steel fibres inside because in controls energy is decreasing with number of cycles or it is almost constant.

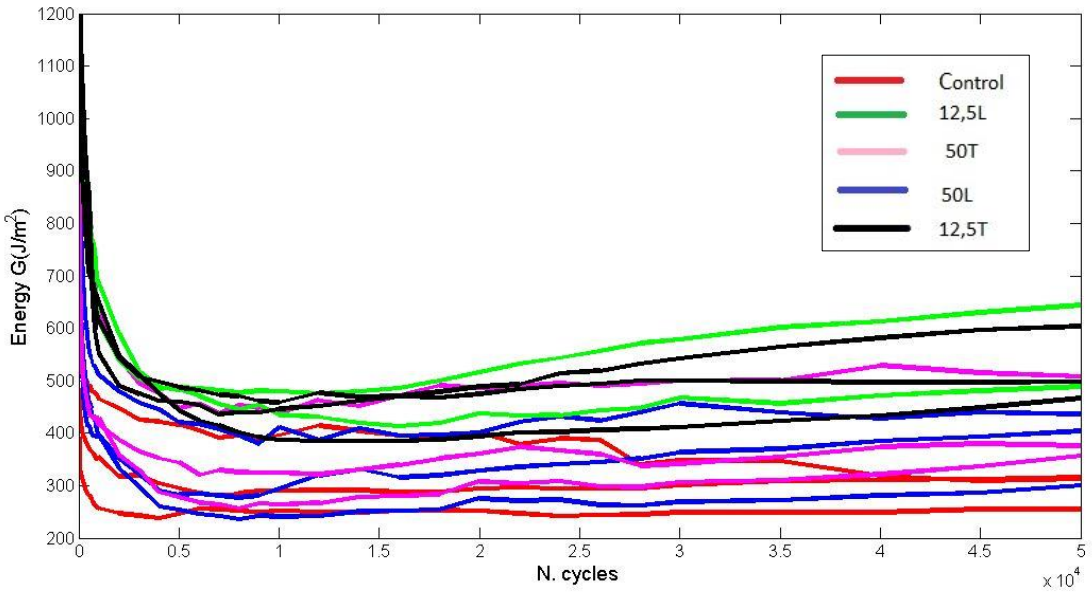

Figure 9.7 Energy vs number of cycles of all samples

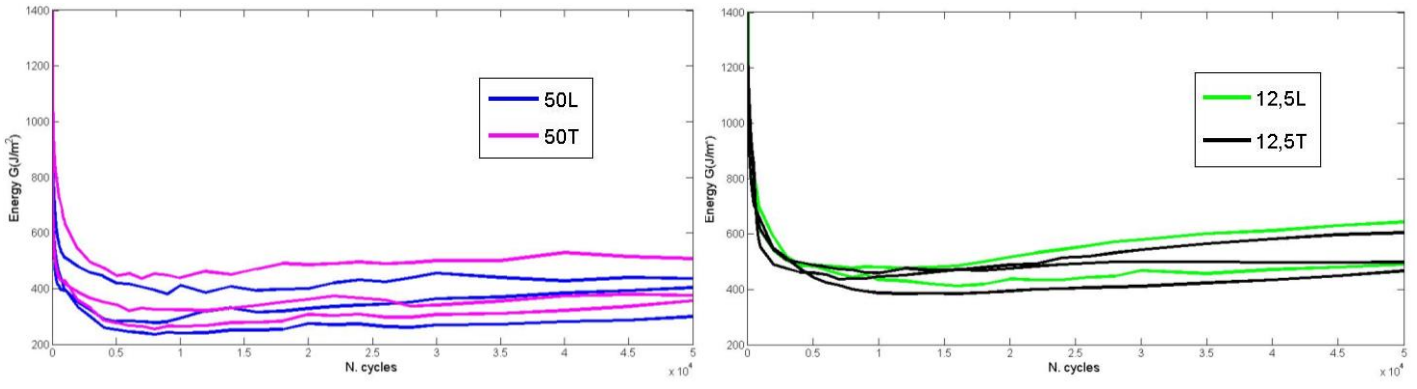

Figure 9.8 Energy vs number of cycles in samples with steel fibres

In figure 9.8 it is possible to see the increasing of energy in particular in samples with 4000 fibres every 12,5mm.

9.1.4 Load-displacement curve

Plotting all the force-displacement curves on a single graph it is possible to get a good visual representation of how much the specimens deviate for each other (Figure 9.9).

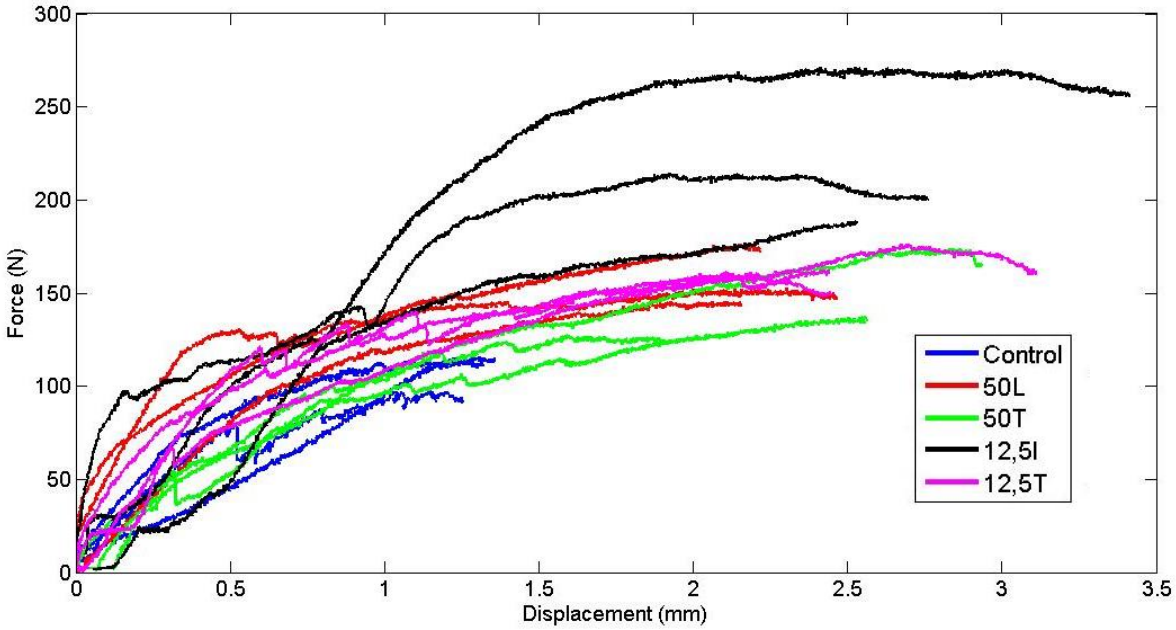

Figure 9.9 Load-displacement curves

It is possible to notice that samples with steel fibres inside reach higher loads and also bigger displacements. Maximum load values go from about 150 to 200N in samples with steel fibres, while the maximum force measured in controls is almost 100N. This causes higher amplitudes during fatigue tests in steel reinforced samples so lower frequencies. Curves present some oscillations due to the presence of fibres bridging during the creation of the precrack. Displacement is below 1,5mm for controls while it goes from 2,5 to more than 3mm in samples with steel inside.

A clearer trend is shown in Figure 9.10 where a mean value of load and displacement is plotted for each type of specimen. It is more evident that steel fibres require higher loads and in particular it is possible to conclude that samples with longitudinal steel fibres reach higher loads while that one with transversal steel fibres higher displacements.

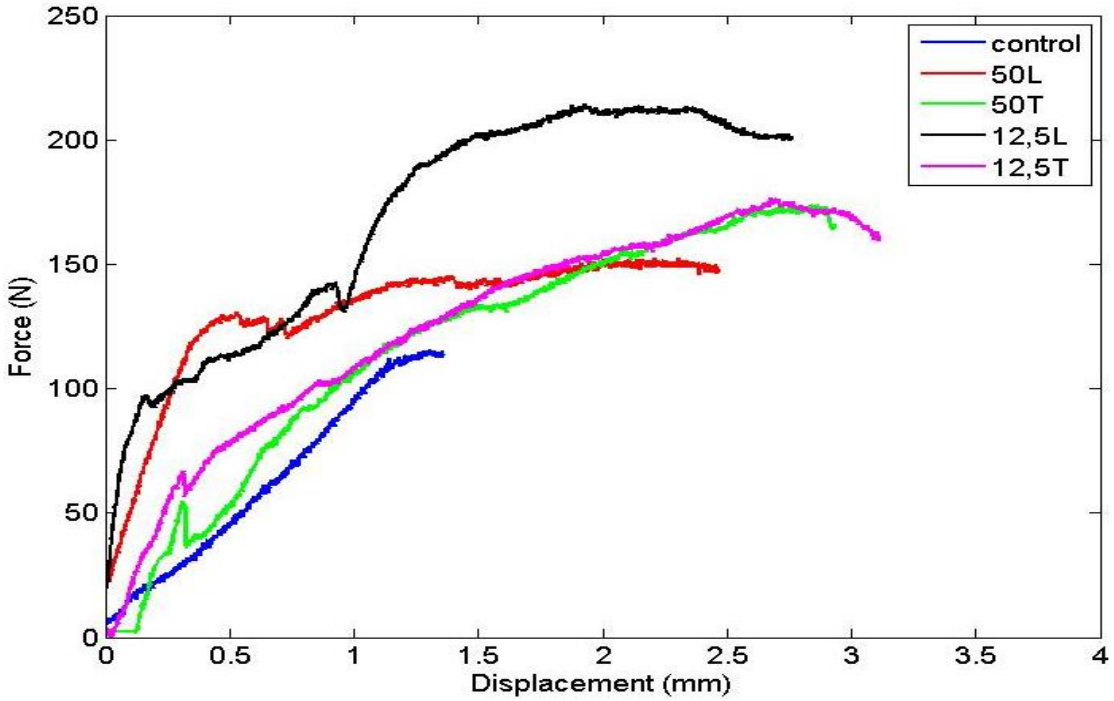

Figure 9.10 Force-displacement based on the mean value

9.1.5 Paris plot

G_I values under fatigue were used to build the Paris curve, as outlined in Chapter 6. From the fatigue data the function of log(da/dN) vs. log G_I was plotted. The slope of this plot is described by the exponent n (see Eq. 9.1).

$$\frac{da}{dN} = C G_{I,max}^{n} \tag{9.1}$$

Where C and n are still power law constants. The crack growth rate, da/dN, was calculated using the 7 point method described in chapter 6.

Figure 9.11 show Paris curve for all samples to let a comparison between different specimens.

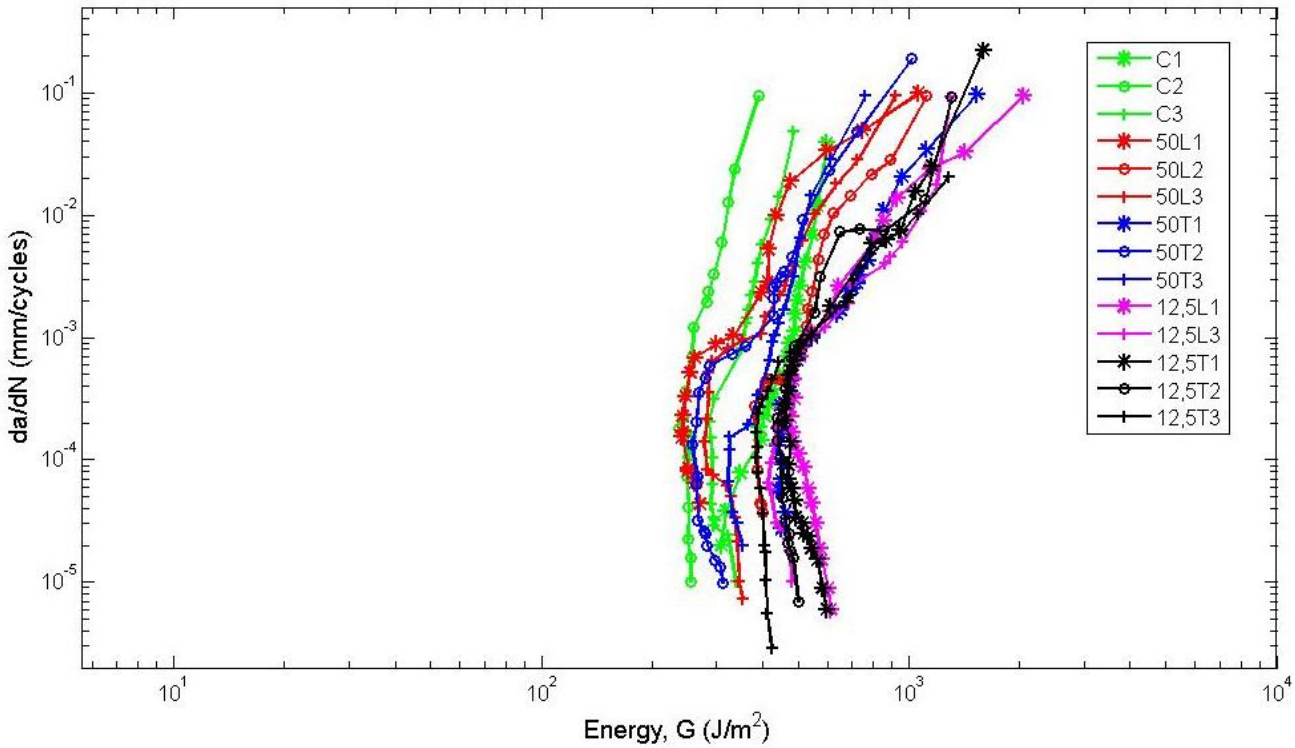

Figure 9.11 Paris plot for all samples tested

It is possible to see that specimens with steel fibres are shifted more on the right due to higher energy of propagation required. Curves seem to respect a 'S' trend as described in the theory but there is some scatter due also to the increase of energy in particular on steel fibres samples maybe linked to fibres bridging. Samples with steel fibres reduce the slope so improve the performance because energy is decreasing slowly. From the graph it is possible to notice that samples with highest fracture toughness are that one with 4000 steel filaments every 12,5 mm. Moreover, the threshold is not well defined in all samples but to reach that, it is required a longer test and higher resolution of load and displacement and also specimen geometry should be changed to have less compliant beams.

9.2 Repeated fatigue tests analysis

Following paragraphs show results about the continuation of fatigue test on same samples tested previously to compare the materials' behaviour during a repeated fatigue test and when tested at the virgin state.

9.2.1 Crack propagation rate

The average crack growth for the second set of fatigue tests is plotted in Figure 9.12. Following table 9.3 shows the crack growth for each sample and the average value for every type of material tested.

Table 9.3 Crack growth results for all samples

	C1	C2	C3	50L1	50L2	50L3	50T1	50T2	50T3	12,5L1	12,5L2	12,5L3	12,5T1	12,5T2	12,5T3
Crack growth (mm)	8,7	6,3	7,5	12	8	14	12,5	-	12	17,2	-	14	7,3	13	15
Average (mm)	7,5			11,3			12,25			15,6			11,75		

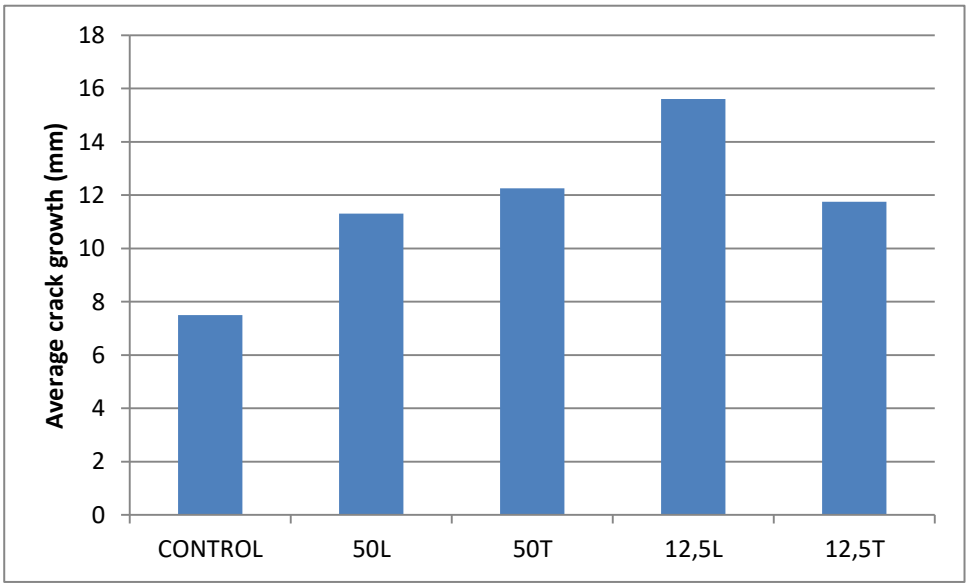

Figure 9.12 Average crack growth for different samples

From this graph it is possible to see that crack growth is bigger in samples with steel fibres and in particular the maximum crack growth is measured for samples with 4000 steel filaments every 12,5mm. Crack growth values are around 7mm in controls while in steel reinforced CFRPs they go from 11 to 15mm.

In figure 9.13 crack growth propagation of the first and second fatigue test are compared.

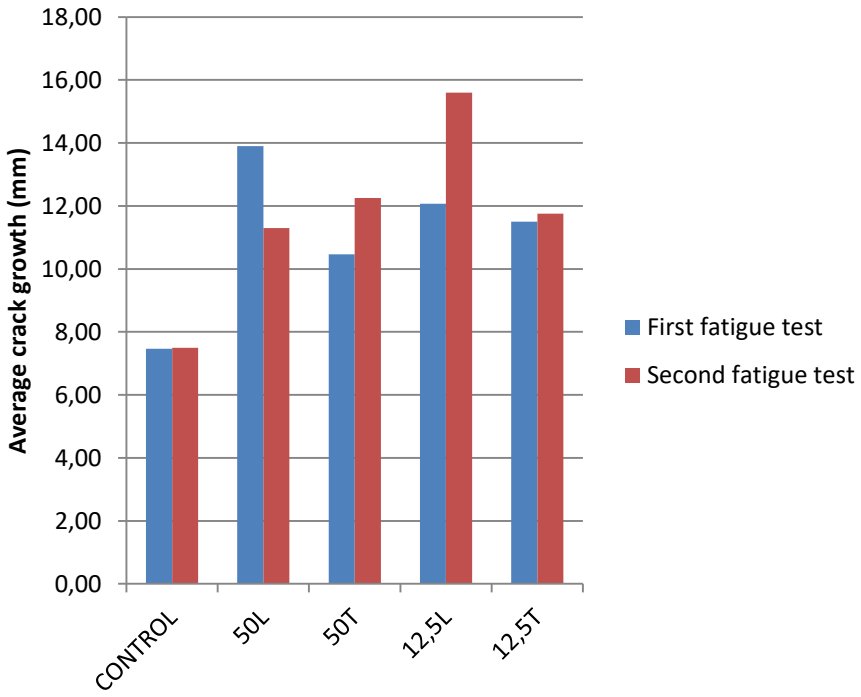

Figure 9.13 Crack growth comparison between first and second fatigue test

Comparing the average crack growth from both tests it is possible to realise that for controls there is almost the same average crack propagation and in general it is possible to say that the crack grew more during the second fatigue test done on samples except for samples with 4000 steel fibres every 50mm.

9.2.2 Energy release rate

Making the same calculation used in first fatigue tests analysis, so reporting the average energy for each sample (Figure 9.14), it can be seen that energy required for crack propagation is higher in samples with steel fibres and in particular the highest values correspond to materials with filaments inserted in the transversal direction thus it is possible to say that they have a strong bridging behaviour which competes with the crack propagation. It is also possible to see that controls average energy is almost the same measured in 50L specimens.
Estimated energy is 316,12 J/m^2 in controls, 316,35 J/m^2 in 50L samples, 495,31 J/m^2 in 50T, 425,75 J/m^2 in 12,5L and 525 J/m^2 in 12,5 T samples.

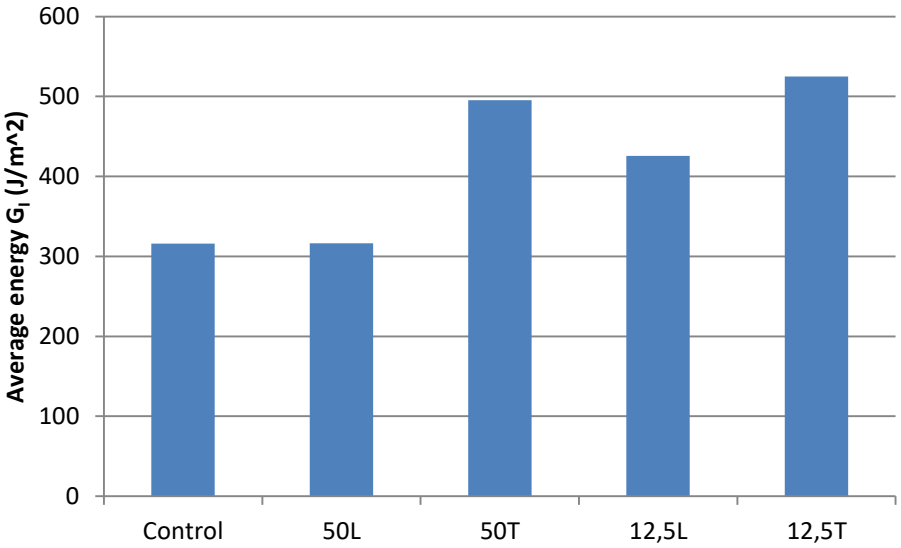

Figure 9.14 Average energy release for each sample

Calculating mean energy for every type of specimen and comparing it with results from first set of fatigue test (Figure 9.15) it is possible to conclude that for almost all samples, stopping fatigue load and reapply it, brings to lower energies but in 50T samples a higher energy is required to propagate the crack during second fatigue test.

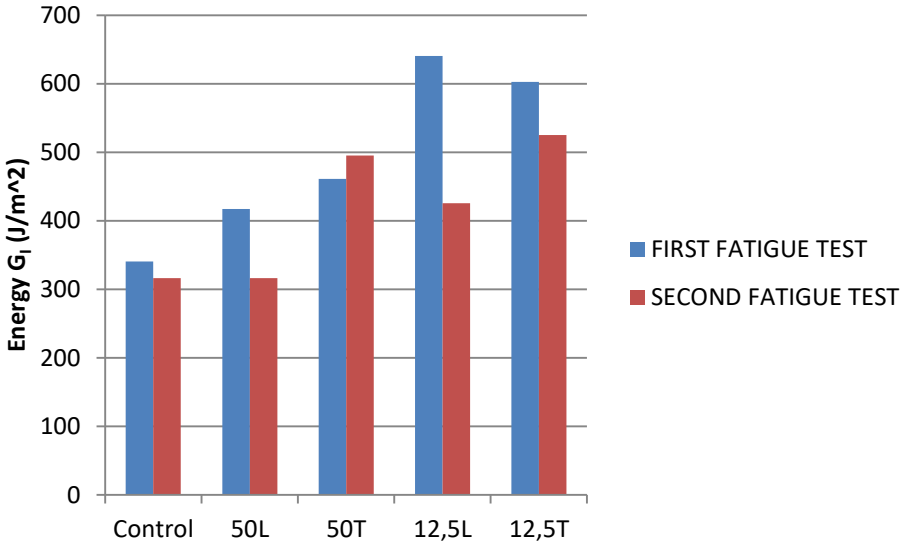

Figure 9.15 Energy average values for first and second fatigue tests

Furthermore, in general it is possible to say that during second fatigue tests higher displacements and lower loads are reached during quasi static tensile test.

9.2.3 Paris plot

Figure 9.16 compares Paris plot obtained from the second fatigue test.

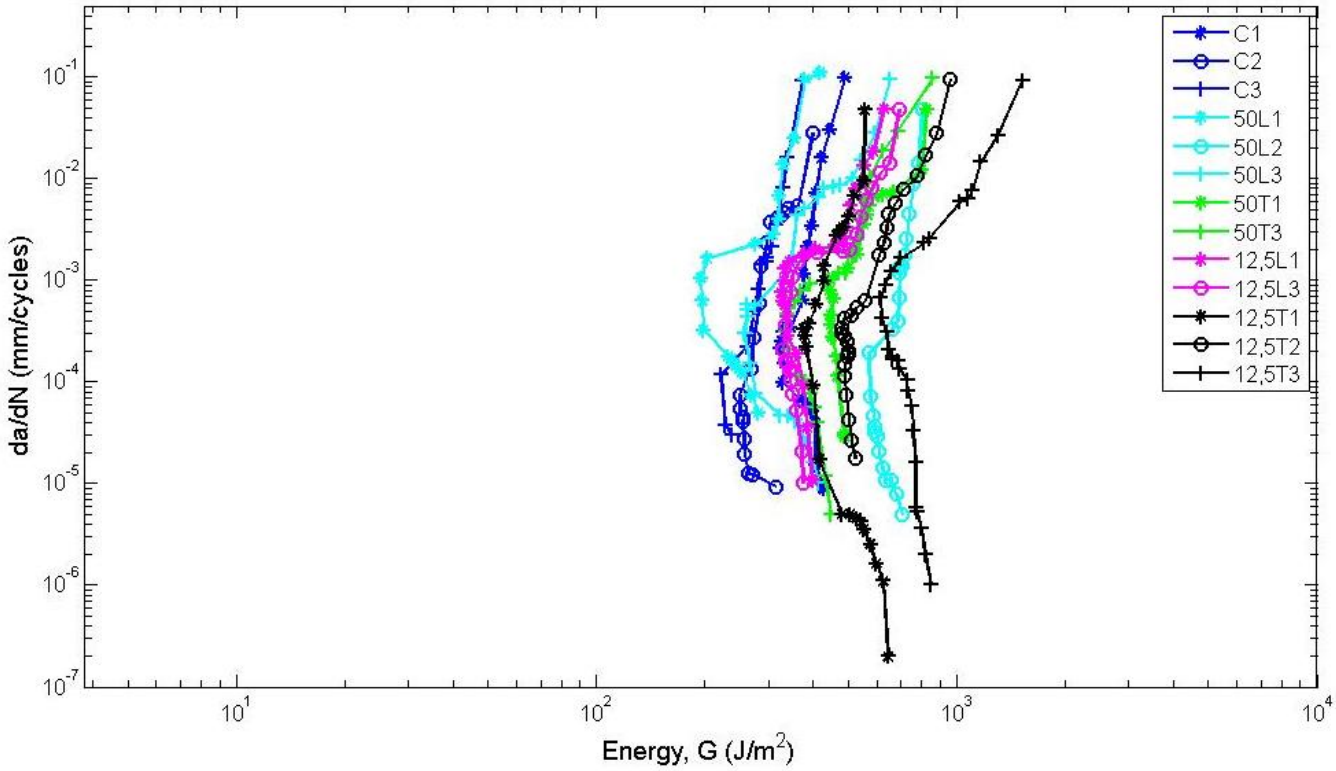

Figure 9.16 Paris plot obtained from second fatigue test data

The general trend is similar to that of Figure 9.11, so samples with steel fibres show curves to higher energies, in particular for material with transversal filaments. Moreover it is possible to see that the slope decrease in samples with steel inside so these materials are safer during applications because the energy required to propagate the crack reduces slower.

Comparing Paris curves obtained from the first and the second fatigue test (Figure 9.17, 9.18, 9.19, 9.20, 9.21)

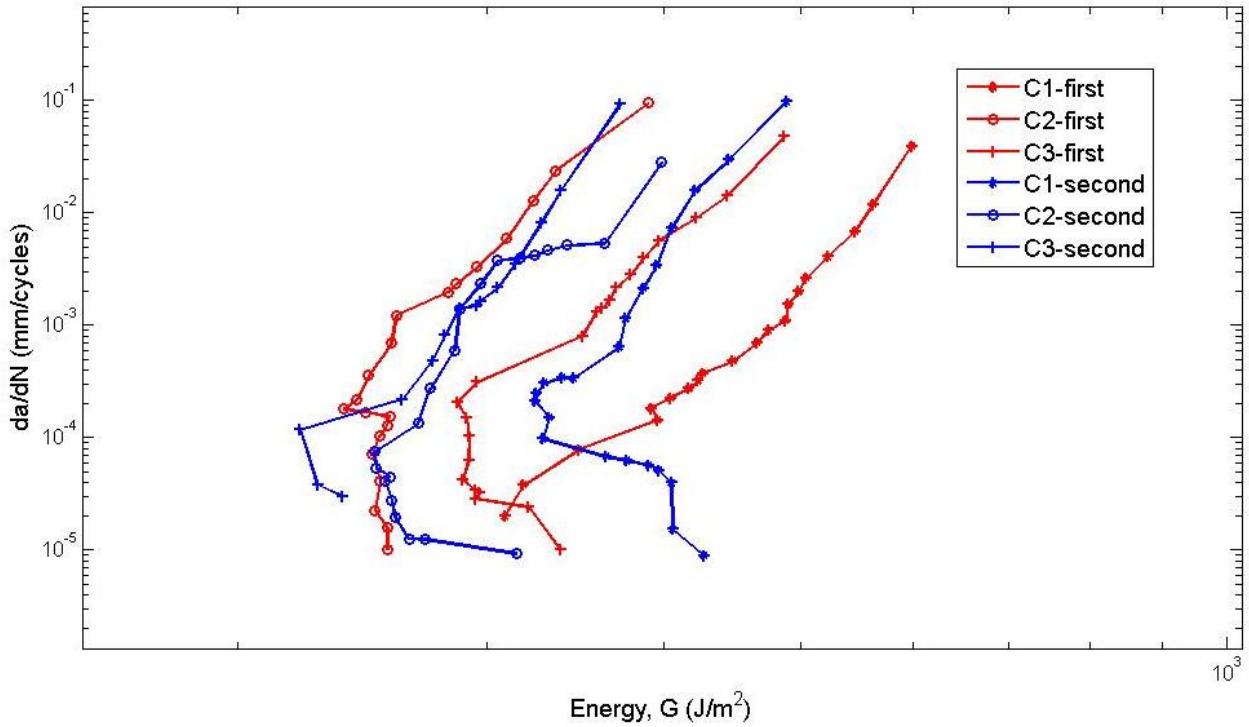

Figure 9.17 Paris control plot for first and second fatigue test

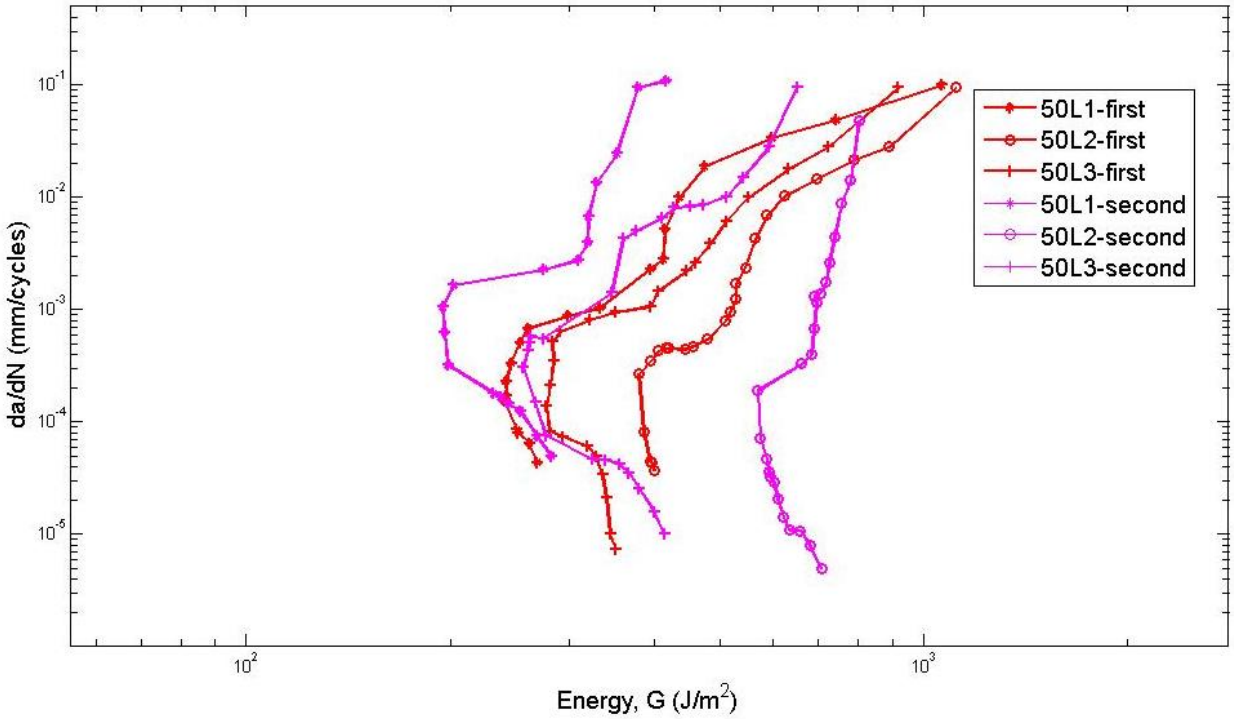

Figure 9.18 Paris 50L plot for first and second fatigue test

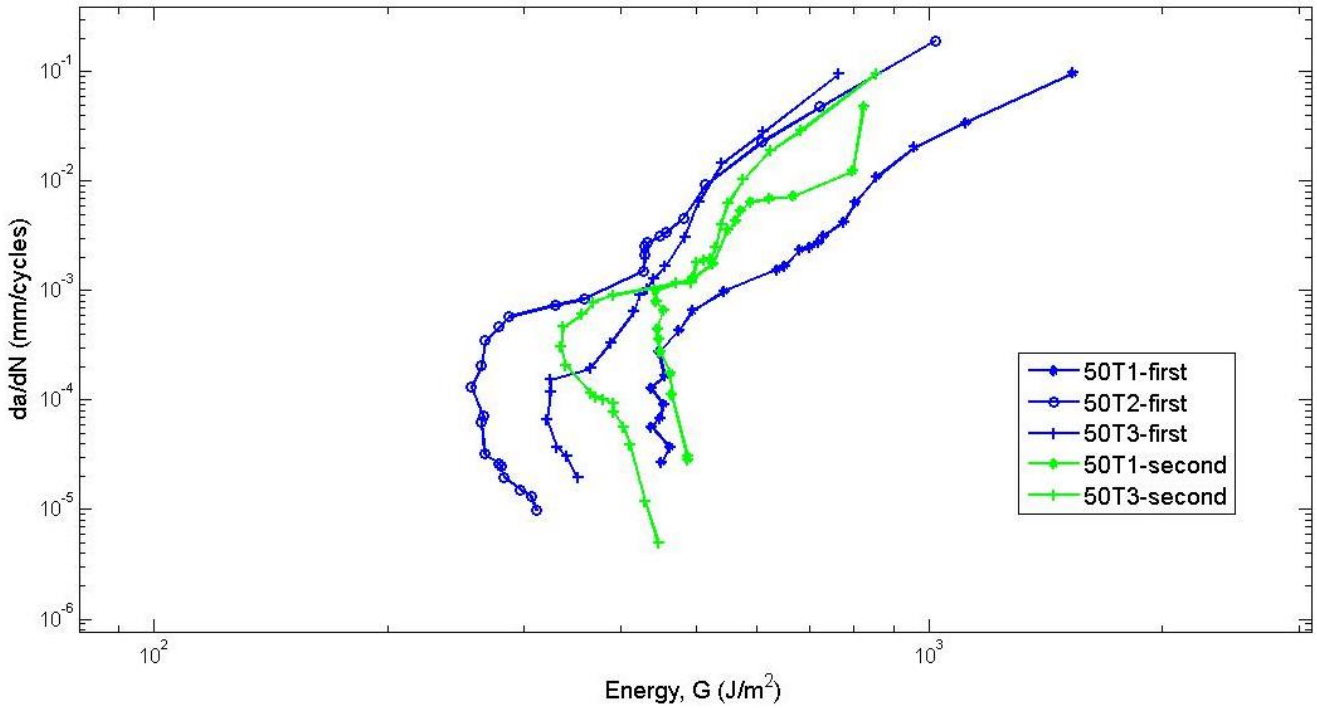

Figure 9.19 Paris 50T plot for first and second fatigue test

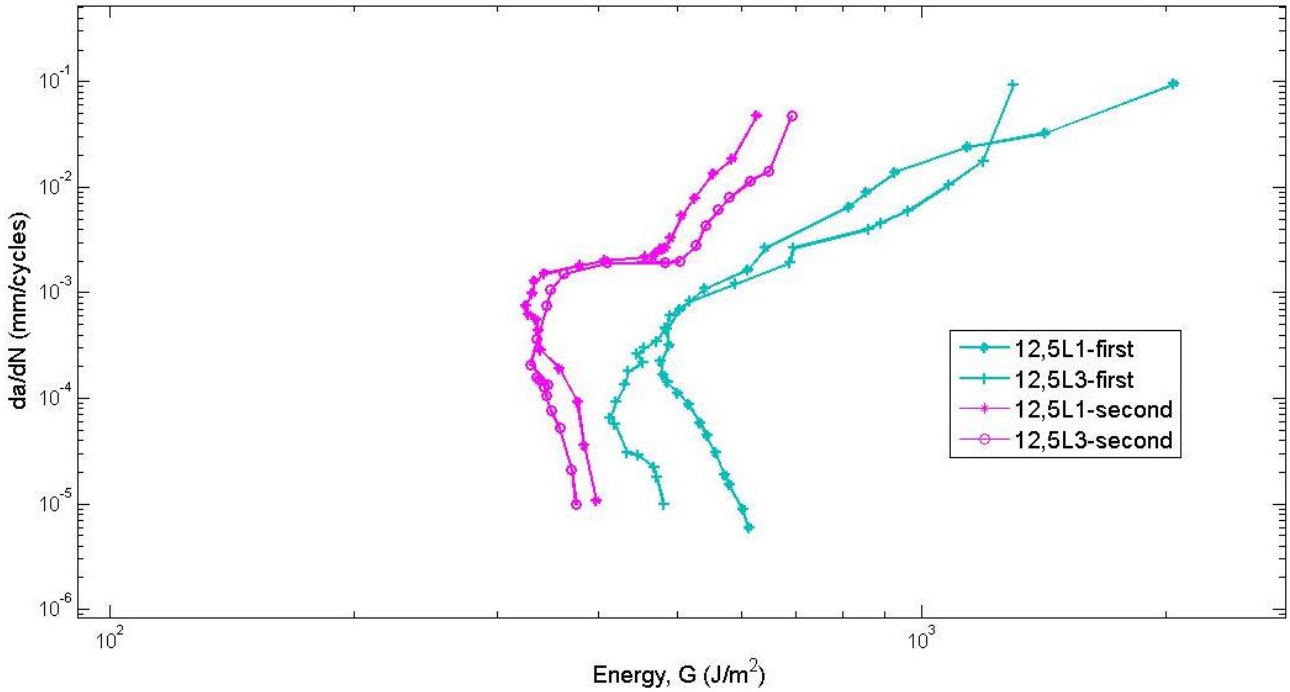

Figure 9.20 Paris 12,5L plot for first and second fatigue test

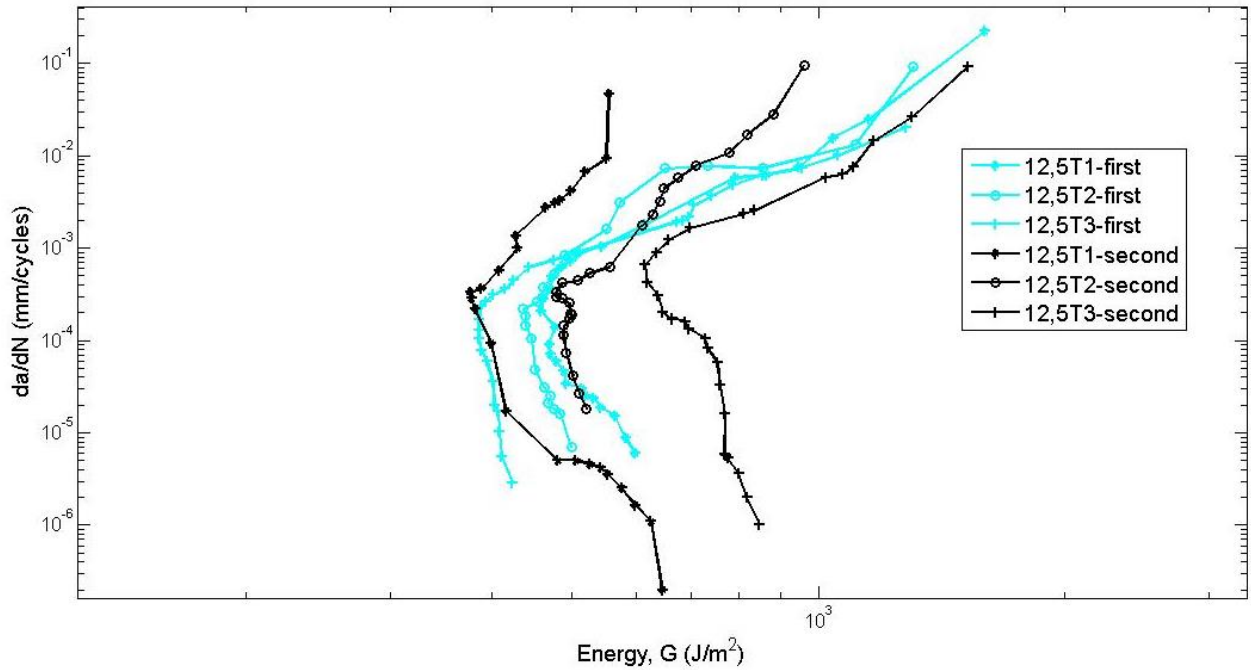

Figure 9.21 Paris 12,5T plot for first and second fatigue test

Graphs are overlapped while from previous experiments done at UCD (TU-Delft) it was expected to find second fatigue test curves more on the left as happens in Figure 9.20. To describe and generalise CFPRs with steel fibres behaviour during second fatigue tests, it should be used some new standards that have not already introduced in literature. It is important to notice that crack initial length is much longer than the first-run test, so this can influence results and data analysis. Moreover, using ESIS-TC4 'round-robin' analysis, as happened in NASA and TU-Delft experiments [57], it is possible to notice that existing fatigue test standards give rise of a large degree of scatter. Hence, these testing standards are not useful for material selection and comparison study purpose. This work aims to study the effect of the initial crack length on the fatigue resistance of CFRPs, however, results show that the initial crack length has some effects on the fatigue resistance, so the reason behind need to be further investigated.

Conclusions

The aim of this thesis project was to determine mode I delamination fatigue characteristics of a variety of CFRPs specimens to study the possibility of increasing fracture toughness adding steel fibres in different amount and disposition inside the composite. Samples were subjected to DCB test and they were tested twice under fatigue load to see how they answered while they were solicited. As part of the project, Instron 250kN machine was used. Appropriate grips and fixtures were designed and manufactured to carry out the tests following standards. Test procedure consisted on a first quasi-static load to create a sharp and natural crack, then a fatigue load was applied and data recorded.

CFRPs are a new materials with a lot of positive properties as low weight, high strength, corrosion resistance and high stiffness. However, they have also some weak points such as poor out-of-plane impact resistance, low fracture toughness and poor delamination resistance. As delamination, due to poor fracture toughness, is one of the biggest causes of failure especially under cyclic load, new research works are investigating a solution to this problem. One of the possibilities is to insert a second material layer inside the composite to increase the crack propagation energy.

In total 5 different materials were tested: controls with only carbon fibres inside, CFRPs with 4000 steel fibres every 50mm disposed in longitudinal and transversal way respect carbon fibres and CFRPs with 4000 steel filaments every 12,5mm disposed in longitudinally and transversally.

A standard fracture mechanics based approach was employed; Beam Theory (BT) calculations were compared to the ones obtained from two corrected LEFM approaches based on specimen compliance: Corrected Beam Theory (CBT). From the results, conclusions can be made about the performance of the different composites under mode I fatigue loading. Three samples were tested for each amount and disposition of steel fibres and results were compared with controls samples. Each sample was tested twice to characterise the material's response to fatigue test when the load was applied after a first solicitation. Values of the strain energy release rate $G_{I,max}$ were calculated for each specimen tested, considering the maximum load P_{max} measured by the machine every cycle. Using values of G_I, the two methods of calculation were compared. In the literature, BT method usually produces lower values than CBT; so CBT values were used to make the analysis because they take into account all the geometric issues of the test caused by the crack growth, using correction factors.

Results from first fatigue test done on samples showed longer crack length in samples with steel fibres especially the ones with longitudinal filaments inside. Considering the maximum load registered by the machine it is possible to see a different behaviour in samples with steel fibres than in controls. In samples without steel filaments the load has a decreasing trend, as expected in this kind of test, while samples with steel filaments after some cycles the load starts to increase a bit probably due to the bridging effect of fibres inside the material.

Comparing energy values it is possible to notice that in samples with steel fibres, to let the crack propagate, higher energies are required. Considering the mean energy value, obtained from energies

measured during the whole fatigue test, controls need 340,8 J/m^2 to let the crack grow. Mean energy for 50L samples was 417,14 J/m^2 and for 50T 461,18 J/m^2. In 12,L a value of 640,53 J/m^2 was measured, while in 12,5T 602,37 J/m^2.

Energies increased respectively of 22% and 35% in samples with 4000 steel filaments every 50mm and of 88% and 77% in samples with 4000 filaments every 12,5mm. In conclusion, from first fatigue run test it is possible to confirm results obtained from previous quasi-static test indeed steel fibres inside CFRPs increase energies so fracture toughness. In particular higher energies are measured in samples with more steel filaments.
Analysing Paris plots it is possible to see that curves of samples with steel inserted are moved to the right to higher energies and their slope is reduced so they show a potentially safer behaviour when used in applications.

Results obtained from second fatigue test done on previous samples show the same trend in crack growth of the first fatigue test, so higher crack propagation in samples with steel fibres inside and generally higher growth were recorded during the repeated test than in the first one.

Comparing energy results, using CBT method, it is possible to observe that higher energies are required to propagate the crack in samples with steel filaments inserted. In particular the mean energy values are 316,12 J/m^2 in controls, 316,35 J/m^2 in 50L samples, 495,31 J/m^2 in 50T, 425,75 J/m^2 in 12,5L and 525 J/m^2 in 12,5 T samples. Analysing data from both tests, it is possible to conclude that during second run test, equal or lower energies were required maybe because some bridges among fibres were ruined after the first test.

In general from this work it is possible to conclude that steel fibres inside CFRPs increase fracture energy so improve the fatigue resistance of these materials and they lower delamination effect. It is difficult to compare the first and the second fatigue test in particular because there are no standards and rules available for reapplication of cyclic load on samples and it is not properly correct to examine data using the same rules adopted in the first test analysis especially because initial crack length is much bigger and this influence the results.

Future work is required to better analyse the repeated cyclic load on already tested samples to find new regulations. This topic is of huge interest in this years and it can bring to big improvement in knowledge of composite properties and it can let safer application of these new materials.

Bibliography

[1] ISO, International Organisation for Standardization. ISO-15024, Fibre-reinforced plastic composites — *Determination of mode I interlaminar fracture toughness, G_{IC}, for unidirectionally reinforced materials*, 2001

[2]Murphy N., Rouge C., *Determination of the mode I delamination resistance, G_{IC}, of a composite material using the double cantilever beam (DCB) specimen*, Fracture Mechanics, UCD Dublin

[3] "What are composite?" [Online]. Available at: https://acmanet.org/what-are-composites/

[4] Composite UK. [Online]. Available at: https://compositesuk.co.uk/composite-material

[5] Advancing the chemical science, Composite material, Royal Society of Chemistry. [Online]. Available at: http://www.rsc.org/Education/Teachers/Resources/Inspirational/resources/4.3.1.pdf

[6] "Development of Carbon Fibre Technologies." [Online]. Available: http://www.bbc.com/news/technology-12691062

[7] Composite manufacturing magazine. [Online]. Available at: http://compositesmanufacturingmagazine.com/2018/03/2018-geneva-motor-show-features-european-debuts-of-new-composite-intensive-models/

[8] Huda M.S. , L.T. Drzal, D. Ray, A.K. Mohanty, M. Mishra, *Natural-fiber composites in the automotive sector*, 2014

[9] Mohan J. D., *An Investigation of Composite-to-Composite Bonding*, UCD, Dublin 2010

[10] Appunti dal corso 'Materiali compositi', A. Maddalena, 2016/2017

[11] Nikhil V Nayak, *Composite Materials in Aerospace Applications*, Mechanical, B.V. Bhoomaraddi College of Engineering & Technology, 2014

[12] *How to win in carbon composites for the automotive market*, Composite world. [Online]. Available at: https://www.compositesworld.com/columns/how-to-win-in-carbon-composites-for-the-automotive-market

[13] Xie, D. and Biggers, S.B., *Delamination growth and residual strength of Compressively loaded sandwich panels with stiffness tailored face sheets*, Journal of Sandwich Structures and Materials, 11(2-3), pp. 133–15, 2009

[14] Pardini L.C, Levy Neto F, McEnaney B., *Modelling of Mechanical Properties of CRFC Composites Under Flexure Loading.* J. Braz. Soc. Mech. Sci.vol.22, pp.203-216, 2000

[15] Murphy C., *Determination of the Fatigue Properties of High Performance Composite Materials*, UCD 2016

[16] Van Velthem P., W. Ballout, J. Horion, Y. A. Janssens, V. Destoop, T. Pardoen, and C. Bailly, *Morphology and fracture properties of toughened highly crosslinked epoxy composites: A comparative study between high and low Tg tougheners*, Composites Part B: Engineering, vol. 101, pp. 14–20, 2016.

[17] Abdussalam S., *Damage and fracture mechanics of composite material*, University of Manitoba, Canada 1999

[18] Carolan D., Ivankovic A., Kinloch A. J., Sprenger S., Taylor A. C., *Toughening of epoxy-based hybrid nanocomposites*, Polymer 97 (2016) 179–190.

[19] Rahmanian S., Suraya A., Roshanravan B., Othman R., Nasser A., Zahari R., Zainudin E., *The influence of multiscale fillers on the rheological and mechanical properties of carbon-nanotube silica-reinforced epoxy composite*, Materials & Design (2015) 227 –235.

[20] Quan D., Ivankovic A., *Effect of core shell rubber (CSR) nano-particles on mechanical properties and fracture toughness of an epoxy polymer*, Polymer 66 (2015) 16 – 28.

[21] Quan D., Murphy N., Ivankovic A., *Fracture behaviour of epoxy adhesive joints modified with core-shell rubber nanoparticles*, Engineering Fracture Mechanics 182 (2017) 566–576.

[22] Ayatollahi M. R., S. Shadlou, M. M. Shokrieh, *Fracture toughness of epoxy/multiwalled carbon nanotube nano-composites under bending and shear loading conditions*, Materials&Design (2011) 2115–2124.

[23] Subhani T., M. Latif, I. Ahmad, S. A. Rakha, N. Ali, A. A. Khurram, *Mechanical performance of epoxy matrix hybrid nanocomposites containing carbon nanotubes and nanodiamonds*, Materials & Design 87 (2015)

[24] Quan D., D. Carolan, C. Rouge, N. Murphy, A. Ivankovic, *Carbon nanotubes and core– shell rubber nanoparticles modified structural epoxy adhesives*, Journal of Materials Science (2017) 4493–4508.

[25] Ahmadi-Moghadam B., M. Sharafimasooleh, S. Shadlou, F. Taheri, *Effect of functionalization of graphene nanoplatelets on the mechanical response of graphene/epoxy composites*, Materials & Design 66, Part A (2015) 142 – 149.

[26] Li P., Y. Zheng, M. Li, T. Shi, D. Li, A. Zhang, *Enhanced toughness and glass transition temperature of epoxy nanocomposites filled with solvent-free liquid-like nanocrystal functionalized graphene oxide*, Materials & Design 89 (Supplement C), 2016

[27] B. C. Kim, S. W. Park, D. G. Lee, *Fracture toughness of the nano-particle reinforced epoxy composite*, Composite Structures 86 (1) (2008) 69–77.

[28] B. Qi, Q. Zhang, M. Bannister, Y.-W. Mai, *Investigation of the mechanical properties of DGEBA-based epoxy resin with nanoclay additives*, Composite Structures 75 (1) (2006) 514–519.

[29] M.-W. Ho, C.-K. Lam, K. tak Lau, D. H. Ng, D. Hui, Mechanical properties of epoxy based composites using nanoclays, Composite Structures (2006) 415–421.

[30] M. Hosur, A. Mohammed, S. Zainuddin, S. Jeelani, *Processing of nanoclay filled sandwich composites and their response to low-velocity impact loading,* Composite Structures (2008) 101–116.

[31] Hufenbach W., R. Bohm, M. Thieme, A. Winkler, E. Mader, J. Rausch, and M. Schade, *Polypropylene/glass fibre 3D-textile reinforced composites for automotive applications,* Materials and Design, vol. 32, no. 3, pp. 1468–1476, 2011

[32] Mouritz A. P., M. K. Bannister, P. J. Falzon, and K. H. Leong, *Review of applications for advanced three-dimensional fibre textile composites,* Composites Part A: Applied Science and Manufacturing, vol. 30, no. 12, pp. 1445–1461, 1999.

[33] Dexter H. B. and J. G. Funk., *Impact Resistance and Interlaminar Fracture Toughness of Through-the-Thickness Reinforced Graphite/Epoxy In The Proceedings of 27th Structures,* Structural Dynamics and Mat. Conference, San Antonio. TX, May 1986

[34] Mouritz A. P., *Review of z-pinned composite laminates,* Composites Part A: Applied Science and Manufacturing, vol. 38, no. 12, pp. 2383–2397, 2007

[35] Cui H., M. Yasaee, G. Kalwak, A. Pellegrino, I. K. Partridge, S. R. Hallett, G. Allegri, and N. Petrinic, *Bridging mechanisms of through-thickness reinforcement in dynamic mode I&II delamination*, Composites Part A: Applied Science and Manufacturing, vol. 99, pp. 198–207, 2017

[36] Kim R. Y., *A Technique for Preventation of Delamination*, AFWAL-TR-82- 4007,1982.

[37] Ramirez V. A., P. J. Hogg, and W. W. Sampson, *The influence of the nonwoven veil architectures on interlaminar fracture toughness of interleaved composites,* Composites Science and Technology, vol. 110, pp. 103–110, 2015.

[38] Beckermann G. W. and K. L. Pickering, *Mode I and Mode II interlaminar fracture toughness of composite laminates interleaved with electrospun nanofibre veils*, Composites Part A: Applied Science and Manufacturing, vol. 72, pp. 11–21, 2015. 13, 16, 17

[39] Daelemans L., S. van der Heijden, I. De Baere, H. Rahier, W. Van Paepegem, and K. De Clerck, *Nanofibre bridging as a toughening mechanism in carbon/epoxy composite laminates interleaved with electrospun polyamide nanofibrous veils,* Composites Science and Technology, vol. 117, 2015

[40] Zhang J., T. Lin, and X. Wang, *Electrospun nanofibre toughened carbon/epoxy composites: Effects of polyetherketone cardo (PEK-C) nanofibre diameter and interlayer thickness,* Composites Science and Technology, vol. 70, no. 11, pp. 1660–1666, 2010.

[41] K. N. Shivakumar, R. Panduranga, and M. Sharpe, *Interleaved Polymer Matrix Composites - A Review,* 54th AIAA/ASME/ASCE/AHS/ASC Structures, Structural Dynamics, and Materials Conference, pp. 1–13, 2013.

[42] Borowski E., E. Soliman, U. F. Kandil et al., *Interlaminar Fracture Toughness of CFRP Laminates Incorporating Multi-Walled Carbon Nanotube,* 2015

[43] Callens M. G., L. Gorbatikh, and I. Verpoest, *Composites: Part A Ductile steel fibre composites with brittle and ductile matrices*, COMPOSITES PART A, vol. 61, pp. 235–244, 2014.

[44] Guy M., L. Gorbatikh, E. Bertels, B. Goderis, M. Smet, and I. Verpoest, *Tensile behaviour of stainless steel fibre / epoxy composites with modified adhesion*," COMPOSITES PART A, vol. 69, pp.208–218, 2015. ix, 21, 23, 64, 66, 67

[45] Callens, Verpoest, Gorbatikh, *Ductility of steel fibre/epoxy composite in function of their microstructure*, Leuven 2017

[46] Swolfs Y., P. De Cuyper, M. G. Callens, *Hybridisation of two ductile materials – Steel fibre and self-reinforced polypropylene composite*, Leuven 2017

[47] Callens M. G., P. D. Cuyper, L. Gorbatikh, and I. Verpoest, *Effect of fibre architecture on the tensile and impact behaviour of ductile stainless steel fibre polypropylene composites*, COMPOSITE STRUCTURES, vol. 119, pp. 528–533, 2015. ix, 21, 24, 64, 67

[48] Murphy B., M. D. Gilchrist, A. Ivankovic, D. Quan, C. Roug, *Developing High Performance Glass Fibre Composites Using Carbon Fibre Veils*, UCD, Ireland 2018

[49] Jollivet T., C. Peyrac, F. Lefebvre, *Damage of composite materials*, Polymer & Composite Engineering Department, Chemin du Chaffault, France 2013

[50] Allen D.H, Harris C. E., *A thermomechanical constitutive theory for elastic composites with distributed damage—II. Application to matrix cracking in laminated composite.* International Journal of Solids and Structures. Volume 23, Issue 9, 1987, Pages 1319-1338

[51] Adams R.D, Maheri M. R., *Damping in advanced polymer–matrix composites*, Journal of alloys and compound, Volume 355, 2003

[52] Manivasagam S., Chandrasekaran K., *Characterization of damage progression in layered composites*, Journal of Sound and Vibration 1992

[53]ASTM E647-00 Standard Test Method for Measurement of Fatigue Crack Growth Rates

[54] Brunner A., S. Stelzer, G. Pinter, ESIS-TC4-Protocol, *Determination of Mode I Fatigue Delamination Propagation in Unidirectionally Reinforced Materials*, Draft Test Protocol, Austria 2015

[55] J. G. Williams. *The fracture mechanics of delamination tests*. Journal of strain analysis for engineering design, 24(4):207–214. ISSN 0309-3247

[56] Schijve J. *The Accumulation of Fatigue Damage in Aircraft Materials and Structures*, AGARD Ag-157, North Atlantic Treaty Organisation Advisory Group for Aerospace Research and Development, 1972

[57] Alderliesten R., *Mode I fatigue delamination in composite DCB specimen-Discussing standardization*. TU-Delf.

Acknowledgments

First, I would like to thank Dr. Alojz Ivankovic, who was my supervisor at UCD School of Mechanical and Materials Engineering, giving me the opportunity to work on fatigue behavior of composites. Thank you to Dong Quan, my tutor at UCD, who followed me during the work and gave me some advises. Massimo Guglielmi is gratefully acknowledged for the final thesis revision but especially for his support and availability during all my experience abroad. Many thanks also to UCD workshop staff, for their precious help with machines and fixtures. in particular to Mr. John Gahan who helped me during experiments being always available, patient and especially because he found time to chat with me during my long fatigue tests even if he was always busy. I want to thank all the colleagues I met during my stay at UCD, who were always willing to help me in hard times, who always found some way to make me laugh with jokes. They taught me a lot about Dublin, how to survive there during strong winter and cloudy days; they let me to learn a lot about different countries and cultures sharing with me their food and traditions. Thank you to all friends I met during my Erasmus, we spent nice time and we discovered Ireland together. A huge thank you is to my 'Irish family', the landlady and her daughters were as second family and I will never forget them. I would like to thank my Italian friends and colleagues I met during my university period, they have made my time more pleasant during lessons and breaks.
Last but not less important, a very big thank you to my family, my boyfriend and relatives, who supported me, stood me and endured me during my studies.